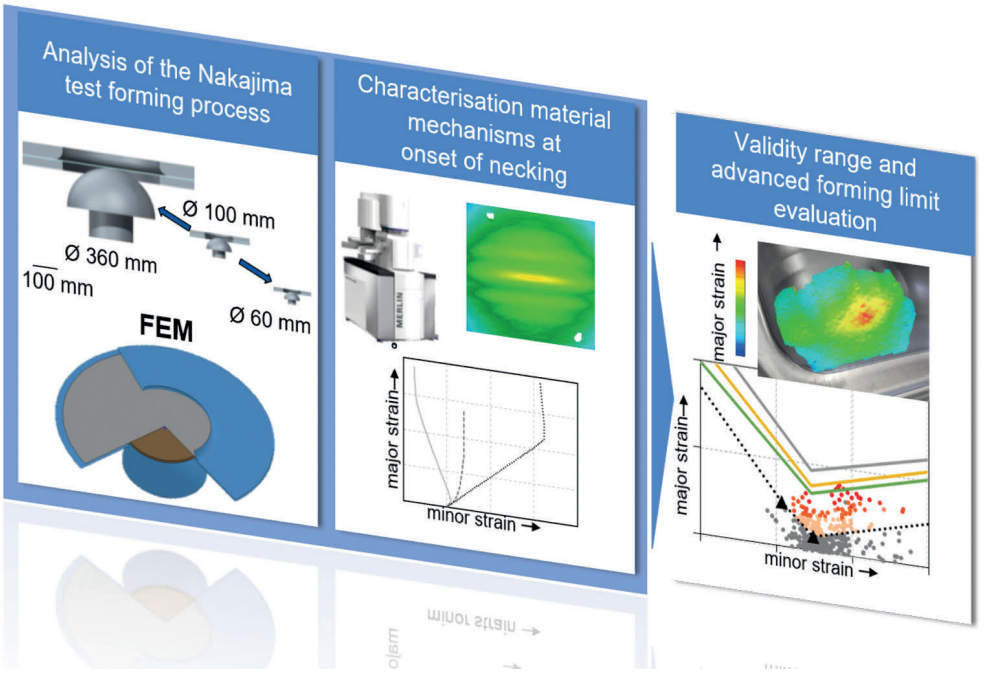


FAU Studien aus dem Maschinenbau 342

**Emanuela Affronti**

# Evaluation of failure behaviour of sheet metals

FAU UNIVERSITY PRESS

Emanuela Affronti

Evaluation of failure behaviour of sheet metals

# FAU Studien aus dem Maschinenbau

## Band 342

Herausgeber der Reihe:

Prof. Dr.-Ing. Jörg Franke
Prof. Dr.-Ing. Nico Hanenkamp
Prof. Dr.-Ing. habil. Marion Merklein
Prof. Dr.-Ing. Michael Schmidt
Prof. Dr.-Ing. Sandro Wartzack

Emanuela Affronti

# Evaluation of failure behaviour of sheet metals

Dissertation aus dem Lehrstuhl für Fertigungstechnologie (LFT)
Prof. Dr.-Ing. habil. Marion Merklein

Erlangen
FAU University Press
2020

Bibliografische Information der Deutschen Nationalbibliothek:
Die Deutsche Nationalbibliothek verzeichnet diese Publikation in der Deutschen Nationalbibliografie; detaillierte bibliografische Daten sind im Internet über http://dnb.d-nb.de abrufbar.

Bitte zitieren als
Affronti, Emanuela. 2020. *Evaluation of failure behaviour of sheet metals.*
FAU Studien aus dem Maschinenbau Band 342.
Erlangen: FAU University Press. DOI: 10.25593/978-3-96147-304-5.



Verlag und Auslieferung:
FAU University Press, Universitätsstraße 4, 91054 Erlangen

Druck: docupoint GmbH

ISBN: 978-3-96147-303-8 (Druckausgabe)
eISBN: 978-3-96147-304-5 (Online-Ausgabe)
ISSN: 2625-9974
DOI: 10.25593/978-3-96147-304-5

**Evaluation of failure behaviour of sheet metals**

Der Technischen Fakultät
der Friedrich-Alexander-Universität
Erlangen-Nürnberg

zur
Erlangung des Doktorgrades Dr.-Ing.

vorgelegt von

Emanuela Affronti, M.Sc.

aus Palermo

Als Dissertation genehmigt
von der Technischen Fakultät
der Friedrich-Alexander-Universität Erlangen-Nürnberg

| | |
|---|---|
| Tag der mündlichen Prüfung: | 09.12.2019 |
| Vorsitzender des Promotionsorgans: | Prof. Dr.-Ing. habil. Andreas Paul Fröba |
| Gutachter: | Prof. Dr.-Ing. habil. Marion Merklein<br>Prof. Dr. Livan Fratini, Università di Palermo<br>Prof. Dr.-Ing. habil. Andreas Maier |

# Vorwort

Die vorliegende Dissertation entstand im Rahmen meiner Tätigkeit als wissenschaftliche Mitarbeiterin am Lehrstuhl für Fertigungstechnologie der Friedrich-Alexander-Universität Erlangen-Nürnberg. Die wesentlichen Ergebnisse der Arbeit wurden im Rahmen des EFB Projekts 08/212 „Verbesserung der zeitlichen Auswertemethoden von Versuchen zur Ermittlung der Grenzformänderung und Ableitung eines virtuellen Ersatzmodells“ und von der Deutschen Forschungsgemeinschaft geförderten Projekt ME 2043/59-1 „Verbesserte Charakterisierung des Versagensverhaltens von Blechwerkstoffen durch den Einsatz von Mustererkennungsmethoden“ erarbeitet. Mein besonderer Dank gilt der Ordinaria des Lehrstuhls für Fertigungstechnologie Frau Prof. Dr.-Ing. habil. Marion Merklein für die intensive wissenschaftliche Betreuung bei der Erstellung der Arbeit. Prof. Dr. Livan Fratini danke ich für die Übernahme des Koreferats und bei Prof. Dr.-Ing. habil. Prof Andreas Meier möchte ich mich für seine Mitwirkung an meinem Promotionsverfahren als fachfremder Gutachter und die gute Zusammenarbeit im Rahmen des DFG Projekts bedanken. Ich möchte mich beim Prof. Dr. -Ing. habil. Dipl.-Inf. Hinnerk Hagenah für den Prüfungsvorsitz bedanken. Für die fachliche die gute Zusammenarbeit möchte ich mich bei meiner Projektpartnern Herrn Dr. David Jocham und Herr Christian Jaremenko bedanken. Mein Dank gilt den Kollegen am Lehrstuhl für Fertigungstechnologie. Den Mitgliedern der Forschungsgruppen „Werkstoffcharakterisierung und Modellierung“ gilt mein Dank, sowie Dr.-Ing. Dipl.-Wirtsch.-Ing. Univ. Michael Lechner für die vielen fachlichen Diskussionen und Anregungen zur vorliegenden Arbeit. Mein Dank gilt allen technischen Mitarbeitern, den Teams aus Sekretariat, Buchhaltung und Systemadministration. Einen besonderen Dank richte ich an Janine Schmidt, Philipp Sachse, Jürgen Hermann, Philipp Frey, Matthias Lenzen und Martin Rosenschon für die konstruktive Zusammenarbeit. Ebenso danke ich den Studenten und Hilfswissenschaftlern, welche durch Ihre Arbeit zum Gelingen dieser Dissertation beigetragen haben, besonders an Herrn Michael Beneder und Herrn Mario Weidinger. An der Stelle möchte ich mich bei meiner Familie in Italien sowie in Deutschland für die Unterstützung bedanken. Abschließend geht mein größter Dank an meinen Lebensgefährten Christian, für seine bedingungslose Unterstützung und sein liebevolles Verständnis.

Amberg, im Januar 2020 Emanuela Affronti

# Table of contents

# Symbols and abbreviations

| *Symbols* | *Unit* | *Description* |
|---|---|---|
| *b,c,a* | - | extrapolation parameters |
| eMMFC | | Enhanced Modified Maximum Force Criterion |
| eps | - | FLC point at plane strain |
| k | - | thickness ratio |
| m,a,b,c,f,g,h | - | coefficients of Yld91 model |
| n | - | hardening exponent |
| p | - | number of evaluation points |
| $r_0$ | - | Lankford coefficient in rolling direction |
| $r_{90}$ | - | Lankford coefficient perpendicular to the rolling direction |
| $t_0$ | mm | thickness in millimetres |
| $t_A$ | mm | thickness sheet metal |
| $t_B$ | mm | thickness sheet metal in the groove |
| u | mm | displacement in the groove |
| w | mm | specimen width |
| A,B,C,D,E | - | constants of M-K model |
| BBC05 | | Banabic yield model of 2005 |
| $D_{bh}$ | mm | blank holder diameter |
| $D_p$ | mm | punch diameter |
| DIC | | Digital Image Correlation |
| DP | | Dual-Phase |
| EFB | | Europäische Forschungsgesellschaft für Blech-verarbeitung e.V. |
| FEA | | Finite Element Analysis |
| FEM | | Finite Element Method |
| Fexperiment | kN | experimental force |
| FLB | | Forming Limit Band |

| | | |
|---|---|---|
| FLC | | Forming Limit Curve |
| FLSD | | Forming Limit Stress Diagram |
| Fsimulation | kN | numerical force |
| GDDRG | | German Deep Drawing Research Group |
| GFLC | | General Forming Limit Curve |
| H-N | | Hutchinson-Neale |
| IDDRG | | International Deep Drawing Research Group |
| IF | | Interstitial-Free |
| Kcr | - | critical value |
| M-K | | Marciniak-Kuczynski |
| MMFC | | Modified Maximum Force Criterion |
| NA | | Bending Neutral Axis |
| NADDRG | | North America Deep Drawing Research Group |
| PLC | | Portevin-LeChatelier |
| PVC | | Polyvinyl chloride |
| R | mm | punch radius |
| RF | | Random Forest |
| RMSE | | Root Mean Square Error |
| SEM | | Scanning Electron Microscope |
| T | in | sheet thickness in inches |
| TRIP | | Transformation Induced Plasticity |
| TS | MPa | tensile strength |
| UE | % | uniform elongation |
| Yld2003 | | Barlat yield model of 2003 |
| Yld91 | | Barlat yield model of 1991 |
| YS | MPa | yield strength |
| $\overline{R}$ | - | planar anisotropy |
| $\vec{v}$ | mm/s | relative velocity |
| μ-DIC | | Micro Digital Image Correlation |
| $\alpha$ | - | imperfection factor |
| $\gamma$ | - | stress ratio |
| $\varepsilon_1$ | - | major strain |

| *Symbols* | *Unit* | *Description* |
|---|---|---|
| $\varepsilon_{12middle}$ | - | strains on the inner surface |
| $\varepsilon_{12outer}$ | - | strains on the outer surface |
| $\varepsilon_{1b2b}$ | - | biaxial pre-straining |
| $\varepsilon_2$ | - | minor strain |
| $\varepsilon_3$ | - | 3rd component of principal strains |
| $\rho$ | | Pearson correlation coefficient |
| *б1* | MPa | principal stress |
| *бx* | - | standard deviation in the x-direction |
| *бy* | - | standard deviation in the y-direction |

# 1 Introduction

Sheet metals are an integral part of our everyday life. From preserves packages to automotive constructions, up to large structures such as aeroplanes or solar panels, the forming of sheet metals plays an important role in the world economy and the trend seems to increase. Sheet metal is defined as metal in form to thin and flat pieces. The advantage of the sheet employing is the high versatility thanks to the combination of good formability and high resistance.
The production trend goes to an increase in products complexity, close to the costumers' needs, with a possible high-profit margin. In order to exploit the full potential of sheet metals, a comprehensive knowledge of the sheet metal behaviour and the exact evaluation of its formability are crucial. Therefore, in order to optimize the processes, it is important, besides the diversification of the forming processes, to acquire knowledge on the material characteristics.

The formability is defined as the capability to undergo plastic deformation causing a change in shape without failure or defects [1]. The quantification of this sheet metal characteristic is decisive for the design and optimization of forming processes. This information is crucial for the finite element analysis (FEA), in which forming operations, as well as material characteristics, are numerically modelled. It allows the numerical study of the process feasibility saving time and costs. Thus, the quantification of the formability should be precise in order to use the full material potential and at the same time, it should be easy to implement and model. Depending on the forming process, the formability is differently evaluated. Focusing the attention on the stretching, the most used tool for the determination of formability is the forming limit curve (FLC).

The FLC appears for the first time in the 50s, as a set of major and minor strain value pairs that define the onset of instability of sheet metal under different strain conditions. It was designed with a practical orientation, considering the in-situ measurement of formability on test specimens by analysing the strain distribution. Starting with the measurement of the elliptical deformation of circle patterns on the surface, the strain measurement on sheet metal surface has reached nowadays high precision levels thanks to the digital image correlation techniques (DIC). Pictures of the specimen are acquired during the test and the DIC method calculates the pattern displacement using the pictures' development. Thus, to date, the standard for the evaluation of the FLC is represented by the

DIN EN ISO 12004-2 that describes the test procedure as well as the evaluation method. The development of the standard has tried to keep the simplicity of the FLC definition. In fact, despite the huge number of test setups available for materials characterisations, such as tensile test, bulge test, plane strain tests, the standard prescribes the use of only a stretching setup with two punch variations, namely a hemispherical punch according to Nakajima [2] and a flat punch according to Marciniak [3]. The use of only one setup guarantees a better comparison of the forming limits by different strain conditions that are obtained by changing the geometry width. The evaluation method, named cross-section method was proposed in the 70s. Sections are defined on the strain distribution perpendicular to the crack initiation, and the strain development on them are interpolated with a second order function in order to achieve values corresponding to the last stable level of forming. The answer in reply to the question, why an old method still represents the standard, lies to the fact that the method is simple, easy to apply and works for most of the conventional materials in which the limit of the formability is represented by strain localization.

However, the diversification of materials, as well as the complexity of the material structures, is growing. The trend shows that sheet metals with high strength are increasingly used. For those materials, the conventional method shows weaknesses. In the last two decades, the research has been focused on alternative evaluation methods that are valid for any material characteristic, by using the advantages of the DIC techniques with time-dependent evaluation methods. However, the methods still have aspects that need more investigations such as the definition of the evaluation zone or the influencing parameters deriving to the optical measurement system. Moreover, even using the standard procedure and using setups with a slight difference in the range of the ISO validity, FLC results show discrepancies suggesting that further analyses are required. Process- as well as material-dependent parameters, influences the FLC results. For example, the hemispherical form of the Nakajima punch causes undesired effects like bending and an initial biaxial pre-stretching. Despite several proposed correction methods in the literature, a thorough quantification of their mechanisms and its dependence on the material characteristics are required. Considering the material aspect, an analysis of the material mechanisms during Nakajima tests depending on the material structure is also missed.

The objective of the present research is a more precise evaluation of the FLC thanks to a better understanding of the test process of the Nakajima

test. The research will focus on the material mechanisms during Nakajima tests for three different sheet metals, namely ductile deep-drawing steel, high strength steel and aluminium alloy. The material mechanisms will be related to the measured distribution in order to recognize surface pattern useful for the definition of the onset of instabilities during Nakajima tests. Finally, the effects of the setup-dependent influencing parameters will be analysed and the limit of validity of the evaluated FLC will be set. The acquired knowledge can be used for the further development of the evaluation method. A possible application is represented by the advanced evaluation of the strain distribution using automatic pattern recognition. The pattern recognition is a field of machine learning and deals with the irregularities and peculiarities in data. This innovative approach allows an automatic determination and can represent the future of the experimental evaluation of the FLC.

# 2 State of the art and research

In this chapter, an overview of the history and the state-of-the-art in the field of forming limits in sheet metal forming is given. In section 2.1 the aspect of formability is summarised. In particular, the attention is focused on the evaluation of sheet metal formability in industrial processes. The formability is the sheet metal characteristic to undergo plastic deformation without damage occurs. This capability is the fundamental of every production chain in which sheet metal is involved. Nevertheless, the progress in technology involves increasingly complex manufacturing processes and the limits of the material capability are reached quickly. Consequently, the evaluation of the forming behaviours is crucial nowadays. The most used tool for the determination of forming limits in sheet metal forming is represented by the forming limit curve (FLC). It collects the forming limits in terms of major and minor strain pairs and can include strain paths from the biaxial stretching to the uniaxial tension condition. Its simplicity makes the FLC very popular in press shop applications and it is mostly used for the forming characterisation in finite-element-analysis (FEM). section 2.2 deals with the FLC, from its definition to the evaluation. In section 2.2.1 the experimental procedure for the evolution of the FLC is discussed. The different setups, as well as the current standard, are presented. section 2.2.2 briefly outlines the developments in measurement techniques and the fundamentals of digital image correlation (DIC). The evaluation methodologies for the determination of the FLC are discussed in section 2.2.3. The most important analytical approaches for the definition of the forming limit curve are summarised in section 2.2.4. Moreover, the effect of process parameters and material characteristics on the FLC is discussed in section 2.2.5. Finally, a general assessment of the current state of the arts is given in section 2.3.

## 2.1 Formability in sheet metals

Metals are part of the human history since the antiquity when the first gold jewellery products can be found. The production of metals in the sheet is also ancient. Firstly it was produced by hammering and after, thanks to Da Vinci's invention, by rolling. Sheet metal has numerous advantages: it is easy to work with, it is easy to shape and can be used to make products from small to large scales [4]. Due to their formability, in fact, sheet metals have the capability to bear plastic deformation and

change in shape without defects [1]. This useful characteristic permits the construction of complex structures and nowadays can be observed regarding many aspects of our daily lives, from food packaging to cars and plane construction. The goal of product design engineering is to use the full potential of material and minimize the cost of production processes. Thus, the correct evaluation of formability is a crucial point for the manufacturing industry. The formability depends on two main influencing factors: the material characteristics and the process parameters [5]. Focusing only on the material, the evaluation of formability usually starts with the material characterisation. The tensile test [6] or the bulge test [7] are only some examples of the possibilities for testing sheet metals. In order to evaluate specific material parameters, the characterisation tests should be designed to cover only a specific forming condition (uniaxial tension, biaxial tension, etc.). However, in industrial applications, the forming processes are more complex and multiple forming conditions can coexist. Already in 1946 Gensamer [8] pointed out the importance to investigate the relationship between the measured mechanical characteristics of metal and their mechanical behaviour in service. Generally, the main material characteristics can be summarised in strength and ductility. The strength, considered the resistance of the material to undergo distortion or fracture, can be easily determined by the tensile test. The ductility is defined with the material potential to be deformed without fracture. The condition of loading is hereby much more important and thus the only tensile test cannot be used for the general evaluation of this characteristic. Gansamer evaluated the ductility for different material tests, from uniaxial to biaxial test and depicted the results in a transverse principal strain/longitudinal principal strain diagram. He discovered that the deformation at the point of fractures varies with the ratio of the principal strain. Therefore, a more general tool, able to collect a broad-spectrum of formability characteristics, is required for those applications. Moreover, Gansamer distinguished between the local material deformation and the homogeneous strain distribution. The local deformation, considered as strain localisation, represents the forming limit since it is the first step of the onset of fracture. The pioneering work of Gansamer led to the evaluation of formability at several strain conditions and to the definition of the forming limit curve.

## 2.2 Forming limit curve

As mentioned above, the first concept of a diagram collecting forming information at several strain conditions was produced by Gensamer

in 1946 [8]. Unfortunately, as observed years later by Col [9], the new idea had resonated only in the academic field and its potential for the press shop was unknown. Only in 1963, thanks to Keeler and Backofen [10], the possibility of analysing the forming limits in stretching processes were examined. The authors studied stretching processes and measured the strains through the deformation of circles drawn on the surface before deformation. After the analysis of several materials, from aluminium to copper and steel, they concluded that the instability under biaxial stretching occurs by diffuse necking and ductile fracture. Moreover, they observed that the fracture behaviour depends on the processing history and material microstructure. The study of Keeler and Backofen covered only processes under positive minor strain. The concept of forming limit curve, as it is known today also for negative minor strain, was developed by Goodwin in 1968 [11]. The basic idea was to define a universal, easy and practical tool for the analysis and optimization in stamping processes. Goodwin compared his results with Keeler outcomes and observed that his curve achieved higher values. The reason can be found in the definition of the limits they used: Keeler considered the diffuse necking and the onset of "surface depression" as a limit. On the contrary, Goodwin took the fracture as limits and thus reached a higher value of formability. It was clear, that the definition of limit plays an important role for a universal definition of the FLC. As summarised by Col [12], the failure criterion can be selected as fracture, pronounced necking, the onset of localised necking and onset of diffuse necking. Due to the safety rules in the press shop, the later studies have considered the onset of necking as a failure, since it represents the stage before undesired crack initiation. A schematic representation of the forming limit curve according to [1] is depicted in Figure 1.

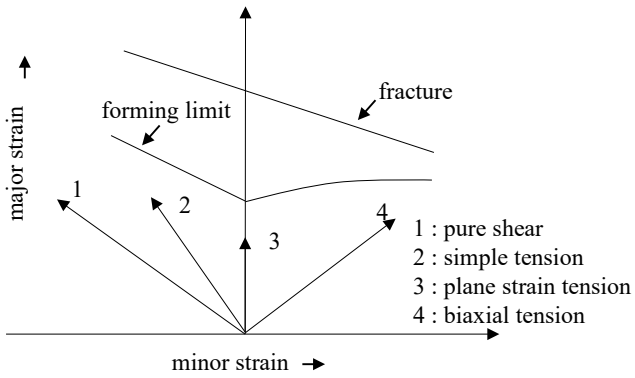


Figure 1: Schematic representation of the forming limit curves (according to [1]).

### 2.2.1 Experimental evaluation of the forming limit curve

The first approach for the evaluation of the FLC considered different tests setups, from tensile test and bulge test to direct measurements on press shop. In order to find a universal definition of the forming limit curve, Nakajima et al. [2] proposed a test setup for the analysis of diverse strain conditions by using a unique tool configuration. The so-called Nakajima test is composed of a clamping unit and a hemispherical punch. The different strain configurations are achieved with several sample geometries. The specimens are strips whose width changes according to the desired strain history. It can be varied from biaxial condition with the full geometry to uniaxial stress using small widths. They also observed that the most severe strain condition, in which the lowest point of the FLC is achieved, corresponds to the plane strain condition. Marciniak [3] proposed a machine setup similar to the Nakajima test but with the employing of a flat punch. Due to the critical contact condition between the sheet and the flat punch, the so-called Marciniak-test requires a carrier blank between the two contact surfaces. The carrier blank assures a homogeneous strain distribution. In Figure 2 the two setups are represented according to the standard DIN EN ISO 12004-2 [13]. With a view of a more symmetrical strain distribution, Hasek [14] proposed a modification of the Nakajima test samples. He reached more stability by substituting the Nakajima strips with round specimens with a central parallel shaft with a fillet radius. By changing the width of the parallel shaft, the various strain paths could be realised. In the second part of his research, Hasek [15] put in evidence the influence of the strain path history on the forming limits investigated by Müschenborn and Sonne [16].

In general, a pre-straining has an influence on the FLC that can be positive or negative. They noticed that the highest forming limit results are achieved when the second strain path has a higher strain ratio than the pre-strain path. Higher strain path ratios mean a higher compensation of the volume constancy of the strain component in the thickness $\varepsilon_3$ and thus an increase of the thickness reduction potential. A biaxial pre-straining followed by a uniaxial stress condition, for example, will reach a lower strain limit than a combination of uniaxial pre-straining and secondary biaxial straining.

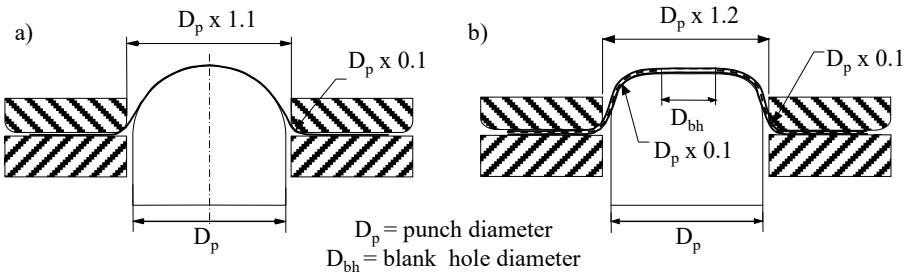


Figure 2: Schematic representation of the a) Nakajima and b) Marciniak setup (according to [13]).

The Hasek geometries are currently part of the standard method, represented by the DIN EN ISO 12004-2 [13] mentioned above. At the Institute of Manufacturing Technology of the Friedrich-Alexander-Universität Erlangen-Nürnberg (LFT), a modification of the Hasek geometries is employed [17]. An example of the LFT geometry and the difference to the Hasek geometry is depicted in Figure 3. The modification affects only the clamping area and the two geometry designs are comparable. The increase of the clamping area in the LFT-geometry allows a secure clamping, given by the clamping force, removing the need to use drawnbeads that can influence the material flows. Moreover, the clamping by force on a symmetrical clamping area assures a more homogeneous pressure distribution, avoiding undesired effects during forming.

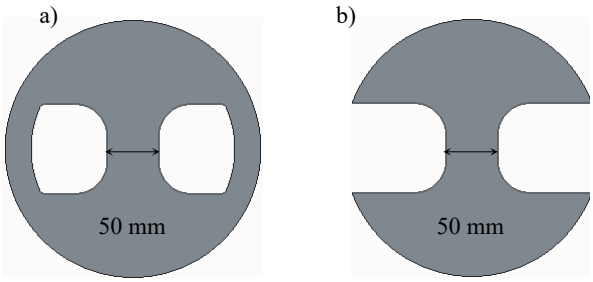


Figure 3: Comparison of the LFT a) Nakajima geometry with the b) Hasek geometry.

### 2.2.2 Measurement techniques

In their investigations, Keeler and Backofen [10] designed a circle pattern on the material surface and measured the deformation considering the final elliptical form of the pattern. This approach permitted the analysis of the total deformation. However, it was not able to consider the strain history during the process. The most important development in this way

came in the '90s with the introduction of the computer era. For the first time, pictures could be digitalised during the deformation and analysed with computer algorithms. This procedure is known as the "digital image correlation" (DIC). An outline of the basic theory, as well as experiments with those techniques, can be found in Chu [18]. The DIC-techniques are the basic principle of the optical measurement system. Thanks to a stochastic pattern on the surface, any deformation can be followed from the first picture before forming to the last step. Chu [18] demonstrated the validity of the method and its possible application in experimental mechanics. In 1989, Bruck et al. [19] proposed a correction technique based on the Newton Raphson method to improve the accuracy of the digital image correlation measurements. The development of the digital image correlation techniques in the more complex 3D coordinates followed some years later with Luo et al. [20]. In 1999, Galanulis and Hofmann [21] used the optical measurement system to achieve the forming limit curve. The typically used digital image system, ARAMIS (gom GmbH), takes pictures using two CCD cameras and collects the strain history of the specimen from the beginning to the end of the Nakajima test. The first approach considered in a classic manner only the strain distribution at cracking. In contrast to the past, the use of the optical measurement system permitted a higher resolution and considerable time saving by preparing the specimen with coloured spray instead of using etching methods. Lewinson and Lee [22] used the potential of the technique and analysed the strain development of the Nakajima and Marciniak specimen. Shortly before the crack initiates, the strain path diverged from the linear behaviour with a sudden increment. The change in the gradient occurs due to the necking (diffuse and local). Thanks to the new information achieved, the researcher continued to investigate the change of gradient as an effect of the necking initiation. In 1999, Vacher et al. [23] mapped the gradient between two consecutive frames. They considered that the necking occurs when the strains are located in a restricted area of the image and defined this strain condition as forming limit. The advanced possibility to analyse the strain distribution became an area of interest for the international deep drawing researching group (IDDRG). In particular, the German division (GDDRG) took into consideration the definition of a standardized method. Part of their research can be found in Liebertz et al. [24]. Conducting a round-robin tests procedure with several labours, they attested that the forming limit curve strongly depends on the test parameters, evaluation procedure, and measurement techniques. In [24] the author proposed a development of the Bregard method. This method, as well as its development, is discussed in section 2.2.3. The digital image

correlation system started to be more and more important in material characterisation and forming limit evaluation. In 2006 two different DIC system producers, ViALUX GmbH [25] and gom GmbH [26] presented their results for the FLC and proposed an automatic evaluation procedure. Feldmann and Schatz [25] worked with the Autogrid system (ViALUX GmbH). They used 4 cameras and a frame rate of 10 Hz. Firstly, the last picture before crack was selected. Secondly, the last 20 images before crack were analysed. Two areas in the crack zone were defined: a "running maximum", in which the crack occurs, and the "stopping environment", named the neighbouring area, in which the major strain stops to decrease due to the localization. After the definition of an upper boundary of the major strain, the first image set over this value was defined as the beginning of the local necking. The analysis of Friebe et al. [26] was conducted with the abovementioned system ARAMIS (gom GmbH). Thanks to the progress on the measurement techniques, the need for a standardization of the method became possible and the DIC-technique was considered in the revision of the DIN EN ISO 12004-2 in 2008 [13]. To date, the standard remains the same, since 2008.

### 2.2.3 Evaluation methods

In 1972 Bragard et al. [27] observed a local necking in form of multiple peaks in the strain distribution during stretching tests. They proposed to apply a parabolic regression on the strain distribution across the necking area to achieving a safe value of principal strains before crack initiation. In the same year, Kobayashi et al. [28] proposed an evaluation method based on surface roughness measurement with stylus instrument measurements. They observed that during stretching the granulation in surface texture increases immediately before necking. Many years later, in 1997, Marron [29] used the digital image correlation to analyse the strain history on the necking zone. Observing that the major strain rate in the necking zone can be interpolated with two lines before and after the necking initiation, he proposed a criterion based on the major strain ratio and its development during the test. Before necking, the strain distribution is homogeneous and increases linearly. The area of necking develops rapidly and the strains increase. Both developments are almost linear and their intercepts can be considered as the onset of instability. Vacher et al. [23] proposed a method based on the potential of the digital image correlation. They investigated the strain distribution on Marciniak tests at a different time during the forming. The evaluation of the strain velocity as the difference between two subsequent frames allows the observation of

localisation with high major strain velocity. They analysed a deep drawing steel with a frame rate of 4 pictures per second. Even with a low frame rate, it was detected that the localisation was not a sudden phenomenon and occurred with a different pattern for distinct strain paths. After the definition of the frame at necking initiation, the stain values for the FLC were evaluated as an average of the 100 higher values of the considered image. In 2001, Janssens et al. [30] conducted an investigation on the accuracy and precision of the FLC. They considered 10 repetitions for three specimen width and two setups combination, Marciniak and Nakajima.

The Bragard method was used for the determination of the FLC points and a "reference" FLC based on the average value was evaluated. The deviation from the reference was calculated. They defined a factor of uncertainty based on the standard deviation. Moreover, a global precision factor based on X-squared distribution was considered. It was observed that the uncertainty increased by strain path with higher major strain (stretching). However, only 10 repetitions were not enough for a full statistical analysis and thus the authors' contribution has to be considered as the first approach in this direction. Nevertheless, it is important to note, that the authors suggested substituting the concept of forming limit curve with the forming limit band (FLB), in which a certain safety margin should be considered. Geiger and Merklein [31] remarked the increasing quality and quantity of information about forming due to DIC-techniques.

DIC-techniques represent a huge advantage, since more data are collected and can be used for an accurate evaluation of the forming limits. However, a way to manage this vast amount of data should be found. The development of the method should consider the use of a computing device. The authors raised the image acquisition rate at 15 Hz and analysed the loading instability due to necking on the automotive steel H360LA during Nakajima tests in a cross-section on the surface. The onset of necking was defined based on the major strain gradient in the cross section during the time at a critical value. Nevertheless, the progress of the concept of forming limit curve had to take account of those two important aspects. On the one hand, it had to be precise, accurate and reliable. Thus, the modern measurement techniques, the achieving of more information and using advanced computer-aided method contribute to this side. On the other hand, the forming limit curve definition had to stay true to its original definition of easy and practical characterisation tool. Some researchers stayed faithful to the second aspect. Keeler [32] analysed a large number of HSLA steels to acquire a good number of experimental points. He found a relation between the sheet thickness, the strain hardening expo-

nent (n) and the FLC. He proposed a correction of the FLC based on thickness and hardening exponent and introduced the possibility to model the FLC for a material without experimental stretching tests but only based on the material behaviours. In [33] the concept was extended to an enhanced forming limit curve, focused on press shop application. The increase of interest in the FLC and the proliferation of evaluation methods pointed out the necessity to standardize the procedure [34]. The GDDRG presented a draft on 2004 and 2006 to put some order in the variety of testing possibilities and evaluation methods [35]. Firstly, they proposed to limit the test options to Nakajima and Marciniak setups. Moreover, a difference between laboratory and press shop should be considered. In the first case, the determination of the forming limits is done in the press shop in the same condition as that of the final part will be formed. In the second case, the characterisation of the forming limits is lab-controlled and collects the experimental points in the forming limit diagram. The FLC should be a reliable material characteristic and independent on the laboratory conditions. The standardisation proposed in 2008 [36] is currently the standard in force and is divided in the DIN EN ISO 12004-1 for the press shop [37] and the DIN EN ISO 12004-2 for the lab-testing [13]. Focusing on the second part, the setups, the lubrication conditions, the test geometries and the number of samples are defined and standardised. The evaluation method is based on the principle suggested by Bragard [27] and its application is prescribed with the distinction of three analysis modes:

*Analysis modus 1*- evaluation offline after failure

*Analysis modus 2*- evaluation offline after failure considering the starting dimension with a regular grid

*Analysis modus 3*- evaluation online before crack

In all three procedures, one or two cameras are used for image acquisition. In the offline modus images are acquired only at the end of the test. The online modus prescribes the use of digital image correlation techniques and the collection of images from the beginning to the end of forming. The advantage of the offline measurement is that no complex measurement techniques are required and the data to be processed are moderate. On the contrary, the online method processes a considerable quantity of data and gives more accurate details. The modified Bragard method is called “cross-section method” and is schematically depicted in Figure *4*.

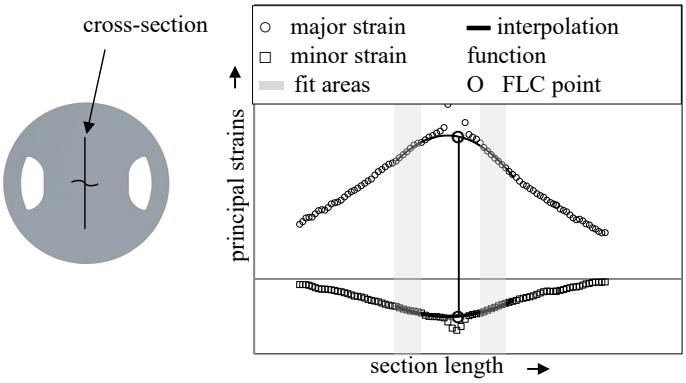


Figure 4: Basic elements of the cross-section evaluation method according to [13].

The strain values on a section perpendicular to crack initiation develop gradually from a homogeneous distribution to a localisation due to the necking. The distribution can be approximated with a "bell-shaped" distribution with a more pronounced dome the more advanced is the forming. After necking, the neighbouring area does not continue its development, while the necking zone increases rapidly. Therefore, this area still maintains the strain level achieved just before necking. By interpolating this zone with an inverse parabola, it is possible to reconstruct the level of strain in the necking zone just before necking. This assumption is in accordance with the experimental evidence for materials with a clear necking phase. For materials with high strength and abrupt crack initiation, the cross-section method shows weakness [38]. For this reason, the research focuses on the time-dependent methods that use the strain history during forming. In 2006, Volk [39] considered the possibility to determine the time at the onset of necking by analysing the strain rate. For the determination of the necking zone, the author proposed to interpret the strain distribution in discrete points like in the FEM analysis. He defined the necking area by evaluating the strain values and their developments for these points. The automatic evaluation on the necking area was presented by Volk et al. in 2011[40] and in [41] also for more complex material with transient local instabilities, like the aluminium alloy AA5182. The method is focused on the thinning rate history of the necking zone, defined as the area with the highest thinning rate. The representative maximum thinning rate is calculated as arithmetic mean value. Furthermore, the points with a thinning rate higher or equal to a certain percentage of the maximum were identified as belonged to the necking zone. The evaluation of the thinning rate is quantifiable and therefore the evaluation of the necking can be computed automatically with computer-aided algo-

rithms. As observed in [42], the results of this automated procedure allow a lower standard deviation, in comparison to the manual analysis. This method is called "line-fit method" and it is nowadays implemented as a time-dependent method in the optical measurement systems ARAMIS (gom GmbH) and Autogrid (ViaLux GmbH). A comprehensive analysis of the method and its comparison with the standard cross-section method was the object of study of the project EFB 08/212 "*Improvement of time-dependent methods for the evaluation of the forming limit curve and the derivation of a virtual simple model*", funded by the European Research Association for Sheet Metal Working [43]. The research has been focused on the analysis of the influencing parameter of the line-fit method regarding the process, the measurement and the evaluation. It has been shown that the line-fit method is suitable for conventional steels as well as lightweight materials and is less conservative as the cross-section method. However, for a reliable evaluation of the FLC, the evaluation and measurement parameters should be strictly defined. Sigvant et al. [44] proposed in 2008 a method that involved the Bragard evaluation. Instead of defining the cross-section after failure (Bragard) or a stage before crack (ISO 12004-2), they suggested taking the strain distribution at the stage of maximum punch force. After that, the maximum and the minimum strain values on a rectangle area on the surface with a dimension of 2 x 30 mm were evaluated. The instability is defined to occur when the difference between maximum and minimum exceeds six standard deviations. However, the authors remarked that in the automobile industry, and by Volvo Cars Centre, in particular, a safety margin of 40 % is usually considered. Merklein et al. [45] proposed the so-called "correlation coefficient method". The method is based on the investigation of the major strain rate. It is conducted a regression analysis on the curve with the correlation coefficient. The coefficient is near to 1 if the points used for the regression are near to a linear interpolation and 0 if the points are not comparable with a linear interpolation. Considering the points of the major strain rate, the trend is linear before necking and changes rapidly its gradient after the onset of necking. The coefficient of correlation achieves a maximum value only just before necking and the stage, in which this maximum occurs, is defined as the onset of necking. The advantage of this method, in contrast to the other time-dependent methods, is that the values after necking are not needed for the evaluation of the onset of instability. The method was improved in [17], with a correction of the initial slope and values dispersion on the major strain rate curve. The correlation-coefficient method was also implemented in the optical measurement system ARAMIS [46]. Further improved versions of the methods can

be found in the literature, such as the gliding correlation coefficient method and the gliding difference of mean median method. In both cases, the thinning rate curve is filtered to achieve a more sensitive analysis of correlation. In the first version, a general slope is added on the curve to avoid the zero values of the coefficient of correlation at the beginning. The second modification makes a difference between a gliding mean and a gliding median of the thinning rate curve.

Vysochinskiy et al. [47] proposed the so-called thickness-control method. Based on a defined area of observation (evaluation radius), the onset of local necking is defined as a rapid local thinning, exactly as observed in the above-mentioned methods. The difference consists in the fact that the limit strain is evaluated on the thickness ratio (*k),* defined as the difference between the thickness at the point of crack and the neighbouring area. The value of *k* at the limit is arbitrarily given to fit the tests values.

### 2.2.4 Analytical method for the forming limits

Alongside the numerous studies on the experimental evaluation of the FLC, a large part of the analysis is focused on the analytical approach in the last 60 years. The principal models used for the determination of the forming limit curve are summarised in [1] and schematically organized in Figure 5. The modelling can be divided into theoretical, with homogeneous and non-homogenous sheet behaviours, and semi-empirical. The semi-empirical models are based on experimental observations and they propose FLC models based on relations with the principal material parameters. However, the most investigated field is still the theoretical one. The models based on homogeneous material behaviour can be divided also into three main theories: necking, bifurcation and linearized theory of perturbations. The main models regarding the necking theory, the non-homogeneity and the semi-empirical methods are discussed more in details below.

In 1952, Hill [48] investigated discontinuities in a plastic-rigid sheet in planar deformation and uniaxial tension and can be classified as a theoretical model based on necking. He considered the localised necking as a discontinuity on strain velocity. If the material is isotropic, the yield function coincides with the plastic potential, the Bauschinger effect is neglected and considering the necking such as discontinuity defined by a relative velocity ($\vec{v}$), he stated that the direction of zero elongation is along the neck and perpendicular to the direction of $\vec{v}$. This method is presented

in [1] for the determination of the critical strain at necking. The method proposed by Marciniak and Kuczynski in 1967 is based on a material non-homogeneity under positive minor strain conditions [49].

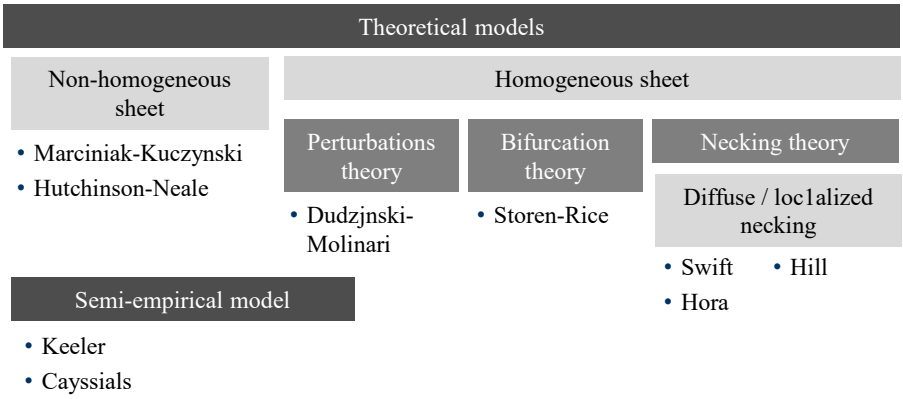


Figure 5: Overview of the principal models for the calculation of the FLC [1].

Assuming an initial inhomogeneity with the thickness $t_B$ lower than the material thickness $t_A$, the zone B with the smallest thickness is predesignated to evolve in a localisation. Considering the yield condition, the strain hardening function and the equilibrium of the force between the two zones, knowing the imperfection factor α:

$$\alpha = t_A/t_B \tag{1}$$

The equation describing the process of groove formation can be written as follows:

$$\frac{du}{u} = \left[\frac{1}{A+B\varepsilon_2} + \left(Cu - \frac{1}{D+B\int[d\varepsilon_2/\sqrt{1-u^2}}\right) * \frac{1}{\sqrt{1-u^2}} - E\right] d\varepsilon_2 \tag{2}$$

The constants A, B, C, D, and E are related to material properties like the anisotropy coefficient, the hardening exponent and the forming loading path. It is supposed that the groove orientation with respect to the principal direction is the same during the forming. That is basically the case of positive minor strain conditions, in which the crack development is perpendicular to the major direction. The method was later extended to the prediction of the whole FLC by Hutchinson-Neale [50]. Using a long-wavelength approximation, and the localisation-band bifurcation analysis, the groove can have any inclination with respect to the main stress direction. Therefore, the method is able to include also the shear necking at negative minor strains. They assumed a time-independent behaviour of the material. Moreover, they analysed the effect of the strain-rate depend-

ence on necking retardation. The dependence of the strain rate basically increases the limit strains in comparison to the independent prediction [51]. The key characteristic of the M-K and H-N method is the assumption of an initial inhomogeneity in the thickness. As observed from Hasek [52], the value of the imperfection factor influences the prediction of the FLC. Hence, it is a disadvantage that the arbitrary value of the imperfection is user-dependent. Moreover, Chan [53] pointed out that the M-K method, as well as the H-N method, are influenced by the choice of the yield function in the field of positive minor strain. Also, the plastic anisotropy plays a role. The forming limit strains increase by a low anisotropy value in the field of positive minor strain but by negative minor strain, the FLC increases with the anisotropy value. The authors suggest that by negative minor strain, high values of R increase the difficulties to achieve the critical thickness strain. Under positive minor strain, a low R-value increases the limit strain due to the less sharp curvature in the initial yield curve. Butuc et al. [54] implemented the M-K model with a series of subroutines that allow flexibility in the choice of yield functions and hardening laws. In order to solve the system of equations, the Newton-Raphson numerical method was used. Thanks to this flexible tools, a comparison between different yield functions and hardening laws were performed [55]. The analysis indicated the importance of the choice of the material model and once again its influence on the FLC determination. A similar approach was also presented by Aretz in 2007 [56]. He proposed a combination of Hill's and M-K model and extended the implementation to more complex yield function: BBC05 [57] and Yld2003 [58]. The author investigated the FLC determination for several aluminium alloys. Even if for several aluminium alloys reliable results were achieved, some weakness was noticed by the 5000 class. The material exhibits the Portervin-LeChatelier (PLC) effect and thus it might cause the promotion of instabilities in the strain distribution. A review of the developments of the M-K model and its implementation can be found in Banabic [59].

More recent is the so-called modified force maximum criterion (MMFC) proposed by Hora et al. [72]. It considers that the hardening depends not only on the material characteristics, but also on the alteration of the stress state. Moreover, it is assumed that during the strain localisation, the necking progresses on a plane strain path. In order to consider also the effect of thickness, an extension of the method in an enhanced modified maximum force criterion (eMMFC) was proposed [60]. Finally, an additional approach was suggested by El-Magd et al. [61]. The method distinguishes the fracture modus in two main mechanisms: ductile fracture and

shear band fracture. For the first modus, there is no coupling between the plasticity model and the fracture criterion. The second approach is dealing with mesoscopic levels: an increasing defect area (i.e. a void) causes a change in the flow stress. Plasticity and fracture are coupled due to a damage parameter. The model is implemented in a generalised form in the so-called Crach FEM add-on module for FEM codes [59], and the modes are extended to three: necking, ductile fracture and shear fracture. With the CRACH algorithm, an initial failure based on the M-K model is used to generate the instability.

The bifurcation theory was developed by Stören and Rice [62] with a prediction of the onset of necking under biaxial stretching with an incremental-stress approach. By using a simplified constitutive model, they derived the condition for strain localization as a consequence of instability in the constitutive description of the material deformation. Gosh [63] proposed a method in which the ductile fracture is modelled with a process of shear joining of voids. It is assumed that the void initiation happens relatively early in the forming process. Thus, the voids responsible for failure have grown before crack. Moreover, only voids generated due to larger inclusions are responsible for shear joining and the number of large inclusions is independent on the loading history. It is assumed that the voids are spherical, uniform sizing and spacing and have the same growth rate. The material is supposed to preserve its characteristics during the voids growth. Finally, it is assumed that shear joining can take place only on the surface. With these assumptions, the fracture condition can be written in relation to a critical value Kcr, the stress ratio γ and the principal stress $\sigma_1$:

$$(1+\gamma)\sigma_1^2=K_{cr} \tag{3}$$

Adding the critical stress condition, the strain limits can be achieved with the conventional Hill's plasticity theory. Arrieux [64] proposed the concept of forming limit stress diagram (FLSD). The advantage of this formulation is that the FLSD is independent on the strain path. However, this calculation assumes conditions that imply some indirect measurements. Firstly, the material is considered stiff plastic. Moreover, the component of stress in the thickness has zero value and the axes of symmetry of the specimen are also the principal directions of stress and strain. Finally, the strain path is calculated incrementally with effective strain by means of von Mises relation. The corresponding stress state is calculated using the hardening relation from the tensile test and the Prandtl-Reuss equations in the case of isotropic materials. In the case of anisotropic material and for in-axes solicitations the strain state is calculated according to the flow

relations. The authors also analysed the condition of off-axis solicitations that are later investigated in [65]. In both cases, they concluded that the forming limit stress curve is independent on the strain path. In [66], Arrieux compared his method based on the plastic calculation along the experimental strain paths and the M-K model, obtaining a good results agreement. He also extended the concept of a forming limit stress surface in three dimensions, collecting all the curves determined along every direction on the sheet surface. Even if the author proposed the forming limit stress surface as failure criteria for the FEA analysis, it has to be noted that the stress state on the specimen can only be indirectly calculated from the strains, since it is not possible to measure the stress state during the test. Moreover, complex calculations are required in comparison to the M-K model.

The semi-empirical models put together the experimental observations for different materials and defined mathematically the main tendencies with respect to the material characteristics. In Bleck et al. [67] the authors conducted a comparative analytical investigation of the FLC achieved with the Hill's [48] and Swift's [68] method and the empirical model proposed by the North America Deep Drawing Research Group (NADDRG) [69]. The empirical model was based on observations of Keeler and Brazier [32]. The NAADRG summed up the consideration of Keeler and Brazier with the following formula:

$$e_{ps}(\%) = (23.3 + 360T)(n/0.21) \quad \text{with } T \leq 0.125 \tag{4}$$

in which $e_{ps}$ is the FLC point at plane strain, T is the thickness expressed in inches, n is the hardening exponent. The comparison of the analytical and empirical models for IF steel, TRIP steel and DP steel pointed out that none of the models could be applied to all of the materials. In particular, in steel with metastable austenite, all the models have difficulties in the evaluation. Thus, the influencing parameters cannot be limited only to the thickness and the hardening exponent. Other material characteristics should be considered: the yield and the tensile strength, the strain hardening and the strain-rate sensitivity. Cayassials [70] tried to implement this dependency on an FLC model. He proposed a new criterion based on the coupling of plastic instability theory with a damaging approach. His solution based on the constitutive law, the equilibrium, the flowing plastic theory and the effect of perturbation due to internal damage effects like cavities, included the effect of strain-rate sensitivity, strain hardening and thickness.

Parallel to the analytical determination of the forming limit curve, there is the possibility to conduct the prediction with numerical analysis. Even if the FLC is usually used as input for the FE-analysis, a modelling of the Nakajima or Marciniak setups allows the investigation of the setups and the material forming limits. Based on the ABAQUS model suggested by Taylor et al. [71], Ozuturk et al. [72], conducted a numerical and experimental analysis of the evolution of the dome test. They mentioned that the model strongly depends on the mesh sensitivity and suggested that the minimum element size should be bigger than the sheet thickness. In 2005, Petek et al. [73] proposed a simulation of the Marciniak setup to evaluate the forming limit curve. The numerical simulation was performed with the ABAQUS software. The stress-strain curve was approximated by the Hollomon potential law and the yield criterion through the Hill's model. Beyond the influence of the material characterisation, the meshing strategy and the numerical parameter, also the definition of the failure criterion plays an important role. In fact, the FLC is here considered as output from the numerical analysis and thus cannot be used for the determination of the failure. The authors took the maximum force achieved as a point of onset of necking. This consideration is also in accordance with the M-K model hypothesis of a critical magnitude in thickness gradient. However, the outcomes were not comparable with the experimental data, since the necking does not necessarily coincide with the maximum force. More promising was the idea to consider the thickness strain rate in the critical zone on the top of the specimen. The first and in particular the second derivative of the thickness strain present a peak at the onset time for the necking, due to the rapid evolution of the localisation. However, the results show some discrepancies if compared to the experimental data. The authors investigated the effect of the friction coefficient and of the mesh sizes, coming to the conclusion that the choice of the numerical parameters may affect the FLC [74]. In [75] a similar model was proposed, using the software PAM-STAMP 2G (ESI). For the investigated materials, an aluminium alloy AA1205, and two stainless steels Al-SI 316L and AI-SI 304L, different model strategies were investigated. The yield locus was modelled with Hill's [76] and Barlat 1991 model [77]. Moreover, the simulation was conducted using both constant and varying normal anisotropy and hardening exponent. For the AA1050, a variable normal anisotropy improved the FLC estimation. In the case of the AISI steel, the model with variable hardening exponent achieved better results. A summary of the most used failure methods in FEM analysis can be found in Mattiason [78].

### 2.2.5 Effects influencing the forming limit curve

In the previous sections, the most significant studies on the experimental and analytical evaluation of the FLC have been shortly presented. Despite the numerous contributions for both methods, there are still discrepancies between experimental and analytical data of the FLC. The main reason for the divergences is the influence of the process and material parameters on the experimental determination of the FLC. While the analytical approach considers ideal conditions and materials, the experimental evaluation is far from being ideal. The influencing parameters are well known in the literature. It should be distinguished between the parameters that had an influence on the forming behaviour and the factors influencing the FLC evaluation itself. An overview of the forming-related factors can be found in [5] and are schematically listed in Table 1 together with the FLC-related parameters.

Table 1: Most important influencing parameters on the FLC.

| **process parameters and testing conditions** | **material influencing factors** |
|---|---|
| tool geometry [5, 79–83] | material thickness [84–88] |
| tribological system [89, 90] | surface quality [91–94] |
| strain condition and strain rate [16, 81, 95–97] | material structure [98–100] |
| temperature [90] | |
| **evaluation parameters [43]*** | |
| evaluation method | |
| measurement mesh grid | |
| frame rate | |

*purely FLC-related parameters

### 2.2.6 Effect of the process parameters on the forming limit curve

In this section, the most relevant contributions to the influencing parameter investigation concerning the determination of the FLC are discussed. In order to focus on the parameters related to the present study, the attention is focused on the influence of the punch tool. The other effects,

such as temperature and evaluation and measurement methods are not discussed here.

The tribological system plays an important role in forming operations. A dry or poor lubricated contact during stretching causes the sticking of the material to the punch destabilising the material flow [89]. As mentioned above, the FLC is defined only for linear strain paths. Such a condition is fulfilled only at the centre of the specimen for the Nakajima setup and away from the punch radius for the Marciniak punch. Hence, the DIN EN ISO 12004-2 describes a tribological system for the Nakajima and the Marciniak configuration that should avoid any type of friction between punch and sheet. Moreover, the validity of a test is limited only to the specimens with a crack initiation at the centre of the specimen or at least no more than 15 mm to the centre.

In 1975, Charpentier [79] analysed the influence of the punch curvature on the FLC. A lower punch curvature increases the strain gradient due to the bending. The presence of a strain gradient modifies the instability condition and retards the formation of local necking. They also came to the very interesting conclusion that the effect of thickness has a stronger influence than curvature. They also warned that the forming limit curve is not an intrinsic material characteristic since the FLC is strongly influenced by the thickness and the punch radius. Marciniak [80] discussed the influence of the tool on the material flow during forming. Tool pressure and tool friction can be stabilizing or destabilizing factors according to the considered forming process. They are, basically, stabilizing factors in the Nakajima test. The contact pressure between punch and sheet initially causes a reduction of the tensile flow stress and facilities the material flow. After necking, the pressure is not uniform due to the thickness reduction and thus the strength of the neck increases in relation to the rest of the contact area, which is still subjected to the contact pressure. The friction can be maintained relatively low on the hemispherical punch, while it represents a destabilizing factor for the Marciniak punch.

The FLC is also dependent on geometrical parameters related to the punch. In [81], Merklein analysed the influence of punch diameter and punch velocity for an interferritic steel IF260 and for the precipitation-hardening aluminium alloy AA6016. While decreasing the punch velocity, the standard deviation of the optical measurement is reduced. In general, the punch velocity seems to not play an important role for these materials if changed in normal ranges. On the contrary, the punch diameter has an influence on the FLC with the tendency of higher FLC by smaller punches.

Moreover, the investigation focused also on the facet size for the optical measurement system. It was pointed out that the size should be considered enough small in order to detect the crack initiation. The geometrical aspects clarified the discrepancies between evaluations on the same materials by different laboratories with different setups [24]. Jocham et al. [101] suggested for the deep drawing steel DC06 also the characterisation of the strain rate sensitivity. Their outcomes for tensile tests and bulge tests indicated a dependency of the rate sensitivity on the material hardening. It is a plausible conclusion since the characterisation tests like tensile and bulge test are in general conducted in quasi-static velocity. The Nakajima tests, on the contrary, were designed with the intent to characterise press-shop conditions, where typical forming velocity are dynamic. The effect of the punch geometry was investigated by Leppin et al. [84]. The comparison of the FLC resulted from Marciniak-tests and Nakajima tests for two 6xxx aluminium alloys put in evidence the deviation of the strain paths achieved with Nakajima test from the ideal linearity with an initial biaxial pre-straining. The authors proposed a correction method based on the observation of Müschenborn and Sonne for linear-combined stain paths [16], that the sum of the equivalent strains reaches a maximum according to the final loading orientation. Considering the Mises equivalent plastic strain at FLC as the maximum and the biaxial pre-straining as the first linear path and the subsequent strain evolution as a second linear path, the corrected value for a Nakajima FLC point can be calculated from the strain path ratio and the Mises equivalent strain. The results after correction show a partial decrease of the Nakajima FLC from the Marciniak-FLC. Similarly, Abspoel et al. [102] investigated the biaxial pre-straining for deep drawing steel DX54D and a multiphase steel HCT780X. Considering a biaxial pre-strain constant for all geometries, they found a linear relationship between the biaxial pre-straining in the FLC and the elongation from the tensile test. In both investigations, the biaxial pre-straining is qualitatively evaluated at plane strain, where the deviation in the minor strain direction can be ideally attributed only to the biaxial pre-straining. Volk and Suh introduced the idea of a general forming limit concept (GFLC) based on a phenomenological approach [103]. The GFLC is valid for bi-linear deformation histories and is based on the concept of the principle of equivalent pre-forming. The total strain path is approximated with a bi-linear strain path and the total strain path length is considered the limit of formability. Based on a meta-model of the strain path length ratio, the total strain path length can be mathematically defined. The bi-linear model was also used for the correction of the non-linearity in the strain path by the Nakajima tests [82]. Min et al. [83] divided the effect of

the punch in three aspects: the punch curvature, the punch pressure and the non-proportional strain path. To overcome the strain path discrepancies due to bending and the contact pressure effects, they defined the limits in terms of stress by considering the forming limit stress curve. An application is presented in [104]. Obviously, for the calculation of the stresses in relation to the measured strains, a constitutive model is needed since only the strains can be directly measured in the experiments. As observed by Xavier et al. for interstitial free steel [94], the concept of the limit stress diagram is useful only in the case of proportional strain paths. Analysing the locus of the plane strain fracture, they concluded that it is dependent on the strain path. Thus, for the determination of the stresses is necessary to calculate the principal stresses in relation to the deformation path, assuming the relationship is known. Non-proportional strain paths and their relation with the stresses may be complex.

### 2.2.7 Effect of material on the forming limit curve

In this section, the most important investigations of the influencing parameter concerning the material for the determination of the FLC are discussed. The focus is on the influence of the materials structures and surfaces. Another important aspect is the influence of the material thickness. Its evaluation can be complex and an evidence of that the opposing outcomes in the literature. For example, by analysing aluminium alloys, Smith [87] discovered that the thickness plays a less important role for the aluminium alloys than for steels with the same hardening behaviour. This is in contrast with the results of Dilmec et al. [88]. It can be explained by the observation, that the manufacturing processes may be diversified for sheet materials with different thickness. The experimental analysis of a steel or aluminium alloys with various thickness show discrepancies that cannot be directly attributed only to the thickness difference, since the material structure can be completely different.

It is well-known from the literature that the main material characteristics such as anisotropy, hardening, strain-rate sensitivity and strength profoundly influence the FLC values [5]. Instead, the analysis of the effect of the material structures is less investigated. On the one hand, the investigation of the material structure during stretching is limited and only possible under some compromises. On the other hand, this complex analysis does not match with the intended purpose of the FLC to be simple and easy to use. Nevertheless, the knowledge of how the structure changes during stretching can be helpful in the investigation of the forming limits

and can support a more precise definition of the FLC. Hiroi and Nishimura [91] found a correlation between FLC and surface defect dimension. They analysed soft and hard aluminium alloys and introduced an artificial machined notch on the surface. They observed that a critical depth of surface defects can be defined considering the material characteristics. In fact, the FLC does not decrease for defects depths of up to 2% of the thickness of the soft sheet and 0.5% for the hard one. For deeper defects, the limit strains decrease. Becker [92] performed numerical simulations of the surface roughening development in sheet forming for low carbon steel. Even if the model did not take into account the grain interactions in the thickness, the precipitates and the grain shape, the conclusions appeared realistic. The outcomes pointed out a relationship between surface roughening and strain localisation that seems to cause the roughening observed on the surface. Al-Qureshi et al. [105] came to the same conclusion with a different approach. With the analytical representation of the surface asperities with a sinusoidal non-linear model and with the assumption that the surface roughness increases proportionally with the grain size, the thickness evolution during forming can be related to the sinusoidal function. The principal strains are then calculated according to a theoretical model proposed by the authors in 1981 [93]. Further analysis conducted on interstitial free steel [94] indicated that the surface roughness increases with the level of plastic deformation and reaches a maximum on the necking region. The changes in texture seem to not have an influence on the roughness since they happen generally only at the late phase of deformation.

Tasan et al. [98] investigated the microstructure evolution of interstitial-free steel and dual-phase steel. While the IF steel is a single phase material with low carbon content, in the DP steel the ferritic and martensitic phase is recognizable. With the two profoundly diverse material structures, it is possible to distinguish the effects of forming accordingly to their characteristics. The SEM analysis of the different level of deformation in Nakajima tests reveals some interesting aspects. In the IF steel, the ferritic grains show an elongation after forming. A nucleation of micro-voids is also visible due to the inclusions on the ferritic matrix. In the DP steel, the hard martensitic component limits the forming of the softer ferritic phase. The damage mechanisms occur therefore due to decohesion and martensitic fracture. The accumulation of damage is also different for the various strain paths and tends to be higher by positive minor strains. The authors concluded that it should be distinguished between materials with homogenous microstructure (IF steel) and materials

with phases with different characteristics (DP steel). For the first material, damage does not contribute to localisation but plays a role only beyond. For strain paths with negative minor strain, the thinning is compensated and thus the material is more damage resistant. For the latter material, damage plays already a role in localisation and occurs due to the structure inhomogeneity. Thus, the material reaches low forming limits and fails without significant further thinning. In a study conducted in 2012, Tasan et al. [99] tried to bypass the necessity of performing several forming levels and designed a miniaturised Marciniak setup for the direct analysis in a Scanning Electron Microscope (SEM). With a punch diameter of 20 mm and with the help of a microscopic digital correlation measurement setup (μ-DIC), they analysed the damage mechanisms during forming and the microstructure evolution. They demonstrated that there are several damage mechanisms in dependence on material structure. The outcomes proved that the DP steel shows martensite-ferrite decohesion while the aluminium alloys fail with damage due to inclusions. In [100], the authors carried the in-situ analysis together with a crystal plasticity simulation (CP) of two DP steel grades. The study indicated those larger ferritic grains plasticises earlier than smaller ones. Moreover, a good dispersion of martensite contributes to hardening. Therefore, a grain refinement with martensitic dispersion improves the mechanical behaviour in DP steels. Similar results for an in-situ analysis of micro-tensile tests for a DP1000 can be found in the research of Ghadbeigi et al. [106]. Clearly, the understanding of the micro-mechanisms is crucial to explain the global material behaviour and failure mechanisms. However, this type of analysis has some challenge that has to be considered. Firstly, the setup design is limited by the small chamber volume of the SEM and the achievable force is limited. Secondly, even if the Marciniak test is more suitable for miniaturising than other setups thanks to the contact-free surface in the zone of forming, the dimensions of the hole on the washer and of the punch diameter have a strong influence on the stress ratio and on the requested force. Even if the in situ analysis shows potential for achieving new information on the material mechanisms during forming, the limitation in design and force as well as the possible effect of miniaturising limit the investigation in terms of strain paths, material thickness and material types. Thirdly, miniaturised tests are not directly comparable with the standard one. Above all, a qualification of setups deviating from the standard ones is necessary for the results reliability. As mentioned above, changes in the setups and geometry can affect the evaluation. Exemplarily, the scaling of tensile tests presents some challenges in the manufacturing and in the qualification of the evaluation. A comprehensive investiga-

tion of the effect of scaling tensile tests was the object of study in the EFB project 11/212 “Optimisation and standardisation of the tensile test with miniaturised samples for an improved characterisation of thin sheet components' local properties” funded by the European research association for sheet metal working [107]. The outcomes for different sheet materials had shown the discrepancies of results between standard and micro setup.

## 2.3 Summarizing evaluation of the state of the art and research

Sheet metal forming processes are part of the human history since the antiquity and nowadays influence many aspects of our daily lives, from food packaging to cars, and plane construction. The metal in form of sheets is easy to shape and flexible and that thanks to its forming capability. The formability is the capacity of sheet metals to undergo plastic deformation without fracture. With the progress of the sheet metal manufacturing the demand of complex structure is also increasing and thus the employ of the full potential of formability is mandatory. The most widely used tool for the determination of forming limits in sheet metal forming is the forming limit curve. The experimental procedure for its determination is standardised by the DIN EN ISO 12004-2 [13]. It considers the use of a Nakajima or a Marciniak setup. The setups differ basically due to the punch form. The Nakajima punch with the hemispherical form causes side effect such as additional bending stress. The Marciniak punch is flat and provides to a homogenous strain distribution during forming. However, the sever contact conditions limit its use in term of materials and thicknesses. Hence, even if both setups are equally qualified for the determination of the FLC, the results show discrepancies. The evaluation method contributes also to the deviation of the FLC. The standard is represented by the cross-section method and requires the interpolation with a second-order function of the strain distribution before necking on a section perpendicular to the crack initiation. The method showed weaknesses if applied to materials without a clear necking transition. Therefore, in the last 20 years, several evaluation time-based methods have been proposed. Thanks to the introduction of the digital image correlation techniques it is nowadays possible to investigate the strain history and use it for a more precise determination of the FLC. Alongside the experimental determination of the FLC, several analytical methods are suggested in the literature. The analytical methods are based on theoretical models and have to be combined with material modelling. The analytical models should be complex enough to consider the real behaviour of the

material depending on its material characteristics, structures, thickness and composition. The analytical determination of the FLC requires, therefore, a precise material characterisation, a time-intensive analysis, validation of the results and costs that, combined with the less transferability of the methodologies, make a replacement of the experimental determination impossible. Moreover, the analytical procedures are based on ideal stress conditions that do not take into account the experimental conditions. The effects influencing the FLC can be divided into process- and material-dependent. The punch shape and dimension, as well as the friction conditions, contribute to the process-dependent effects. It is well-known that the hemispherical Nakajima punch causes a bending contribution on the strain distribution. Moreover, it was observed, that a biaxial pre-straining occurs on the specimen surface before the final strain path is reached. Several correction methods of those effects can be found in the literature. However, a comprehensive investigation and quantification of the two effects, the analysis of their mechanisms and its dependence on the material characteristics are missed. Some interesting contributions can be found in the material structure development during forming. Tasan et al. proposed a miniaturisation of the Marciniak setup for a metallographic in-situ analysis. Nevertheless, scaled setups should be qualified for a comparison of the results and their validation. Moreover, a methodology for the quantification and qualification of the changes in the material structure and surface during Nakajima tests should be examined. Summarising, a more precise evaluation of the FLC should pass through a better understanding of the test process of the Nakajima test, focusing on the effects of the setup parameters on the necking development. Finally, the phenomenon of necking should be investigated according to the material characteristics. The evaluation should be interpreted with a better definition of necking and forming limits.

# 3 Objective and methodologies

The goal of the present work is the investigation of the failure and necking behaviour of sheet metals during Nakajima tests. The main focus is given to the characterisation of the failure mechanism of the materials, to the effect of the punch geometry in terms of bending and to the biaxial-stretching effect. On the one hand, the analysis of failures during Nakajima test will provide an advanced understanding of the material peculiarities regarding the onset of instability under different strain path conditions. The general definition of instability as the onset of necking is explored for the diverse investigated materials and reformulated, considering the different mechanisms. On the other hand, the effect of bending and biaxial pre-stretching is experimentally and numerically analysed, in order to quantify and qualify the effects on the forming limits prediction. The final goal is to find the answers to the following questions:

- Is the FLC definition still valid also for less ductile materials? And how the knowledge on the material behaviours can be used for the estimation of the forming limits?
- What are the limits of validity of the FLC using Nakajima tests considering the undesired effects of bending and biaxial stretching?

The methodology applied for this investigation is depicted in Figure 6. In order to investigate the relationship between material structure and the forming limit curve, materials from different classes are investigated. The evolution of the material failure mechanisms is analysed as a function of the time and as a function of the space, considering the spatial differences on the surface and across the thickness of the specimens. Various stretching levels and the development of several strain paths are considered. By collecting information regarding the change in the material structure, this work explains the failure development through experimental observations and quantitative results, introducing new definitions.

The effect of bending due to the geometry of the Nakajima punch is experimentally and numerically analysed. The bending effect occurs due to the combination of the punch curvature and the material thickness. Up- and down-scaled setups will be used to analyse the effect of the punch curvature on the FLC. The experimental setups have been purposely designed to facilitate the comparison of the outcomes and determine the effects of the punch curvature and of the material characteristics on the

FLC. The analysis of the thickness is conducted also numerically. The results of the numerical simulations are used to determine the validity range for material thickness.

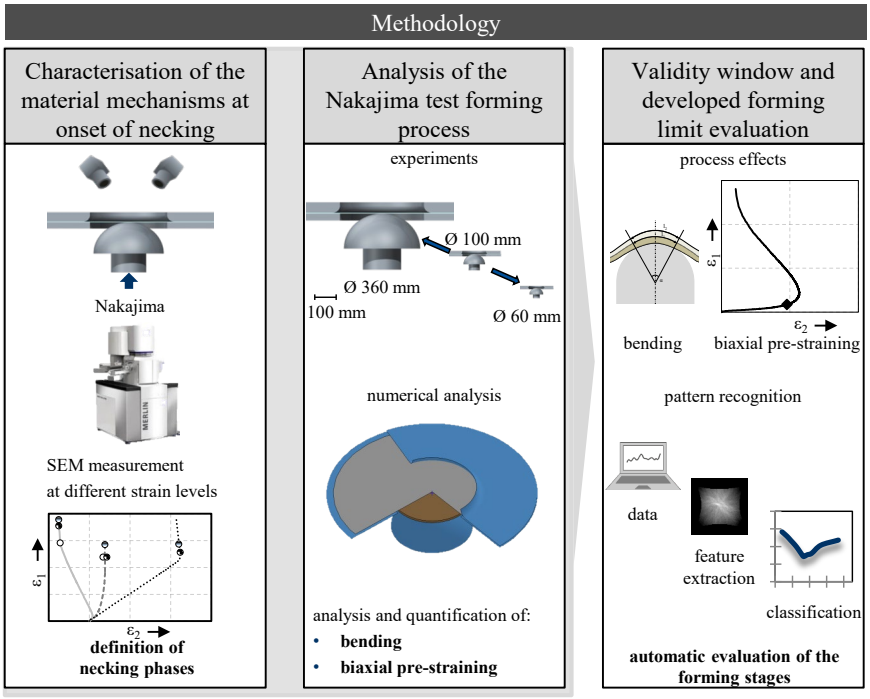


Figure 6: Methodology and investigation milestones of the present work.

The biaxial pre-stretching major effect on the FLC is the shifting of the curve to the right. It is investigated how the thickness and the punch geometry influence this phenomenon. This effect is numerically and experimentally investigated and the effect on the evaluation of the FLC for the different material is evaluated and discussed.

Finally, the practical application of the gained knowledge is discussed. In particular, the material-dependent definition of the onset of instability during Nakajima test is used for an automatic recognition of the surface patterns. This methodology is presented as a valid development for the standard method and its adaptability on the different material peculiarities is presented. The margins of the validity of the standard Nakajima setup are discussed and guidelines for the choice of the setups and procedure for the evaluation of the FLC are given.

# 4 Materials, test equipment and methodology

In this section, the investigated materials, as well as the test equipment, are presented. The methodology used for the metallographic investigation is given in section 4.3. Finally, the fundamentals for the numerical analysis are presented in section 4.4

## 4.1 Materials

In the present study, three sheet metals used in the automotive industries are considered. The choice of the sample materials is guided by the fact that those materials are greatly used in applications, where severe forming conditions are needed. In order to cover a wide range of material structures, the investigated materials are from three material classes with different characteristics. In particular, the analysis is focused on a ductile sheet metal DX54D, a high strength steel DP800 and the aluminium alloy AA5182.

The DX54D steel is conventional deep-drawing steel. It is commonly used in car-body structures for exterior and interior parts. Its composition, according to the DIN EN 10346 [108] is summarised in Table 2. In the present study, a DX54D steel specimen with a thickness of 0.75 mm is investigated. The DX54D steel has a good ductility, with yield strength between 164 and 170 MPa and a uniform elongation up to 23%. The high anisotropy coefficient reveals a tendency of the material to flow more in width direction than in thickness direction.

Table 2: Chemical composition of DX54D steel, according to DIN EN 10346 [108] (max. values).

| Name | C | Si | Mn | P | S | Ti |
|---|---|---|---|---|---|---|
| DX54D | 0.12 | 0.50 | 0.60 | 0.10 | 0.45 | 0.30 |

The dual-phase steel DP800 is a high strength steel; it is used in particular for crash structure component in the automotive industry such as A-pillars. The microstructure is composed of a soft ferrite matrix and martensitic islands at the grain boundaries. The ferrite assures a good formability, while the martensite is responsible for the high strength and harness. The chemical composition according to DIN EN 10346 [108] is listed in Table 3.

Table 3: Chemical composition of DP800 steel, according to DIN EN 10346 [108] (max. values).

| Name | C | Si | Mn | P | S | Al-gesamt | Cr+Mo | Nb+Ti | B |
|---|---|---|---|---|---|---|---|---|---|
| HCT 780X | 0.18 | 0.80 | 2.50 | 0.080 | 0.015 | 2.00 | 1.40 | 0.15 | 0.005 |

The AA5182 aluminium alloy belongs to the 5xxx series of Al-Mg aluminium alloy. It has a good strength/weight ratio and is often employed in car body parts, where a good strength is required. The relatively high presence of magnesium (see *Table 4*) reduces the flow properties by increasing the strengthening. A disadvantage of the AA5182 aluminium alloy is the occurrence of unsteady flow behaviour well-known as PLC effect (Portevin-Le Chatelier effect). The PLC effect causes a visible flow pattern on the surface in form of bands. The exact cause of the behaviour is still under discussion, but it is based on the interaction between free atoms and dislocations and, consequently, the increase of dynamic stress-strain rate dependence [109].

Table 4: Chemical composition of AA2182 according to DIN EN 573-3 [110] (max. values).

| Name | Si | Fe | Cu | Mn | Mg | Cr | Zn | Ti |
|---|---|---|---|---|---|---|---|---|
| EN AW-5182 | 0.20 | 0.35 | 0.15 | 0.20-0.50 | 4.0-5.0 | 0.10 | 0.25 | 0.10 |

The three selected materials offer the possibility to research a wide range of material characteristics, thanks to their dissimilar material parameters. A summary of the most significant characteristics is given in Table 5.

Table 5: Material characteristics of the investigated sheet metals.

| Material | $t_0$ [mm] | n | YS [MPa] | TS [MPa] | UE [%] | $r_0$ | $r_{90}$ | $\bar{R}$ |
|---|---|---|---|---|---|---|---|---|
| DX54D | 0.75 | 0.23 | 164-170 | 297-322 | 22-23 | 1.80 | 2.22 | 1.78 |
| DP800 | 1.0 | 0.16 | 460-470 | 775-797 | 14-16 | 0.76 | 0.90 | 0.895 |
| AA5182 | 1.0 | 0.32 | 130-132 | 265-275 | 20-21 | 0.72 | 0.66 | 0.67 |

## 4.2 Test equipment and testing method

For the experimental analysis, Nakajima, as well as Marciniak tests, are conducted for the different investigated materials. The used setup belongs to the Institute of Manufacturing Technology (LFT) at the Friedrich-Alexander University. The setup consists of a blank holder and a die with an outer diameter of 245 mm, an inner diameter of 110 mm and a round fillet radius of 10 mm. The die movement is regulated by hydraulic cylinders and can achieve a clamping force, which has its maximum at 720 kN. The clamping is assured by force and no draw-beads are used. The clamping force does not allow any material flow in the clamping zone. The hydraulic power unit also regulates the punch movement. The setup consents flexibility by the changeable punch. The Nakajima punch, as well as the Marciniak punch, is used. They are designed according to the DIN EN ISO 12004-2 and have a diameter of 100 mm. The maximum achievable punch force is around 500 kN. A picture of the used setup is depicted in Figure 7.

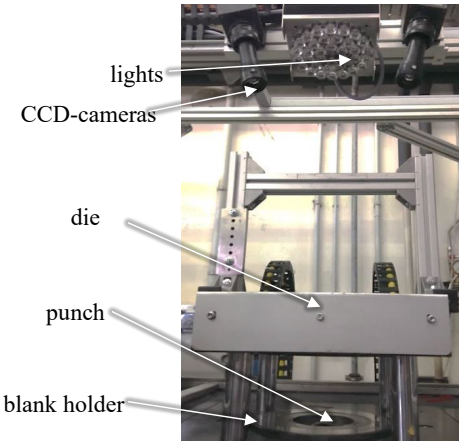


Figure 7: Stretching the test setup at the Institute of Manufacturing Technology.

The friction between punch and specimen is reduced with a sandwich-type lubrication system according to the standard procedure. Teflon foils, a PVC pad with a thickness of 3 mm and grease are the components of the tribological system. In the Marciniak test, the critical contact conditions may not be completely compensated by the lubrication system. Therefore, it is not assured the crack initiation takes place in the specimen centre. For such reason, blank carriers with ductility greater or equal to the tested material are additionally used. The investigation of the influence of the punch diameter is conducted with scaled setups. For up-scaling, the hydraulic press TZP400 from Lasco Umformtechnik GmbH is used (see Fig-

ure 8 a). The maximal press force is 4000 kN and the ram stroke is 800 mm. Die, blank holder and punch are the property of BMW. The tools dimensions are scaled according to the setup at LFT and the punch diameter.

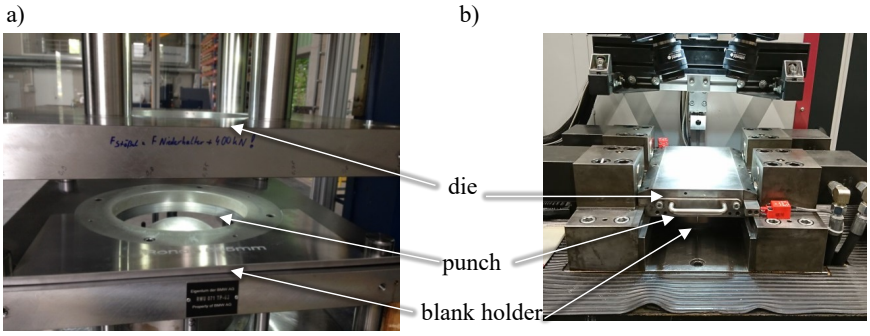


Figure 8: Scaled Nakajima setups with a) 360 mm diameter punch; b) 60 mm diameter punch.

Therefore, for the scaled punch with a diameter of 360 mm, the die inner diameter is 396 mm. The down-scaled setup is mounted on another LFT-developed machine (see Figure 8 b). Once again, the tool sizes are scaled down according to the punch diameter. Therefore, for the punch diameter is equal to 60 mm and the inner diameter of the die is 66 mm. An overview of the principal dimensions of the reference setup and of the two scaled systems is depicted in Figure 9.

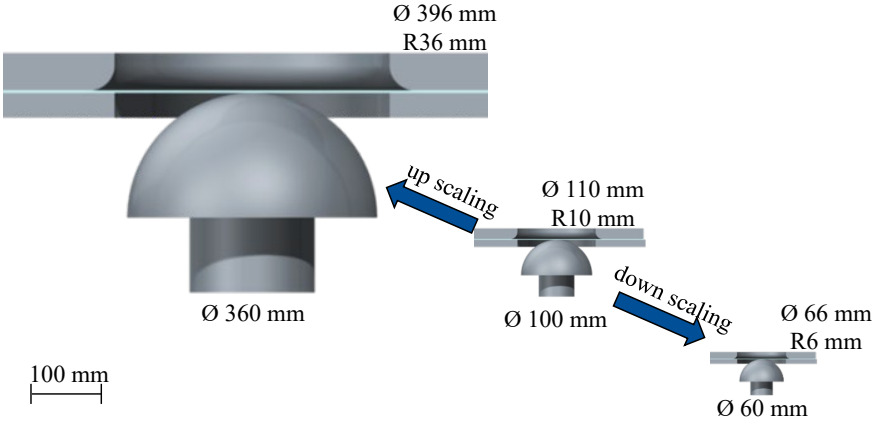


Figure 9: Schematic representation of the Nakajima scaled setups.

For a reliable comparison, the test specimens' widths are also proportionally scaled according to the punch diameter. An exception is represented

by the full geometry under biaxial stretching. The full geometry has no cuts and the scaling of the forming zone is assured by the scaling of the setups itself, specifically the punch diameter and the die inner diameter. The outer diameter of the full geometry specimen is defined by the outer tool diameter and does not affect the forming zone. However, for convenience, the names of those specimens refer to the outer diameter. The investigated geometries cover the strain paths from the biaxial test (full geometry), to near plane strain and uniaxial tension condition. A review of the samples for each setup is given in Table 6. An example of the investigated geometries is given in Figure 10.

Table 6: List of tested Nakajima/ Marciniak geometries.

| **Strain condition** | **Nakajima/ Marciniak D = 100 mm** | | **Nakajima D = 60 mm** | | **Nakajima D = 360 mm** | |
|---|---|---|---|---|---|---|
| | **Name** | **Width [mm]** | **Name** | **Width [mm]** | **Name** | **Width [mm]** |
| Biaxial strain | S245 | full geometry | S156 | full geometry | S595 | full geometry |
| Near plane strain | S125 | 125 | S075 | 75 | S450 | 450 |
| Near plane strain | S110 | 110 | S066 | 66 | S396 | 396 |
| Near uniaxial condition | S050 | 50 | S030 | 30 | S180 | 180 |

For the comparison of the strain paths with pure linear tests, tensile and plane strain tests are additionally performed. The experiments are conducted with the universal test machine Z100 form Zwick AG. The strain distributions during Nakajima tests are achieved using an optical measurement system. The DIC technique discussed in section 2.2.2 is based on the evaluation of displacements following surface patterns and correlating the different collected images during the time. The specimen surface is prepared with white varnish in order to avoid light reflexion. Afterwards, a speckle graphite distribution is applied. The stochastic points are followed in each picture and their displacement is used for determining the strain distributions. All three mentioned above setups are furnished with an optical measurement system ARA-MIS (gom GmbH). Due to the differences in the measured area from the up-scaled to the down-scaled setup, the requirements of image resolution and measuring volume are dif-

ferent. The reference setup with a punch diameter of 100 mm is equipped with the high-speed system ARAMIS HS.

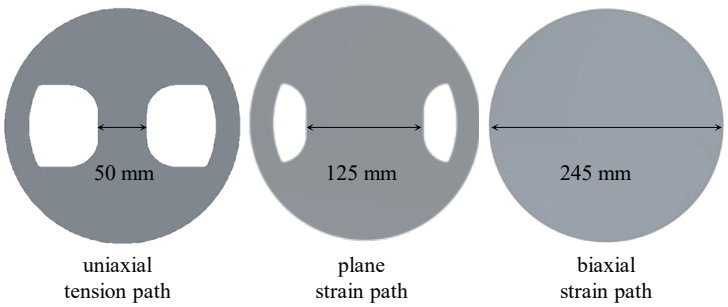


Figure 10: Schematic representation of the investigated geometries.

The cameras are A504k from Balser with a maximal frame resolution of 500 fps and a resolution of 1280x1024 pixels. The camera lens is 135 mm and allows a nominal measuring volume of 75x55 mm. For the setups on the hydraulic press with a punch diameter of 360 mm, an ARAMIS 4M system (with a resolution of 1280x1024) in combination with Dalsa Falcon cameras is used. The used camera lenses are 20 mm. The nominal measuring volume is 300x220 mm. Finally, the down-scaled setup is equipped with an ARAMIS 5M-system with Baumer TXG50 cameras and 50 mm lens. The nominal measuring volume is 65x55 mm.

## 4.3 Metallographic analysis

For the metallographic analysis, several measurement systems are used. The reflected-light microscope Aristomet (Leica Camera AG) has a zoom range between 25 and 1000x magnification. Due to the large view field, it is used for the microstructure image acquisition. The used camera is the DP35 (Olympus Europa SE & Co. KG) with a resolution of 5 megapixels. For the image recording and editing, the Stream Essentials 1.4 software is used. The maximal resolution is 2560x1920 pixels. The Datinf Measure 2.2 software (DatInf GmbH) is used for the measurement of thickness in formed specimens. It enables length determination in digital images and vector-based measurements. For the 3D measurement of the specimens' surface and the analysis of the microstructure, the scanning electron microscope MERLIN (Zeiss AG) is employed with the electron optics GEMINI II. The surface topography is evaluated through the detection of the secondary electrons, which are electrons repelled from the test surface and have energy lower than 50 eV. Pictures are finally recorded

with the Smart SEM 5.07 software (Zeiss). The editing of 3D surface analysis data is performed through the MeX 6.1 software (Alicona Imaging GmbH). The editing consists of overlaying two stereo pictures with a tilt angle. Moreover, the specimen curvature is corrected, in order to analyse the surface asperities.

The quantification of pores, gaps and other patterns in the material thickness is conducted with the open source image processing software ImageJ 1.51j8. It allows the possibility of recognizing and quantifying colours levels. The analysed surface area is defined as 30x30 mm on the top of the specimen. According to the ISO 12004-2, a test is valid if the crack initiation occurs not further than 15 mm from the specimen centre. The evaluation area assures that the instabilities are captured, as it can be observed in Figure 11-a.

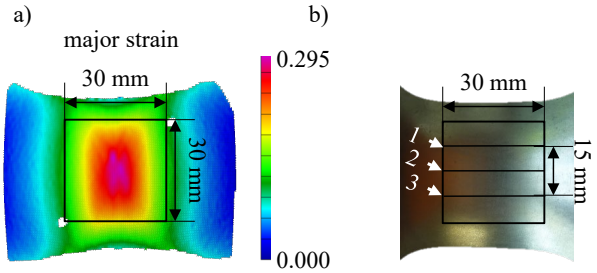


Figure 11: a) Area of the metallographic investigation and b) definition of the section for the analysis of the thickness.

The analysis of the thickness is conducted considering three cut section on the area 30x30 mm, as it is shown in Figure 11-b. Moreover, the sections follow the standard procedure and are oriented perpendicular to the crack or to the instabilities development. The investigation of the thickness and material microstructure needs the embedding and etching tests.

The preparation parameters are chosen considering the material peculiarities. In particular, the etching is crucial for a good evaluation of the microstructure. For the DP800 steel the nital is used. Nital is a solution of nitric acid and alcohol and is a typical etching component for ferritic steels. The AA5182 aluminium alloy is etched with an electrolytic Baker procedure. An overview of the principal test preparation parameters for the metallographic analysis is presented in Table 7.

Table 7: Test preparation parameters for the metallographic analysis.

| Material | Embedding | Sanding | Polishing | Etching |
|---|---|---|---|---|
| DX54D | Epoxy 1000: Room temperature, hardening time: 8 hours | Avg. pressure 20 N, 1 minute | Avg. pressure 20 N, 3 minutes | 3% HNO3 + C2H5OH Etching time: 15 s |
| DP800 | WEM epoxy: Heating 7min (150°C), 250 bar, cooling time: 4 min | Avg. pressure 20 N, 3 minutes | Avg. pressure 20 N, 3 minutes | 3% HNO3 + C2H5OH Etching time: 7 s |
| AA5182 | Epoxy 1000: Room temperature, hardening time: 8 hours | Avg. pressure 20 N, 3 minutes | Avg. pressure 20 N, 3 minutes | 5 ml HBF4 + 100 ml H20 Etching time: 60 s (at 25 V) |

## 4.4 Simulation software and numerical models

The numerical analyses in the present study are conducted with the commercial finite element analysis-software LS-DYNA (Livemore Software Technology Corporation). Whereas the LS-PrePost 4.3 software is used for the pre-processing as well as the post-processing phases, the used solver is the version R9.1. The software offers flexibility with several material models, contact condition and element types. The numerical model of the Nakajima test is defined in the pre-processing phase and built with modules (keywords), from the geometry definition to the boundary conditions. For a correct evaluation of the triaxiality condition in the Nakajima test, the sheet metal is meshed with solid elements. The tools, namely die, blank holder and punch are modelled with shell rigid elements. Finally, the tribological system is represented by solid elements with linear plasticity. An example of the FEM for the configuration with 100 mm is depicted in Figure 12. The material modelling is a crucial element for a correct numerical simulation.

Besides the E-modulus for the elasticity, the Poisson ratio and the material density, the yield, as well as the flow behaviour, should be correctly implemented. Since in the present study different stress conditions (from biaxial stress to uniaxial tension) are investigated, it is needed a yield model that can fit the material behaviour in the field of the forming limit curve.

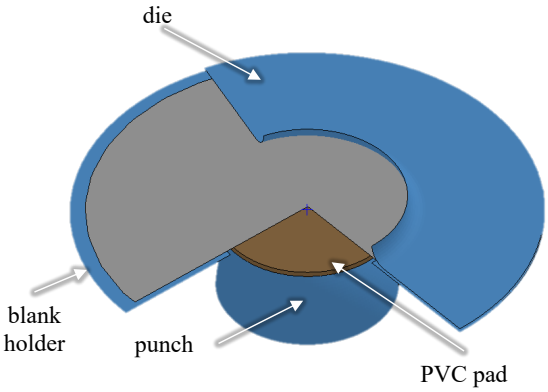


Figure 12: FEM model of the Nakajima setup in LS-DYNA.

The anisotropic model according to Yld91 [77] is used, defining six variables. The six variables can be reduced to four in the case of three-dimensional plane stresses. Therefore, the out-of-plane components f and g can be set to 1. For the fitting, the anisotropy coefficient and the yielding by tensile tests in the 0°, 90° and 45° to rolling direction are used in the superimposed condition. Table 8 reports the yield parameter for the investigated materials

Table 8: Yld91 model parameter values for the investigated materials.

| | Parameter Yld91 | | | | | | |
|---|---|---|---|---|---|---|---|
| **Material** | **m** | **a** | **b** | **c** | **f** | **g** | **h** |
| DX54D | 6 | 0.844900 | 0.891269 | 1.147185 | 1 | 1 | 0.977868 |
| DP800 | 6 | 1.000551 | 1.061809 | 1.960477 | 1 | 1 | 1.019377 |
| AA5182 | 8 | 1.085120 | 1.053358 | 0.958584 | 1 | 1 | 0.986443 |

For the extrapolation of the flow behaviour, two different models are used for steel and aluminium alloy respectively. While the steels are modelled with the Swift approach [68], the aluminium alloy flow behaviour is extrapolated according to the Hocket-Sherby [111] estimation. An overview of the extrapolation parameters is given in Table 9 for steels and aluminium alloy. As failure criterion, the maximum thickness reduction in the experiments is used, according to the method proposed by Pepelnjak et al. [112]. The element with the highest thinning is considered and the thinning acceleration is calculated at several stages. The stage in which the second derivate of the thinning reaches a maximum is considered for the evaluation of the FLC.

Table 9: Extrapolation parameters according to the Swift and Hocket-Sherby estimation, for steels and the aluminium alloy respectively.

**Swift**

| Material | $t_0$ [mm] | *b* | *a* | n |
|---|---|---|---|---|
| DX54D | 0.75 | 553.97 | 0.0063969 | 0.25529 |
| DP800 | 1.0 | 1310.9 | 0.0019445 | 0.19091 |

**Hockett-Sherby**

| Material | $t_0$ [mm] | *b* | *a* | *c* | d |
|---|---|---|---|---|---|
| A5182 | 1.00 | 365.24 | 120.01 | 10.22 | 1 |

# 5 Characterisation of the failure mechanism during Nakajima tests for the investigated materials

The material formability changes with the material structure and characteristics. In sheet metal forming the ductility, the strength, and the material local inhomogeneity are only a part of the several parameters that have to be taken into account when choosing a metal [5]. In section 4.1, the investigated materials are shortly presented by giving the main qualities. The FLC is typically defined considering the onset of necking. On the one hand, the evaluation method considers the forming just before crack, ignoring the strain history and assuming a linear strain path. On the other hand, the evaluation of the FLC at the onset of necking presumes that the material evolves with a recognizable strain localisation. Brittle materials instead fail with a sudden crack initiation. Therefore, the FLC in its classical definition may not fit with modern materials behaviours [38]. In order to better understand the process of failure during Nakajima, an investigation of the material mechanism during stretching is needed. In this section, the material response during Nakajima forming, under different strain paths, is investigated and related to the material structure. In section 5.1, the onset of necking as well as the failure phases during Nakajima test is discussed for the various materials. The strain distribution and evolution are observed using the optical measurement systems, considering the Nakajima tests characteristics as the stretching process. Moreover, the response of the material under various strain paths is compared. In section 5.2, the methodology used for the metallographic investigation is considered. The strategy is defined according to the evaluation of section 5.1 and adapted for the different material behaviours. In section 5.2, the results of the investigation are presented and discussed. The analysis of surface and thickness changes is achieved for the diverse strain paths and materials. Finally, in section 5.4, the outcomes are used for a more precise definition of the failure phases according to the strain paths and material behaviour. The proposed classification is compared to the classical FLC definition, in order to evaluate discrepancies and matches.

## 5.1 Characterisation of the onset of necking in the Nakajima test and classification of different failure phases

Using the cross-section method, according to the DIN EN ISO 12004-2, the forming limit curves obtained for the investigated materials are depicted in

Figure 13. As summarised in [113], the geometry under plane strain is not the same for all materials.

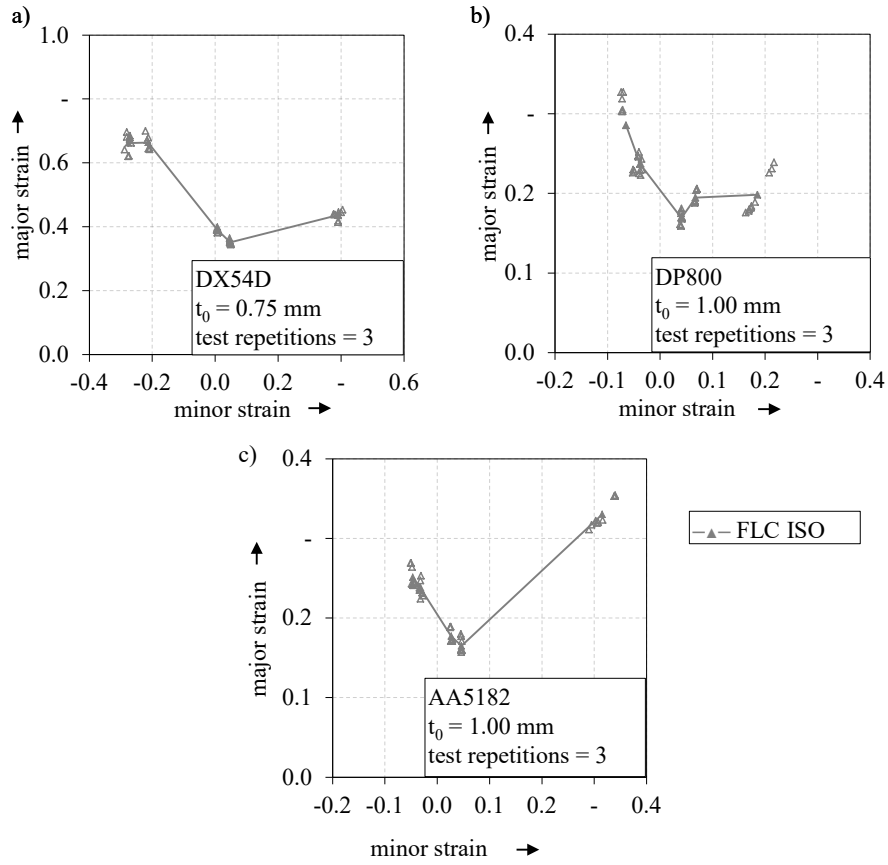


Figure 13: Forming limit curve for the investigated materials evaluated according to the DIN EN ISO 12004-2 method [113].

While the DP800 steel has its minimum with the geometry S110 with a width of 110 mm, the minimum for the DX54D steel and the AA5182 aluminium alloy is represented by the geometry S125 with a width of 125 mm. This can be related to the material behaviour. In fact, the coefficient of

anisotropy [49] and the hardening exponent (n) [114] influence the position and the form of the FLC. Higher values of Lankford coefficient ($r_0$, $r_{90}$) increase the forming limit values and may shift the FLC to the left. By increasing the hardening, also the uniform elongation increases and the forming limit raises to higher values.

The DP800 steel shows a high deviation on the FLC point value under biaxial stain condition. It is due to the fact that this material shows several local maxima in the strain distribution that develops in a sudden strong localization and crack initiation (see Figure 15). This kind of failure behaviour represents a challenge for the standardized evaluation method, which is mainly applied to materials with a pronounced necking development. In addition, it is expected that the FLC develops linearly in the field of the positive minor strain. However, in Figure 13 is the forming limit for the geometry S125 by the steel DP800 has a major strain value comparable with the biaxial strain condition, deviating to the usual FLC behaviour. This effect can be related two different factors. One reason is the specimen slipping at the cut radius as depicted in Figure 14. As can be observed, although the high clamping force, the material flows slightly on the corner and that causes a reduction of the stretching in the x direction, since in y direction the clamping is assured by the full material. Thus, the FLC point tends to be shifting to the left by constant major strain, causing a bend in the curve. Another reason is the high results deviation observable in Figure 13 for the full geometry. The high material strength causes a sudden crack without necking and in particular by the biaxial strain condition.

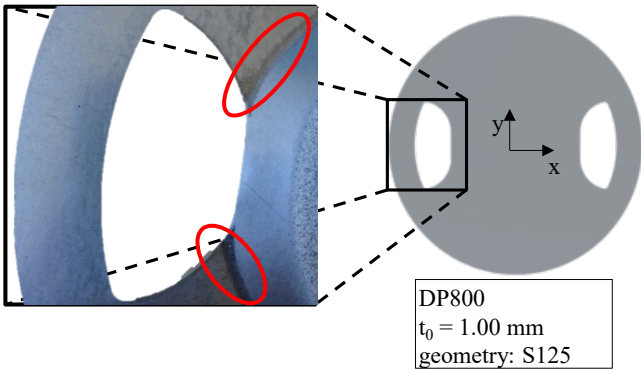


Figure 14: Specimen sliding by the geometry S125 for the DP800 steel.

The difference of the instabilities development for the different materials is also observed in the global strain distribution during forming [43]. The major strain condition on the measured area one instant before cracking

is depicted by several strain paths for the investigated materials in Figure 15. The DX54D steel shows a clear local necking area. Under uniaxial tension path, the localised area of necking has an X shape, well-known from the tensile test [115]. From one side, due to the small width of the geometry, the material compensates the high major strain with a negative minor strain, causing the reduction of the width. From the other side, the thinning causes a strain localisation at the maximum. The material flows along the length from the middle to the margin and from the margins to the centre along the width causing the formation of a transition zone in an X shape. Also by near plane strain, a localisation is visible.

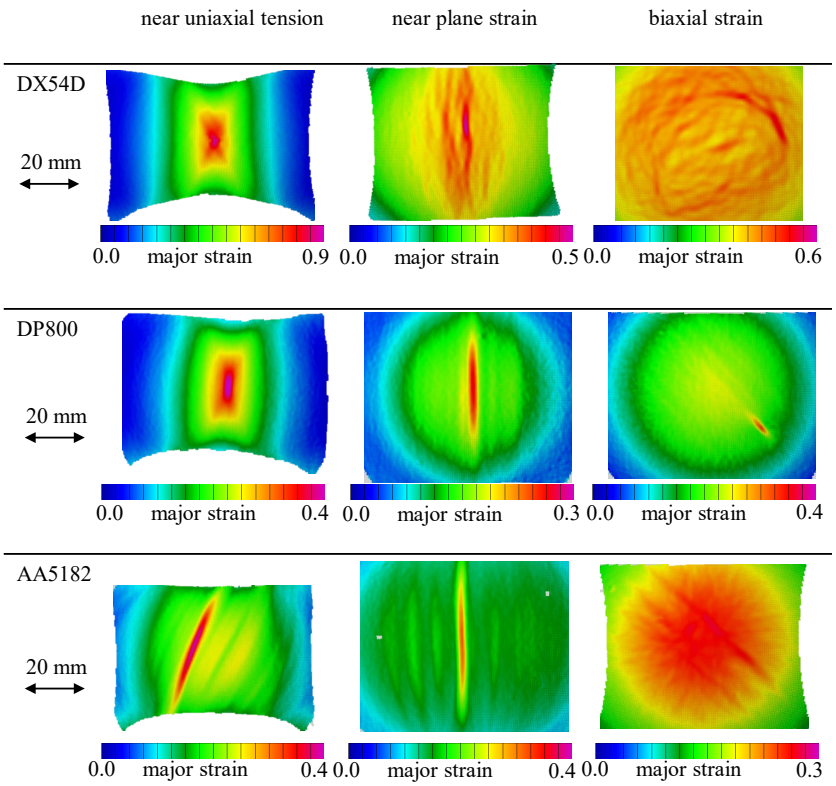


Figure 15: Examples of major strain distribution before crack for the investigated materials.

The crack initiation occurs along the width at the low level of major strain, since the minor stain is geometrically limited and thus the strain along the thickness is high. By the biaxial condition, the localisation occurs mainly in the plane along the thickness, making it difficult to detect

the instability pattern. The DP800 steel shows a localisation under the uniaxial tension path, even if less highlighted than the DX54D steel.

Under plane strain, as well as under biaxial pre-strain multiple local maxima are detectable. Similarly, the AA5182 aluminium alloy shows several maxima related to the FLC effect under uniaxial and plane strain. This is typical for this alloy. Whereas the shear bands are inclined with respect to the parallel shaft under uniaxial tension, they are perpendicular to it in the near plane strain condition. It is also important to note, that the strain distribution appears to smoother under biaxial strain, without the occurrence of shear bands. That is in accordance with the outcomes found by Romhanji et al. in [116].

The heterogeneity of instability modes pointed out from the analysis of the strain distribution partially clarifies the weakness of the cross-section method of the ISO 12004-2 for brittle material. Figure 16 shows the major strain distribution development along the section perpendicular to the crack initiation, for the DX54 and the AA5182 aluminium alloy specimens. As it can be observed, the major strain evolves regularly until it assumes a bell-shape. The assumption of the cross-section method of a distribution fitting with a parabola matches the reality here. Considering the distribution of the AA5182 aluminium alloy, instead, the local shear bands cause an irregular strain profile, even for some stages before crack. The fit area for the cross-section method includes also the neighbour shear bands, giving an incorrect parabola-fitting.

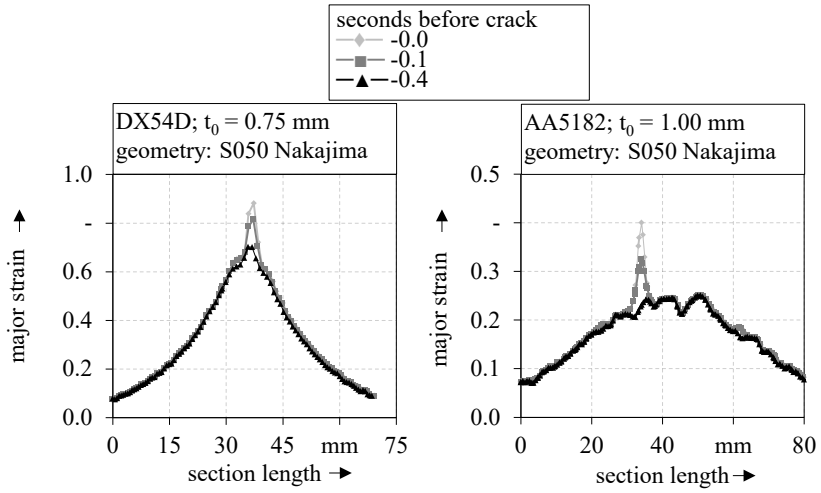


Figure 16: Strain distribution in sections perpendicular to crack initiation.

As it is described in this section, general forming phases are detectable during Nakajima test. Considering the phase concerning the instabilities, the punch force-displacement diagram, as well as the strain path on the top of the specimens, show heterogeneity of behaviour for the different investigated materials. Whereas the DX54D steel develops in a clear necking phase visible in the last few millimetres of the punch stroke, the AA5182 aluminium alloy and the DP800 steel have a brittle behaviour with the generation of multiple peaks in the strain distribution. Hence the cross-section method shows weaknesses for those materials. Regardless of the material characteristics, it is possible to detect the main phases during Nakajima tests. The process phases depend, basically, on the hemispherical punch and is divided into:

First contact punch-specimen: due to the hemispherical form, the contact area between the punch and the specimen increases progressively, starting from the point on the top of the punch. The test specimen is clamping at the margin by the clamping unit and due to the material thickness, a bending stress occurs. The parameters influencing the bending and their investigation is the topic of section 6. The contact area increases up to reaching the maximal contact area is achieved (compatible with the forming behaviour). Due to the geometrical symmetry of the punch, the first steps of the contact area progression are similar in the principal direction, along and perpendicular to the parallel width. The strain path at the top of the specimen is therefore influenced by the neighbourhood, presenting a first biaxial pre-stretching consequence of the contact area development. The magnitude of the biaxial pre-stretching depends on the specimen width, namely on the maximum achievable contact area. This aspect is properly analysed and discussed in section 7.

Homogeneous strain development after the undesired pre-stretching, the strain path on the top of the specimen develops near-linearly. The forming ratio depends on the material characteristics and starts homogeneously with a first diffuse necking phase. The diffuse necking is extended to the contact area, where the material maintains its forming behaviour without instabilities.

The onset of instabilities: the strains start to localise in a small region comparable to the thickness dimension. The reasons may be several, from heterogeneities in the thickness, voids in the microstructures and severe thinning. An overview of the hypothesis of instabilities has been given in section 2. This phase is usually used for the definition of the FLC. However, it is strongly material and strain-history dependent. As a consequence,

the general definition of the FLC as the onset of necking does not fit the diverseness of materials structures and behaviours. It has also to be mentioned that this phase develops rapidly and can be identified with the 2-3 mm of the punch stroke. The investigation of this phase is the topic of the present section.

Crack initiation and failure: the instabilities conditions grow rapidly in a crack initiation, defined as a break in the material structure.

The dependency of phase 3 from the material characteristics can be easily observed considering the force-displacement punch curve. In Figure 17, the punch force-displacement curves for the full geometry of the a) DP800 steel and b) the DX54D steel are depicted. The force increases by increasing the punch stroke. For DX54D steel, the punch reaches its maximum at approximately 46 mm. Then, the force decreases and the crack occurs at 49-50 mm. Conversely, the force development for DP800 steel shows a maximum and a sudden fall, proving a short phase 3. The higher strength of the DP800 steel causes also a higher contact punch force, achieving a maximum of 100 kN, in contrast with the 60 kN maximum of the DX54D steel. The different phases are in part recognizable in the strain path at the centre of the specimen. However, it can also be observed that, in terms of required force, phase 1 and 2 do not cause a discontinuity.

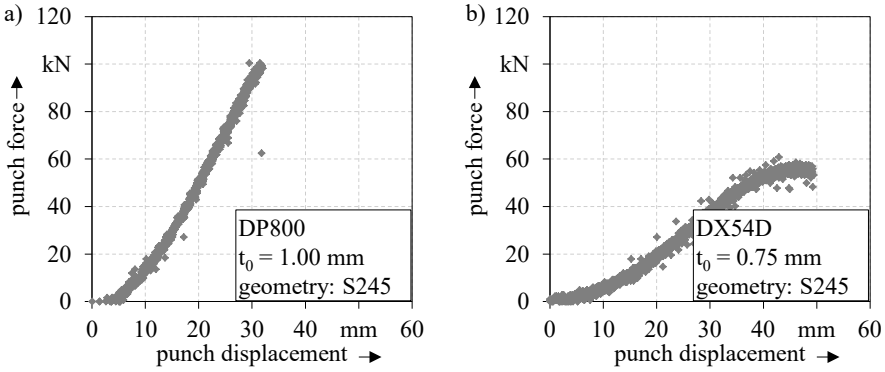


Figure 17: Force-displacement punch for the full geometry for a) the DP800 steel and b) the DX54D steel.

This remarks the challenge of isolating and investigating phase 1. Figure 18 shows the three representative strain paths for the DP800 steel: a) biaxial strain, b) near plane strain and 3) near uniaxial tension. While the bending effect is not recognizable due to the fact that the strain distribution is

measurable only on the outer surface, the biaxial pre-stretching is visible on the strain path.

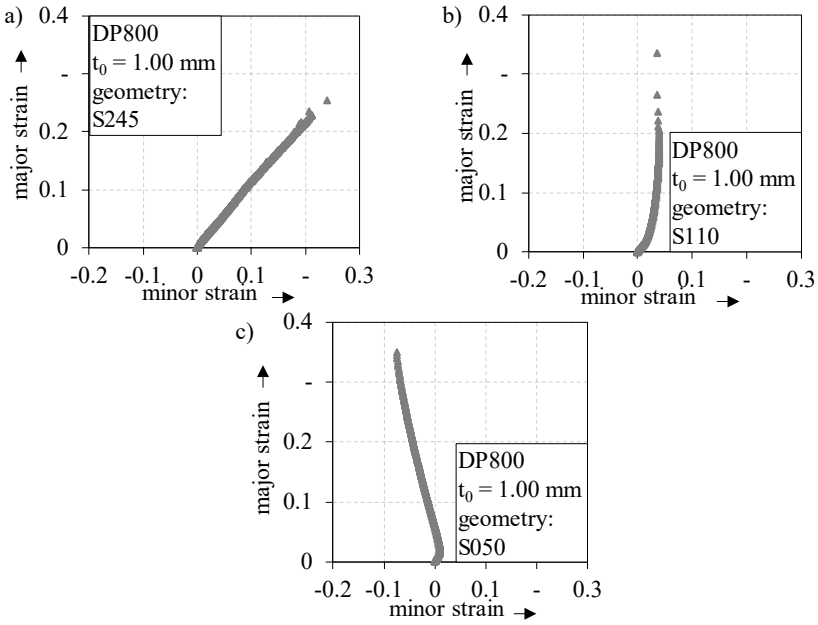


Figure 18: Strain paths evolution for the DP800 steel under a) biaxial strain b) near plane strain and c) near uniaxial tension.

Except for the biaxial strain path, where the strain develops in a biaxial way from the beginning to the end of the test, the pre-stretching is visible for the other two paths in the first steps of the strain development. The paths start with positive major and minor strain and progress according to the geometry in linear strain path. The uniaxial tension path progresses to negative minor strain values, the plane strain path increases vertically at the constant minor strain. These peculiarities of the different geometries in phase 2 are well known from the literature [16] and they are not further discussed herein. Nevertheless, it is important to note that also phase 1 seems to depend on the geometry and the strain path.

In fact, even from a qualitative point of view, a difference of the pre-straining contribution between uniaxial tension and plane strain path is observed in Figure 18. Moreover, the values of major and minor strain increase rapidly immediately before crack initiation, proving the sudden development of the instabilities. To investigate the strain rate more in detail, the thinning rate under near uniaxial tension for the DP800 steel

and DX54D steel is depicted in Figure 19. The grey area corresponds to the last 4 mm punch stroke before crack.

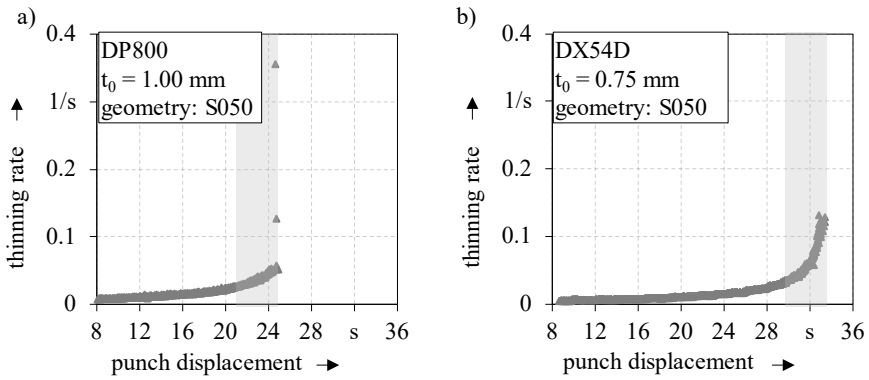


Figure 19: Thinning rate evolution of the necking zone under near uniaxial tensile strain for a) the DP800 steel and b) the DX54D steel.

As it can be observed in Figure 19-a, the DP800 steel shows a sudden increase of the strain rate in the last 4 mm of the punch displacement. This behaviour highlights the lack of a necking phase. In contrast, the strain rate of the DX54D steel rises up regularly and a transition phase between stable and unstable behaviour is detectable and attributable to a strain localisation. In order to evaluate the material characteristics and behaviours that influence the onset of instabilities, a deeper analysis of forming during the last punch steps before cracking has to be conducted. The range of investigation is set to 4 mm of punch stroke before crack for two reasons. Firstly, the experimental knowledge has shown that the instabilities occur in the last 2-3 mm before crack. Secondly, in order to detect the onset of instability, further few punch displacement millimetres should be included in the investigation. Moreover, the value of 4 mm punch stroke before the crack is also the actual parameter considered in the application of the line-fit method for the time-dependent evaluation of the FLC [43].

## 5.2 Development of a topography strategy for the Nakajima test specimen

Figure 20 shows schematically the strategy used for the investigation of the necking phases. The Nakajima experiment, as a typical characterisation test, is normally conducted until material failure. While part of the results of interest, such strain distribution, punch force and punch stroke can be measured and evaluated during the test, the analysis of the microstructure cannot be conducted directly during the test. In order to analyse

the surface topography and the material micro-structure, the test specimen has to be taken out of the test, prepared and investigated.

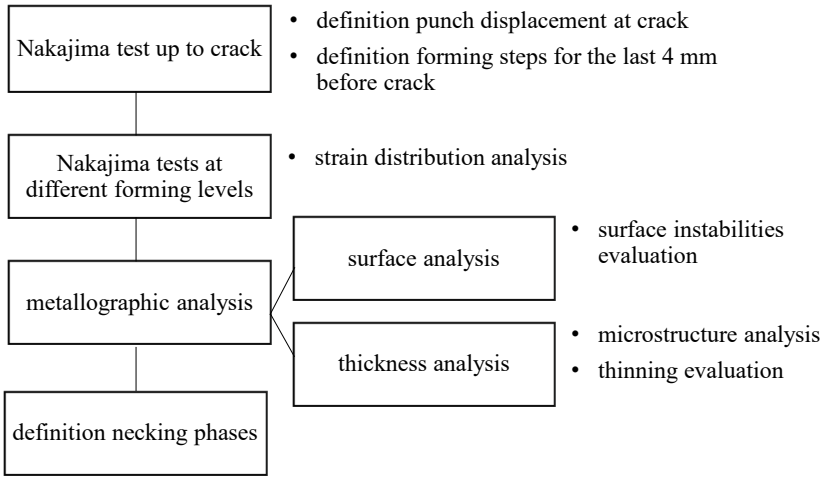


Figure 20: Metallographic analysis procedure of forming limits during Nakajima tests.

A strategy for a metallographic analysis at different strain level for the Nakajima tests is needed. As mentioned in section 2, different strategies can be found in the literature. In the present study, the analysis procedure proposed by Tasan et al. in [98] is modified. The Nakajima test is stopped at various levels of the punch displacement and the specimen is analysed with metallographic procedures. The used method differs from the Tasan method for some aspects. Firstly, the investigation steps are related to the strain path evolution. At the beginning and for the most part of the punch stroke, the forming is homogeneous. In the last 4 mm of punch displacement diffuse as well as local instabilities occur. Secondly, the procedure is applied not only for the investigation of the dual-phase steel but also for the deep-drawing steel and the aluminium alloy. It entails that the procedure should take into account the peculiarities of each different material, assuring a good transferability. Finally, the method is strongly focused on the comparison of the resulting data with the strain distribution achieved with the optical measurement system and the evaluation of the FLC, in order to better understand the forming phase 3 listed in section 5.1.

The different forming levels achieved stopping the Nakajima test at varied punch strokes, are listed in Table 10. For the last 2 mm of punch displacement before crack, a step of 0.2 mm is used. The last investigated step, defined as stage 9, is evaluated at 4 mm punch displacement before crack occurs, except for the material DX54D steel. Due to the long necking phase of DX54D steel the advanced necking at 0.2 mm before crack is

already considered as failure and, therefore, the stage 9 is hereby evaluated at 4.2 mm punch displacement before crack.

Table 10: Investigated drawing depths listed per material and geometries.

| **DX54D** | | **Drawing depths (mm)** | | | | | | | | |
|---|---|---|---|---|---|---|---|---|---|---|
| **Geom.** | **crack** | **1** | **2** | **3** | **4** | **5** | **6** | **7** | **8** | **9** |
| S050 | 34.2 | 34.0 | 33.8 | 33.6 | 33.4 | 33.2 | 33.0 | 32.8 | 32.6 | 30.0 |
| S125 | 40.4 | 40.2 | 40.0 | 39.8 | 39.6 | 39.4 | 39.2 | 39.0 | 38.8 | 36.4 |
| S245 | 50.5 | 50.3 | 50.1 | 49.9 | 49.7 | 49.5 | 49.3 | 49.1 | 48.9 | 46.3 |
| **DP800** | | **Drawing depths (mm)** | | | | | | | | |
| **Geom.** | **crack** | **1** | **2** | **3** | **4** | **5** | **6** | **7** | **8** | **9** |
| S050 | 23.5 | 23.3 | 23.1 | 22.9 | 22.7 | 22.5 | 22.3 | 22.1 | 21.9 | 19.5 |
| S110 | 24.4 | 24.2 | 24.0 | 23.8 | 23.6 | 23.4 | 23.2 | 23.0 | 22.8 | 20.4 |
| S245 | 32.7 | 32.5 | 32.3 | 32.1 | 31.9 | 31.7 | 31.5 | 31.3 | 31.1 | 28.7 |
| **AA5182** | | **Drawing depths (mm)** | | | | | | | | |
| **Geom.** | **crack** | **1** | **2** | **3** | **4** | **5** | **6** | **7** | **8** | **9** |
| S050 | 27.6 | 27.4 | 27.2 | 27.0 | 26.8 | 26.6 | 26.4 | 26.2 | 26.0 | 23.6 |
| S110 | 27.3 | 27.1 | 26.9 | 26.7 | 26.5 | 26.3 | 26.1 | 25.9 | 25.7 | 23.3 |
| S245 | 38.8 | 38.6 | 38.4 | 38.2 | 38.0 | 37.8 | 37.6 | 37.4 | 37.2 | 34.8 |

In order to assure the qualification of this strategy, the deviation of the results due to the elastic compensation by stopping the test before crack should be considered. This aspect may affect the evaluation, in particular for the dual-phase steel that is characterised by a high Young´s modulus and a high strength. A spring-back analysis of the specimen, considering the geometry form with and without clamping, would give only a global evaluation of the phenomenon. The elastic compensation occurs, basically, on the side area between the clamping unit and centre. It causes also a reduction of the specimen height. In order to evaluate if the area of interest, namely the forming zone, is also influenced from the spring-back, a direct evaluation of the strain distribution in this zone with and without punch contact should be considered. The deviation of the strain distribution is measured at the centre of the specimen as well as at 15 mm distance from it, in order to assure the validity of the defined investigation area. The spring-back is evaluated at 4 mm punch displacement before cracking occurs, namely at beginning of the analysed forming steps. It is assumed that the elastic compensation is less significant the higher is the plastic contribution, since the elastic part stays constant while the plastic contribution increases. Thus, the deviation evaluated at the initial forming steps assures lower deviations than the other strain levels. A summary

of the measured major strain deviation between formed specimen before and after spring back for the different materials considering all geometries is presented in Table 11.

Table 11: Evaluation of the major strain deviation on the centre and at 15 mm to the centre of Nakajima tests due spring back effect at stage 4 mm punch displacement before crack.

| | major strain deviation at the centre | major strain deviation 15 mm away from centre | deviation of the strain difference between the centre and at 15 mm |
|---|---|---|---|
| DX54D | 0.001 | 0.001 | 0.001 |
| DP800 | 0.005 | 0.006 | 0.001 |
| AA5182 | 0.052 | 0.080 | 0.028 |

The DP800 steel shows a deviation of the major strain of 0.006 in comparison with the forming values (0.2). Such value can be considered negligible. The difference in shape, considered by evaluating the difference between the point on the centre and the point 15 away from it, shows a small deviation of 0.001 for the AA5182 aluminium alloy. The major strain difference is about 0.08 at 15 mm and 0.052 at the centre (significantly higher than the one observed for DP800 steel). The deviation of the difference between the two evaluated points is 0.028. However, it should be noted, that due to the PLC-effects the strain distribution for the AA5182 aluminium alloy has a high deviation with multiple peaks. Thus, it cannot be deduced if the spring-back evaluation is also affected by this aspect. Nevertheless, due to the low Young´s Modulus of aluminium alloys, it can be considered that the spring back should only have a marginal effect.

## 5.3 Material analysis at different strain development and levels in Nakajima tests

In the present section, the outcomes of the metallographic analysis for the investigated material are presented and discussed. The analysis of the surface is considered. In particular, the occurrence of instabilities and localisations is analysed with the help of REM 3D measurements. For those materials that do not present a clear localisation, further investigations with higher magnification are considered. During the forming, after the homogeneous phase, the material starts to present instabilities. It can be in form of local thinning, reduction of the width, micro-cracks on the surface or, in the case of the AA5182 aluminium alloy, shear bands. The types of instabilities strongly depend on the material structure.

### 5.3.1 DX54D: ductile sheet metal

The DX54D steel shows good ductility thanks to its low-carbon contents and a prevalence of ferritic structure [117]. Due to its ductility, the DX54D steel shows the onset of necking as instability pattern, characterised by a severe thinning. As it can be observed in Figure 15, the localisation is also qualitatively visible on the surface as an inhomogeneity in the thickness and is detectable for a few steps before crack. The localisation is well recognisable on the strain distribution since severe thinning is caused by a strain concentration. The outcomes of the 3D surface analysis conducted with the REM in Figure 21 pointed out that the consideration of the surface topography help with the classification of the instabilities.

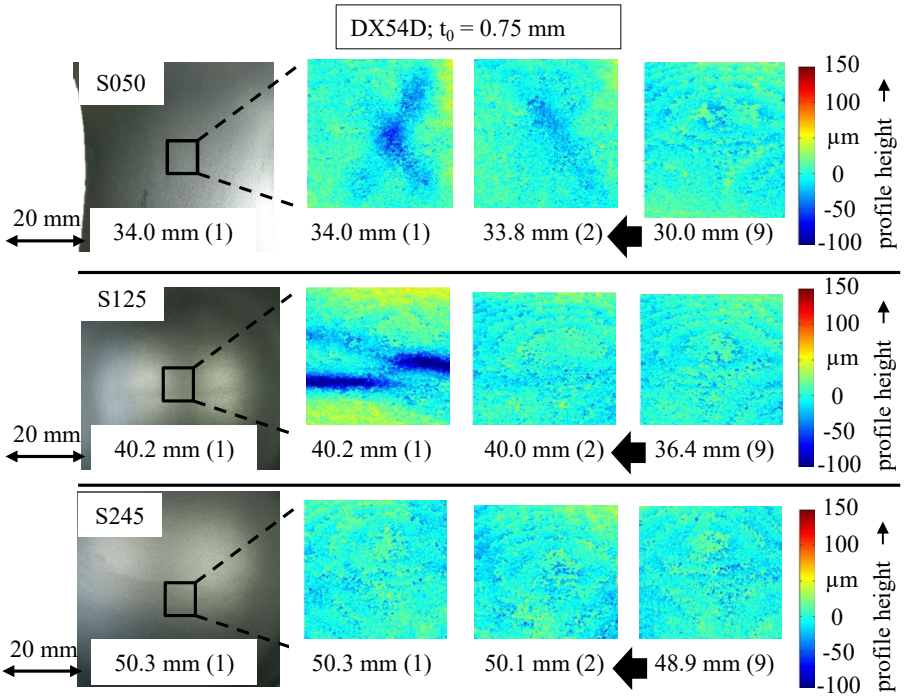


Figure 21: 3D SEM surface evolution of the DX54D steel at different forming stages for the investigated strain conditions.

Considering the geometry under uniaxial tension, the necking is detectable as a localised depth several stages before crack initiates. The strain transition lines by the strain distribution observed in the previous section is detectable also here as thinning localisation at the stage with a depth of about 70 µm. The localisation is detectable several stages before crack. At stage 9, the roughness of the surface is between -20 and 20 µm and no

localisation is visible. Under near plane strain, the necking is visible only a few stages before crack initiates.

The geometry width has an allowance with respect to the diameter of the clamping area of 5 mm since the die inner diameter is 110 mm with a radius of 10 mm. Consequently, the material flow along the width is impeded and the flow occurs basically on the principal strain and thickness direction. Thus, the main material flow plan does not correspond with the test surface.

The thinning causes a visible necking on the topography some stages before crack occurs. The localisation occurs with two local maxima in the investigated area. A correspondence can also be found in the strain distribution in Figure 15. This behaviour suggests that the heterogeneous surface topography at stage 9 and visible also in the later stages may have an influence on the localisation before crack.

The topography is also heterogeneous under biaxial strain condition. The geometry shows a mapping similar to the plane strain condition and no necking is observed, even by stage 1. Due to the strain condition, the material flows in both principal directions and the thinning develops in a diffuse manner. The results are in accordance with the investigations on the DX54D steel with a thickness of 2 mm presented in [118] and show that the observation does not depend on the material thickness. In order to analyse the topography heterogeneity, sections perpendicular to the necking orientations have been analysed with the microscope. In Figure 22, a picture of the stage just before the crack is compared with the stage at 4 mm punch displacement before crack for the geometry S050.

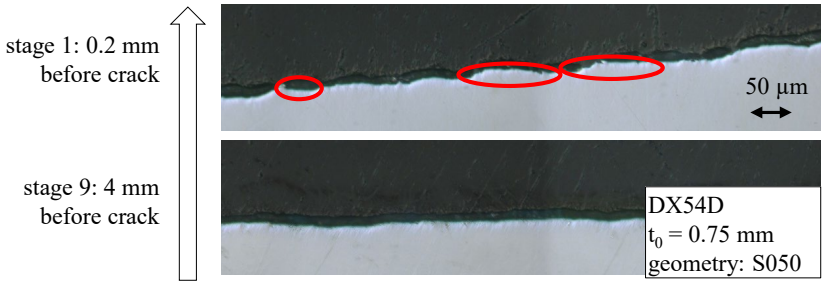


Figure 22: Microscopic thickness analysis of the Nakajima geometry S050 of DX54D steel at stage 9 (4 mm punch displacement before crack) and stage 1 (0.2 mm before crack), see Table 10.

At stage 9 (4 mm before crack), the surface profile is homogeneous in comparison to the profile at stage 1 (0.2 mm before crack). The waves

increase with the forming, develop in necking, and reach peaks of 20 µm, as also observed in the REM evaluation.

On the contrary, in Figure 23, the sections of the geometry S245 at the same strain stages show fewer differences in the surface profile. Waves are visible and develop almost constantly, proving the topography heterogeneity under biaxial strain condition and the challenge to detect an onset of localisation for this strain path condition.

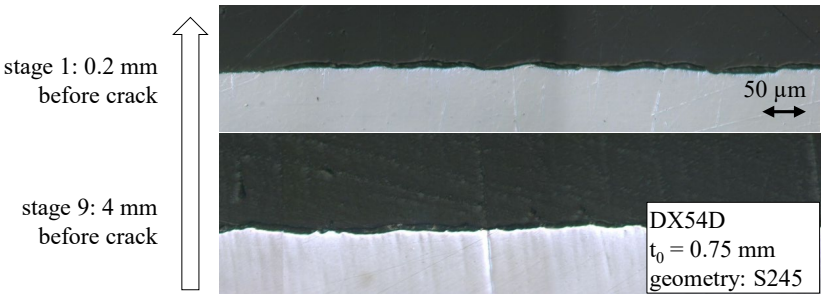


Figure 23: Microscopic thickness analysis of the Nakajima geometry S245 of DX54D steel at stage 9 (4 mm punch displacement before crack) and stage 1 (0.2 mm before crack), see Table 10.

### 5.3.2 DP800: high strength steel with brittle behaviour

The dual phase steel DP800 is characterised by a non-homogenous structure. Its failure occurs basically due to crack initiation at the grain margin between ferrite and martensite [98]. The 3D analysis conducted at different forming steps and strain paths are depicted in Figure 24. Considering the state under uniaxial tension path, a necking several steps before crack with a maximum depth of 250 µm is detectable.

Under uniaxial tension state, the material flows from the width to the centre of the specimen supporting a reduction of the width. Simultaneously, the material along the major strain direction continues to flow from the centre to the side. It follows that on the area in contact with the punch the strain distribution can be divided into 4 zones: the two zones in which the material flows from the top to the side in major strain direction, and the zones that flow from the width to the centre in minor strain direction.

The transition areas between those zones give the typical X form on the strain distribution and also cause the necking localization in the centre of the specimen. Observing the surface with a magnification of 2500x, a

micro-crack is visible one step before crack occurs, attesting the validity of the onset of necking as forming limit.

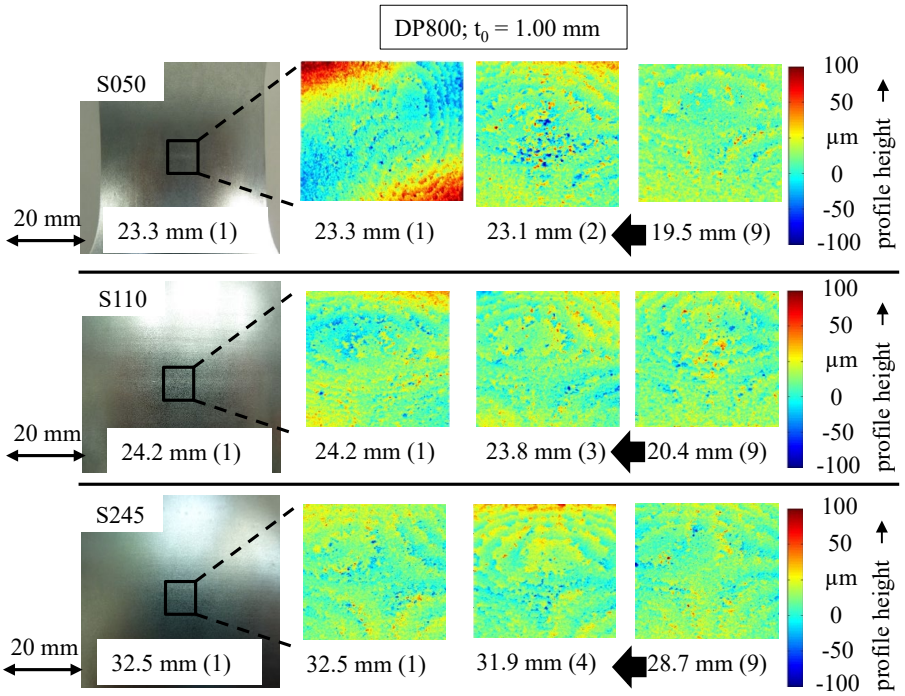


Figure 24: 3D SEM surface evolution of the DP800 steel at different forming stages for the investigated strain conditions.

Under plane strain state a necking is visible only 0.2 mm punch displacement before crack. The depth achieved is 150 µm. In general, the surface topography is heterogeneous. The peaks on the surfaces can be related with the local maxima observed on the strain distribution development. The geometry width is between the die inner diameter and the inner diameter of the clamped area.

The material flow in this direction is limited and the minor strain on the top of the specimen is near to zero, excepting the biaxial pre-stretching contribution that is discussed in section 7. Due to the limited opportunity, the flow on the top of the specimen occurs principally on the major strain- thickness plan, causing a thinning. Due to the inhomogeneous material structure, this condition causes a heterogeneous topography. Considering this aspect more deeply, in Figure 25, SEM pictures of the surface with a magnification of 2500x are depicted. The local maxima are caused by micro-cracks on the surface. Moreover, multiple consecutive

micro-voids proved the occurrence of multiple local maxima on the strain distribution during forming.

The biaxial strain condition is characterised by a diffuse necking without localisation. Due to the volume constancy, the material should flow in the thickness direction compensating the flow on the major and minor strain direction, causing a severe thinning. Therefore, even if the strain distribution is homogeneous due to the symmetry of the strain condition, the surface topography reveals a heterogeneous development with a sudden crack initiation.

Similarly to the consideration done for the plane strain condition, the coexistence of the high strength martensitic component and the softer ferrite causes heterogeneities on the local material developments, causing cracks on the phase's boundaries. The investigation on the surface with a magnification of 2500x depicted in Figure 25 reveals also for this strain condition the occurrence of micro-cracks. The micro-cracks on the surfaces are detectable some stages before the macro-crack is visible. In the strain distribution measurement, they correspond in particular to a local necking by the geometry S050, to multiple local maxima under plane strain condition and to a sudden localisation under biaxial strain condition, as previously observed in Figure 15.

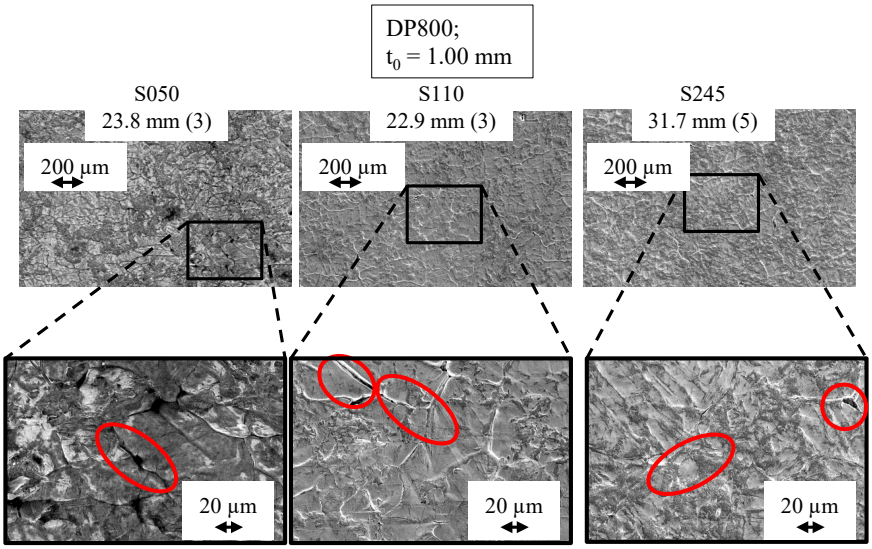


Figure 25: SEM surface investigation of the DP800 steel with 200x magnification at stage 0.2 mm punch displacement before crack [119].

In particular, under plane strain condition, consecutive micro-cracks are responsible for the crack initiation. This outcome seems to attest that the

decohesion of martensite to the ferrite matrix is the main mechanism causing the crack by the DP800 steel, independently to the strain history. Moreover, the presented investigation validates the outcomes from Tasan et al. [98] of an increase of the damage mechanisms under biaxial stress condition due to the higher stress triaxiality. The metallographic analysis, therefore, gives important additional information to the failure mechanisms during Nakajima tests, that can be used for the definition of onset of necking since the micro-crack are visible also on the strain distribution as sudden strain localisations.

To validate the failure mechanism related to the phases decohesion, metallographic analysis along the thickness should also be considered. Observing the thickness structure at different drawing depth steps, the presence of voids was observed. As depicted in Figure 26, the ferrite structure and the martensite particles are well detectable. The decohesion between the phases is recognizable as the darker area between the grains. This characteristic can be used to quantify the void area fraction by processing the images with the program ImageJ. An application of this method can be also found in Tasan et al [98].

The results for the different strain conditions and drawing depths depicted in Figure 27 shows a continuous increase of the void fraction area during forming. Four significant steps are analysed for the geometries: the step 0.2 mm punch displacement before crack, the step where it is considered instabilities start according to the 3D surface measurements, a drawing step 0.4 mm punch displacement before the supposed onset of necking and the drawing step 9, at 4 mm punch displacement before crack.

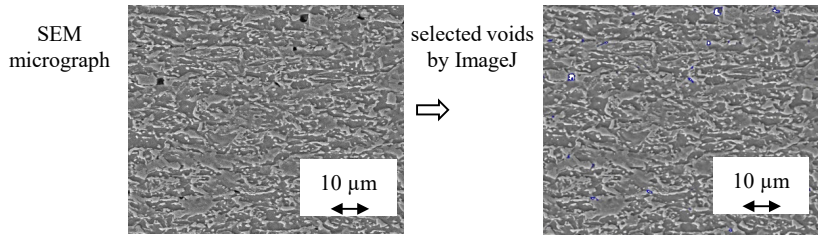


Figure 26: SEM micrograph showing voids (a), influence of drawing depth on void area fraction (b) and sheet thickness (c) [119].

The void fraction of the material in the as-received state is 0.005%. It can be observed that the percentage of the area of voids increases by increasing the forming by all strain state conditions. However, the full geometry under biaxial strain condition shows levels of voids percentage two times higher than the other geometries. The results partially prove the out-

comes of Tasan et al. [12] that observed that in the full geometry the damage mechanism is more active, even if the percentage achieved are dissimilar. It can probably depend on the differences in the dimension of the investigated area. The values of thinning depicted in Table 12 prove a higher forming on the thickness for the geometry under biaxial strain state and a lower thinning by the other two geometries.

The void fraction area is defined as:

$$void\ area\ fraction = \frac{void\ area}{picture\ area} * 100 \quad (5)$$

The grown of the micro-voids observed on the thickness seems to be influenced by the thinning, even if the investigated area is kept constant. At step 9, the thickness is about 0.88-0.86 mm for the geometry S050 and S110. The full geometry shows a thinning with a thickness of 0.68 mm. The increase of voids nucleation develops gradually and continuously during the test and there is not a limit value that can be used for the detection of the onset of instability.

Table 12: Thickness measurement at 0.2 mm (step1) and 4 mm (step 9) [119].

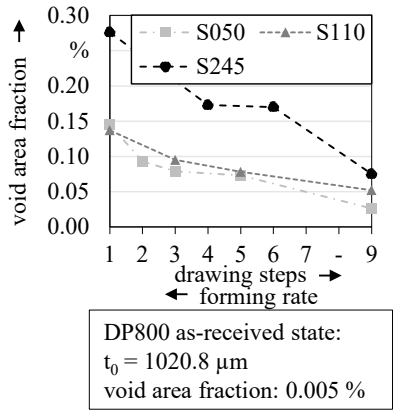


| geometry | drawing step 1 | drawing step 9 |
|---|---|---|
| S050 | 694.7 µm | 881.6 µm |
| S110 | 788.3 µm | 860.2 µm |
| S245 | 591.0 µm | 680.9 µm |

Figure 27: Influence of drawing depth on void area fraction according to [119].

In conclusion, the mechanisms of micro-voids in the thickness are the same as the micro-crack on the surface. For the uniaxial tension condition, in which the main material flow occurs on the surface, the micro-cracks are localized and develop in necking, while on the thickness the voids area increases slowly. Under plane strains condition the main material flow occurs in major strain and thickness direction. Due to the volume constancy, both contributions compensate each other on the top of the specimen, in which the minor strain is near to zero. The micro-cracks

and void-cracks growth develop similarly, causing multiple micro-cracks also on the surface. Finally, under biaxial strain condition, the main material flow occurs on the thickness, causing a high level of micro-voids that develop in micro-cracks on the surface just before crack initiation.

### 5.3.3 AA5182: aluminium alloy with PLC effect

The aluminium alloy AA5182 is characterised by the PLC-effect. Shear bands occur on the surface due to the dynamic interactions of dislocations with the mobile solute atoms [120]. Even if the shear bands are an unstable phenomenon, they can be detected on the surface as well as in the strain distribution as strain discontinuity (see Figure 15). The study of Romhanji et al. [116] mentioned that even the shear band are divided into types from type A to type C, under stretching with the hemispherical punch, the shear band type is limited to type B. Type B is characterised by parallel lines with an angle of 60° to the sample width. A complete overview of the PLC mechanisms theories and studies can be found in [121]. In Figure 28, the 3D topography measurements for the different Nakajima geometries are depicted.

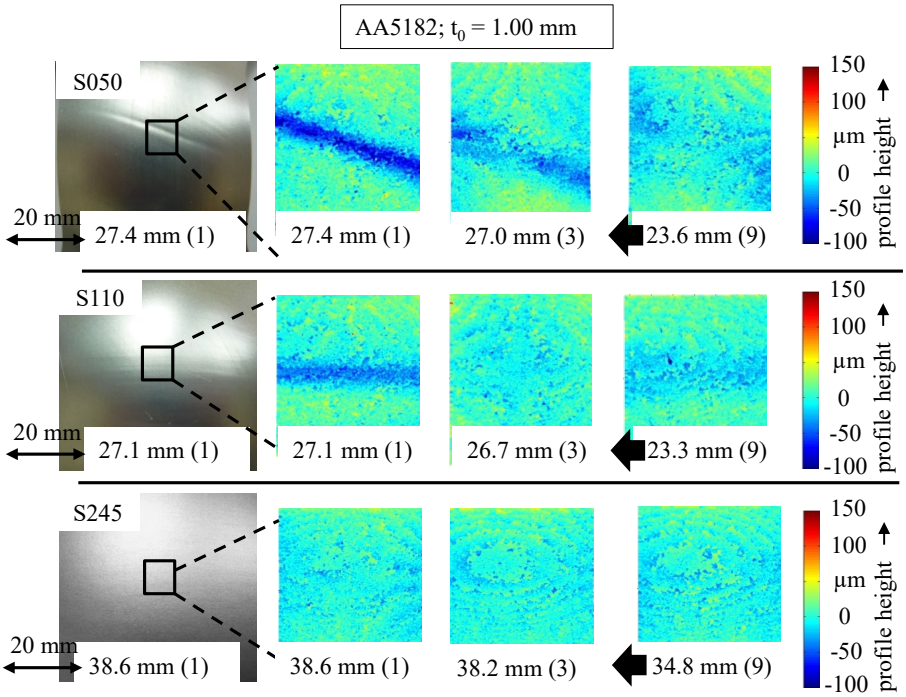


Figure 28: 3D SEM surface evolution of the AA5182 aluminium alloy at different forming stages for the investigated strain conditions.

As can be observed, the phenomenon of the PLC effects depends on the strain path conditions and grades. Under uniaxial tension conditions, the PLC-bands are well recognizable in all investigated stages. Even if the PLC phenomenon is unstable and random bands occur without a clear pattern, it can be noted that the bandwidth decreases by increasing the forming step. The band at necking reaches a depth of 100 µm. The bands can be classified as type B, according to [116].

Similarly, under plane strain conditions, the PLC-bands have an evolution with a reduction of their width. At step 3 (0.6 mm before crack), no PLC-bands are detectable, remarking the unstable behaviour of the PLC-mechanism. The specimens under biaxial strain condition do not present any PLC-bands in all investigated stages. As observed in [116], the PLC-bands are suppressed by increasing the biaxial contribution on the strain paths. Except for the biaxial strain condition, the evolution of the PLC bands can be used for the qualification of the class instability for the AA5182 aluminium alloy.

For the quantification, the pictures depicted in Figure 28 are investigated with the software ImageJ. The bandwidths are quantified using the procedure shown in Figure 29. A section perpendicular to the shear band is defined. The profile height on the section is analysed and the bandwidth is evaluated considering the peak width on the section distribution.

The results shown in the diagram prove that in general there is an evolution of the shear band dimension during forming. For the geometry under uniaxial tension S050 and the geometry under plane strain S110, the bandwidth decreases by increasing the forming grade. The initial width is 8 mm under uniaxial tension and 7 mm under plane strain at 4 mm punch displacement before crack occurs. The bandwidth remains near this value after 2 mm punch displacement. Between stage 7 and 6, the width increases suddenly with a reduction of 2 mm. In the last few stages before crack occurs, the width is reduced to 1-2 mm. It can be concluded that for the geometry S050 and S010 the onset of instability coincides with a sudden reduction of the bandwidth. Instead, the bandwidth for the geometry S245 under biaxial stretching does not show a clear tendency. The margins of bands are not clearly observable and thus the evaluation of the width presents a high deviation from stage to stage. The values are between 8 and 4 mm and a width decrease is not observable. The surface analysis results conducted for the AA5182 aluminium alloy proved the general difficulty to recognize the pattern on the surface for specimens under biaxial stretching.

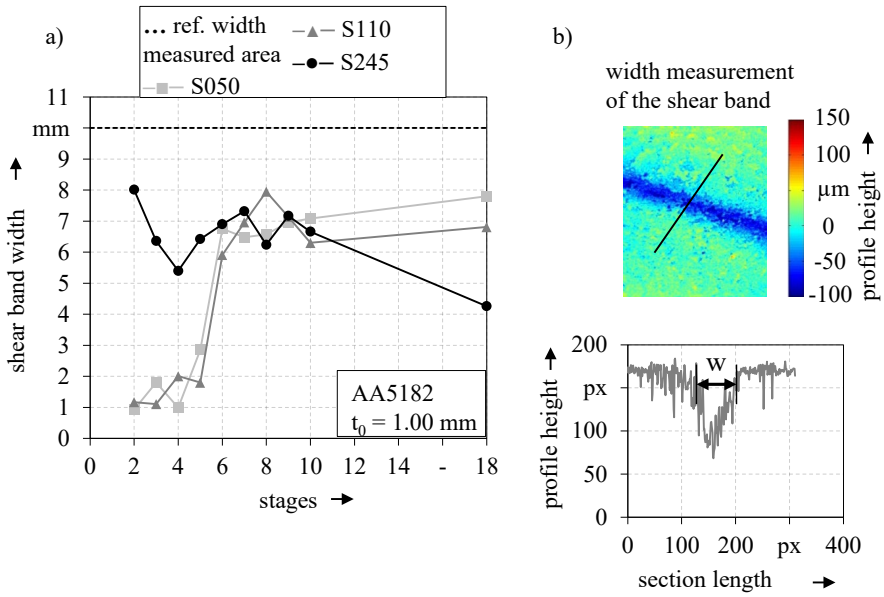


Figure 29: a) Shear bandwidth of AA5182 aluminium alloy during Nakajima test for different geometries; b) procedure for the evaluation of the shear bandwidth with the software ImageJ.

In conclusion, the aluminium alloy AA5182 shows shear bands during Nakajima test in dependence to the strain distribution. For strain condition under uniaxial or plane strain, the PLC effect is visible and quantifiable. In particular, it is observed that by increasing the forming level, the shear bands localise in smaller area reducing their widths. The beginning of the width reduction can be interpreted as the onset of instability and show a clear pattern on the surface. On the contrary, PLC effects are not observable under biaxial strain and in general, the topography of the test specimens under this strain condition does not show any clear pattern.

The analysis of the thickness for the AA5182 aluminium alloy attests that the onset of instability starts with a reduction of the shear bandwidth. In Figure 30 a picture of the thickness at stage 1 is compared with stage 9. At stage 9, namely 4 mm punch displacement before crack, a thinning localisation is not observable, even if large shear bands have been observed on the above-discussed surface analysis. At stage 1, 0.2 mm before crack occurs, the thinning is visible and a surface depression is detectable on the outer surface as well as on the inner surface, confirming that the shear bands, initially considered a surface phenomenon, develops in instability with a thinning and a reduction of the bandwidth.

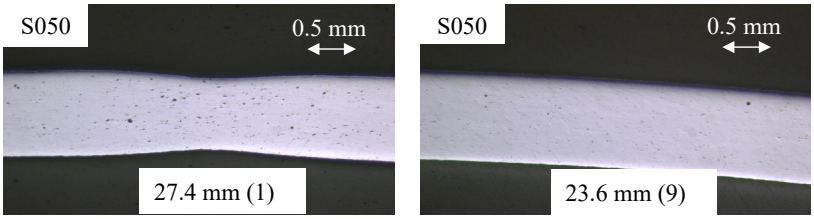


Figure 30: Microscopic thickness analysis of the Nakajima geometry S050 of AA5182 aluminium alloy at stage 9 (4 mm punch displacement before crack) and stage 1 (0.2 mm before crack).

## 5.4 Summarizing considerations on the material mechanisms and peculiarities for the investigated materials

The sheet metal response to the forming during Nakajima test depends basically on the material characteristics and the strain condition. Metallographic analyses have been conducted on Nakajima specimens at diverse strain levels in order to qualify and define the onset of instabilities for the materials. For the investigation, the deep drawing steel DX54D, the dual phase steel DP800 steel and the aluminium alloy AA5182 have been investigated under uniaxial tension state, plane strain and biaxial stretching. The investigations pointed out differences in the material responses due to the different material structure.

The deep drawing steel has a high ductility and shows the onset of necking in form of localisation of thinning at different strain conditions. The thinning is well recognizable on the surface evolution as well on the strain development. Under uniaxial tension condition, the localisation occurs in the middle of the transition zone between major and minor strain direction with a development of the strain distribution in X form. Under plane strain as well as under biaxial strain condition, even if the material flow occurs mainly on the thickness, patterns are recognizable on the surface, even if only a few steps before crack occurs.

The investigation on the dual phase steel indicated that the necking strongly depends on the material ductility and is not always valid as the definition of forming limit. In the case of the DP800 steel, the crack occurs in a sudden manner. Under uniaxial tension condition due to the smaller width, the material is free to flow on the width and a neck is visible on the strain distribution as well as on the topography. Under plane strain as well under biaxial strain, the topography is heterogeneous. The

outcome is also attested from the strain distribution, in which multiple local maxima are visible. The metallographic analysis shows that the heterogeneity is attributable to micro-cracks that occur on the surface due to the decohesion of the martensitic particles to the ferritic matrix. Similar observations have been made along the thickness. However, a clear onset of the micro-voids on the thickness is not observable.

The aluminium alloy AA5182 presents the PLC effect in form of shear bands on the surface during forming. The metallographic analysis shows the tendency of the shear bands to decrease in width by increasing forming. Except for the biaxial strain condition, in which the shear bands are suppressed, the measurement of the band's width can be used for the definition of the onset of instability. An overview of the instability patterns for the investigate materials by different strain conditions is listed in Table 13.

Table 13: Overview of the observable pattern on the surface of Nakajima tests for the investigated materials and geometries with magnification 200 x.

| **Strain condition** | **DX54D** | **DP800** | **AA5182** |
|---|---|---|---|
| Near uniaxial tension | Necking in form of localised thinning | Necking in form of localised thinning | Instability as a reduction of shear bandwidth on the surface |
| Near plane strain | Necking in form of localised thinning | Micro-cracks on surface | Instability as a reduction of shear bandwidth on the surface |
| Biaxial strain | Necking in form of localised thinning few steps before crack | Micro-cracks on surface | No pattern recognizable |

In Figure 31, Figure 32 and Figure 33 the investigated forming steps are depicted together with the strain paths, the FLC according to the DIN EN ISO 12004-2 and the outcomes of the metallographic analysis for the investigated materials. For the ductile DX54D steel, the onset of necking evaluated with the REM analysis is in accordance with the FLC evaluation. The analysis proves that in case of onset of localised necking, the strain distribution on sections perpendicular to the crack initiation evolves in a ring-bell-shaped form and the evaluation with the cross-section method give realistic results.

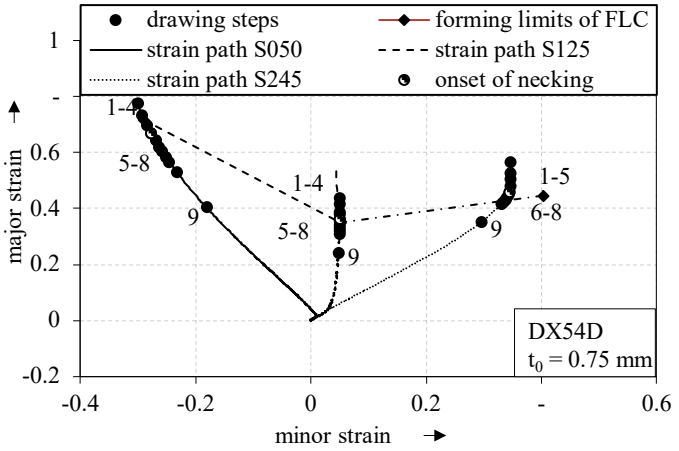


Figure 31: Comparison of the metallographic outcomes with the FLC according to the DIN EN ISO 12004-2 with strain paths and investigated step for the DX54D steel.

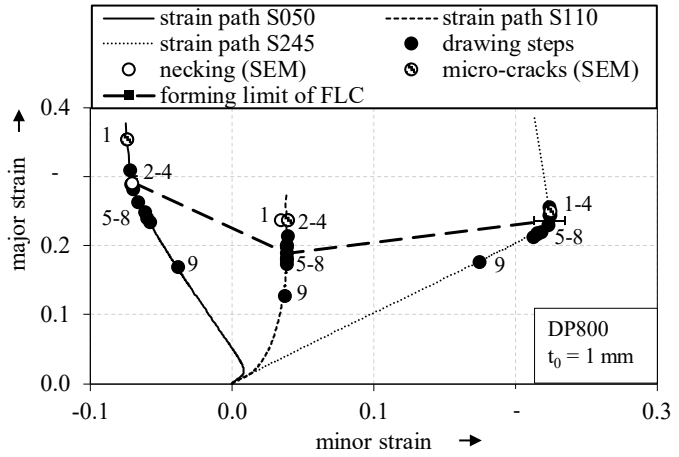


Figure 32: Comparison of the metallographic outcomes with the FLC according to the DIN EN ISO 12004-2 with strain paths and investigated step for the DP800 steel [119].

The micro-cracks observed on the surface of the DP800 steel, on the opposite, are not directly correlated with a homogeneous strain distribution and therefore the FLC deviates from the results of the metallographic analysis. In particular, it can be observed, that in the case of the uniaxial tension condition, in which a necking was visible, the evaluations are in accordance with the cross-section method. For the other two geometries, the ISO method is more conservative than the metallographic observation. The class of instability for the AA5182 aluminium alloy is based on the shear bandwidth. The results, compared to the conventional FLC are lower. The unstable nature of the PLC effect makes the investigation of

the forming steps hard. The several stages performed by stopping the punch at various levels show that the achieved strain levels are often different and sometimes lower levels of forming achieve a higher level of strain values. Therefore, the investigation shows, for example by the plane strain condition, that the steps from 6 to 9 have a similar level of major strain and then there is a sudden change by the step 4. This abrupt change has been also observed by the measurement of the bandwidth. It can be concluded that the PLC effect during Nakajima test can be recognised and quantified and is responsible for the onset of instability for the AA5182 aluminium alloy. However, its unstable nature suggests considering conservative values.

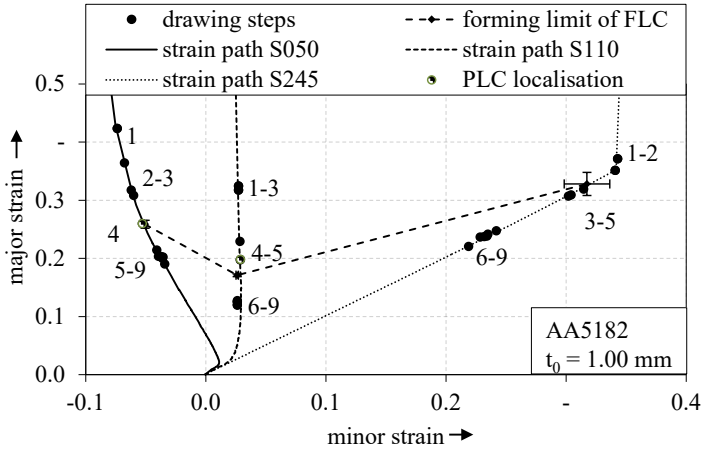


Figure 33: Comparison of the metallographic outcomes with the FLC according to the DIN EN ISO 12004-2 with strain paths and investigated step for the AA5182 aluminium alloy.

The material structure influences the mode of the instability of the materials and patterns on the surface can be detected and used for its definition. However, independently to the material, the specimen under biaxial strain does not show visible pattern during Nakajima tests. On one hand, the biaxial strain condition causes a main flow in the thickness direction due to the volume constancy and the compensation of the biaxial stretching. On the other hand, the strain distribution is homogeneous due to the symmetry of the stress condition. Therefore, instabilities and localisations are suppressed thanks to the symmetrical stretching. Moreover, it has to be noted that the lower is the material plastic anisotropy, the lower are the recognizable patterns on the surface during biaxial stretching. In fact, the DX54D steel has an r-value greater than 1 and it has the tendency to flow more on the width than on the thickness. In general, and apart from

other influence parameters, a necking on the surface is visible, since the flow in the thickness is limited. In contrast, the DP800 steel as well as the AA5182 aluminium alloy have an r-value lower than 1 and tend to flow more on the thickness than on the width and thus the thinning remain homogeneous and the necking diffuse and no pattern are visible on the surface. Finally, the geometry curvature in both major and minor direction by biaxial stretching is considerable. Thus, surface waviness is certainly smaller than the curvature, making their detection challenging.

# 6 Investigation of the bending influence on the determination of the forming limit curve with the Nakajima test

As investigated in the previous section, the onset of instabilities by Nakajima tests starts in the last few millimetres of the punch stroke. The deformation up to this point is homogeneous and nearly linear on the top of the specimen [68]. Nevertheless, it is known from the literature that the strain history has an influence on the forming limit [16]. Besides the non-linear and bi-linear strain paths cases that are not a topic of the present study, the forming limit curve definition is based on the assumption of strain path linearity. This hypothesis only partially matches with the Nakajima tests. As discussed in section 2.2.5, the contributions of bending and biaxial pre-stretching due to the hemispherical punch are the most interesting aspects that play a role. They are undesired process deviations that cannot be completely avoided. The flat Marciniak punch instead is not affected by them but would introduce high contact forces. Moreover, the DIN EN ISO 12004-2 prescribes the margin of testable thickness between 0.3 and 4 mm. Moreover, the punch diameter is prescribed between 98 and 102 mm. Thus, the above-cited process factors may affect the results from different material examiners. As discussed in section 2, the draft of the standard proposed in 2010 by the GDDRG contained a suggestion for the correction of the FLC points for bending and biaxial pre-straining. However, it was not possible to assure the universal validity of the correction methods. Moreover, the forming limit point achieved with the cross-section method comes from the punctual evaluation of necking after the interpolation, increasing the uncertainty factors on the forming limits. For the investigation of a valid correction method, the bending and the biaxial pre-straining should be investigated in their entirety, considering their phenomenology during the test. In this section, the bending contribution during Nakajima tests is investigated. In section 6.1 the origin of the bending and the aspects that have an influence on it, are described. In section 6.2 the bending is experimentally investigated for the different materials. In particular, the analysis of Nakajima tests with upscaling and downscaling tools is presented and discussed. In section 6.3 a numerical analysis for the investigation of the material thickness influence is conducted. Moreover, the effects of material characteristics such as hardening, anisotropy and ductility are analysed. Finally, in section 6.4 the results are summarised and the ranges of validity of the

FLC are given. An overview of the investigation plan for this section is given in Table 14.

Table 14: Summary of the bending investigations in Nakajima tests for this section.

| parameter | range of evaluation | methodology |
|---|---|---|
| material | DX54D; DP800; AA5182 | |
| punch diameter | 60 mm; 100 mm; 360 mm | experimental/numerical |
| strain path | uniaxial; plane; biaxial | |
| material thickness | 1(0.75) mm; 2 mm; 3 mm; 4 mm | numerical |

## 6.1 Identification of the bending in Nakajima tests

The general limitation of testable thickness with Nakajima test is defined as 4 mm for a standard punch between 110 and 100 mm, according to the DIN EN ISO 12004-2. Consequently, the FLC is considered valid in this range. However, the bending contribution is different for the various thicknesses. Moreover, in the standard, no differences for specimen geometries or tested materials are mentioned. The need for a bending correction was proposed in 2008 by the GDDRG [84] and added on the ISO draft. However, the lacking of knowledge regarding the influencing factors and the phenomenon itself caused a rejection of the draft.

The spherical form of the Nakajima punch and its combination with the sheet thickness causes a bending contribution that influences the strain distribution on the surface. In particular, the bending stretches the material on the outer layer and compresses the inner layer. The combination of the stretching and the bending causes a different strain distribution on the layers. A schematic representation of the phenomenon by elastic bending is depicted in Figure 34. Thereby, the FLC based on the strain distribution on the outer surface is affected by a bending component $\varepsilon_{b.}$ As a consequence, the FLC evaluated for various material thicknesses or punch diameters may differ.

However, the design of the Nakajima test does not allow an analysis of the strains through the thickness, the experimental evaluation of the bending effect is difficult. A possible way to overcome the problem is to consider the stresses. A detailed analysis of bending using the analytical approach and the forming limit stress can be found in Min et al. [83].

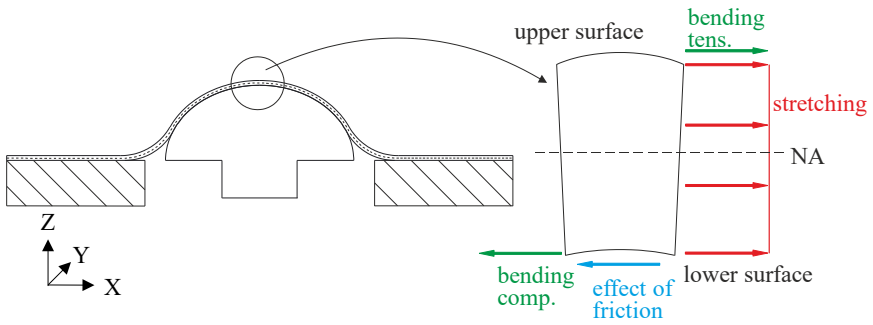


Figure 34: Schematic representation of the strain contribution due to the bending on the sheet thickness.

A second possibility is given by considering a numerical model of the process [122]. Also in this second application, a material modelling and thus a correct constitutive model for the tested metal should be given. Both approaches show the full potential of the forming limit stress and its independence on the strain paths. Moreover, the first approach allows the correction of the forming limits by using the analytical analysis. However, in particular in Europa, the practical use of the forming limit curve in terms of strains is still the preferred one [34]. Firstly, the strains are measurable during experiments, in contrast to the stress. Secondly, an analytical approach requires a profound knowledge of the material behaviour, in order to choose the correct constitutive model. However, the trend of employing new materials and alloys in the press-shop is increasing and thus the immediate approach considering strains is still used for the material characterisation. Nevertheless, the process effects, which are well predicted in the stress-based approach, should be considered in order to clearly define the limits of applicability of the forming limit curve. In order to evaluate the process limits in which the bending contribution may affect the forming limits, both the investigation of different punch diameters and material thickness is conducted. While for the punch diameters an experimental analysis is possible, for the several thickness the numerical approach is used. With the numerical model of the Nakajima test it is possible to have an easy and rapid investigation of the layers through the thickness. Moreover, the same material in different thicknesses can show various behaviours due to the fact that the manufacturing changes. Therefore, the use of the numerical approaches avoids those deviations. The validation of the model based on the experiments assures the plausibility of the results. However, some assumptions should be made. Firstly, a constitutive model should be chosen. The model used for the yield curve and the flow stress curve has been presented in section 4.4. In particular, the

yielding model according to Yld91 [77] supposes a symmetric behaviour in tension and compression. Assuming symmetry of behaviour in tension-compression implies that during bending the contribution on the fibres under tension is the same for the fibres under compression. It follows that the bending neutral axis should be in a symmetric position with respect to the layers and thus in the middle of the thickness. It also assumes that in Nakajima tests the stretching has the prior forming contribution and the bending is considered as a secondary aspect. This simplification is suggested by the geometrical definition of the die and the punch. The standard Nakajima setup is characterized by an inner die diameter of 1.1 times the punch diameter, in order to minimize the bending. Regarding the forming area on the top of the specimen, the bending is expected to be high at the beginning of the contact between the punch and specimen. Moreover, the progressive thinning of the specimen due to stretching should cause a decrease of the bending due to the reduction of the distance between the outer/inner surfaces and the bending-free layer. Taking into account those simplifications, the bending contribution can be calculated as follows, using the strain distribution of the outer-, middle- and inner-layer [113]:

$$\varepsilon_{1b(2b)} = \varepsilon_{1(2)outer} - \varepsilon_{1(2)middle} \tag{6}$$

In the formula, $\varepsilon_{1b(2b)}$ represents the bending contribution, $\varepsilon_{1(2)outer}$ the principal strains on the outer surface, $\varepsilon_{1(2)middle}$ the principal strains on the middle layer. The methodology is similar to the one proposed in [43] for the experimental evaluation of the bending. The difference is in the calculation of the strain at the bending-free layer. In the experimental evaluation, it is assumed that the neutral axis is constant in the middle and that the distance of the outer surface is calculated considering the thickness reduction. In the present investigation, instead, the measurement of the strain is directly evaluated on the middle layer in the numerical model. The advantage is that no assumptions on the thickness or sheet curvature are required.

## 6.2 Experimental analysis of bending

The comparison of the results for the scaled setups has to be preceded to a setups qualification. In fact, the scaling of the punch, the die, and the blank holder, as well as specimen geometries should preserve the strain development. Figure 35 shows the relation of the strain development to the top of the specimen with the normalised dome height exemplary for

the DP800 steel. The reached dome height depends on the punch size. However, the strain distribution should not be dependent on the setups, since it is a material peculiarity. Despite marginal deviations on the major strains and minor strain values due to the eventually different position of the crack initiation, the diagrams show a good agreement of the reached strain path by the diverse Nakajima setups and for all three investigated geometries.

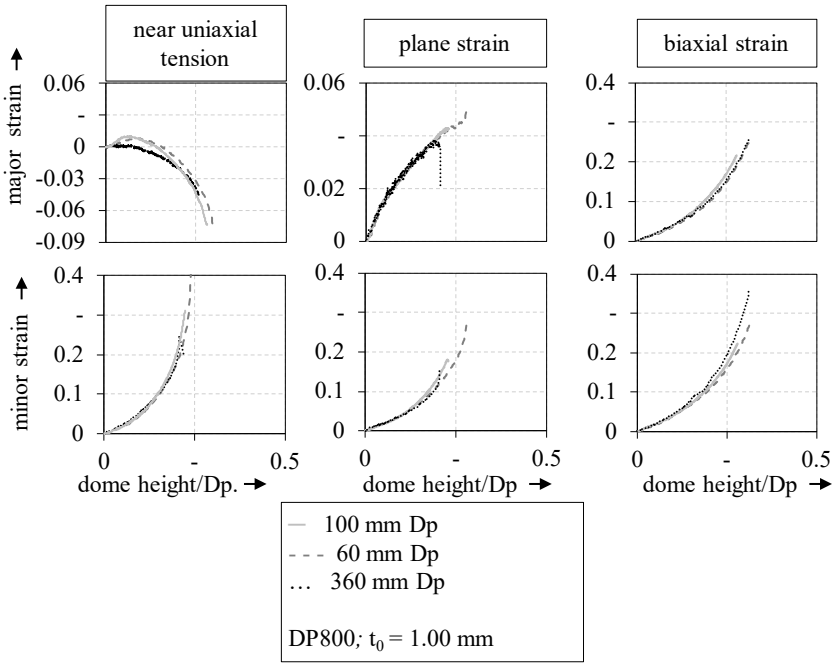


Figure 35: Strain development on the blank dome along the dome height/ punch diameter for the DP800 steel.

In general, the experimental evaluation of the FLC using up- ad down-setups does not show a recognizable tendency on the results, in contrast with Min et al. evaluation [83]. Using a punch of 101.6 mm diameter and comparing the outcomes with a Nakajima punch of 50.8 mm, they found out that their outcomes show shifted values in dependency of the punch curvature. The shifting is here not observable. It may depend on the fact that in the present investigation also the die has been scaled and qualified. Thus, even if the bending slightly increases due to the higher relation thickness/punch diameter, the geometrical distance between the punch contact and the contact of the sheet with the die is scaled consequently, limiting the effect of bending.

For the DX54D steel the deviation of the forming limit is negligible. It has to be supposed that the ductility of the material causes a thinning and a translation of the bending neutral-axes. Moreover, the strain localisation achieves a high level of strains above 0.4 up to 0.7 for the uniaxial condition and thus the stretching prevails on the bending effect.

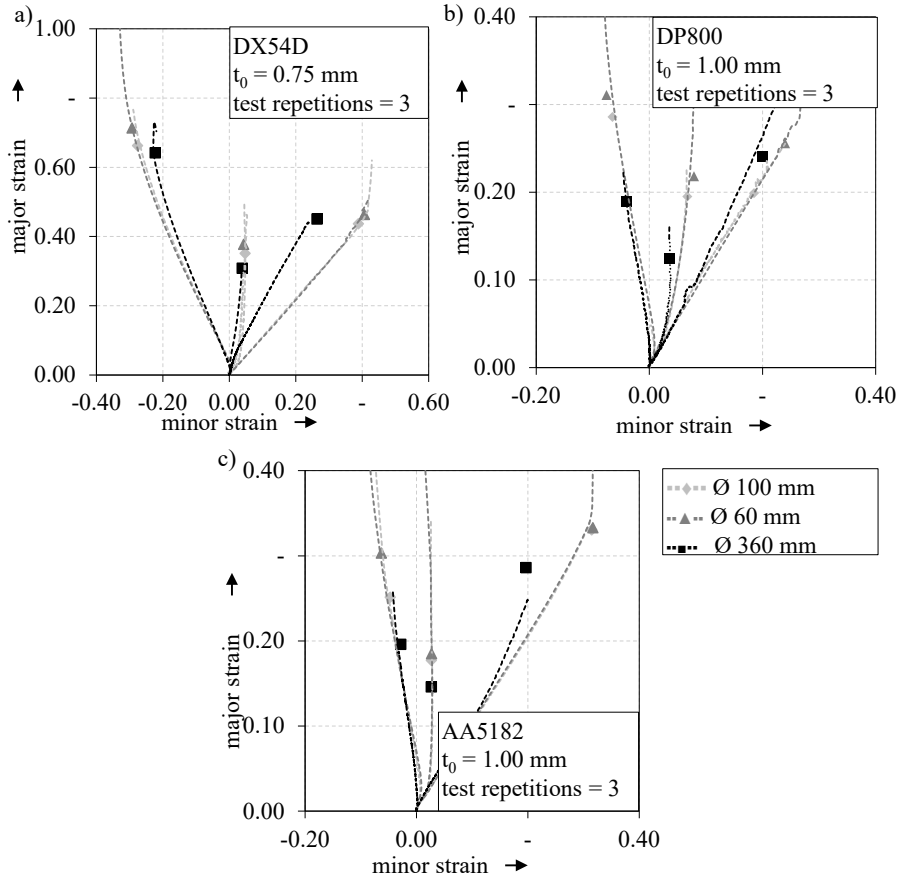


Figure 36: Strain paths and FLC points from the Nakajima test with punch diameter 360 mm (blue), 100 mm (green) and 60 mm (red) for the a) DX54D steel, b) DP800 steel and c) AA5182 aluminium alloy according to [113].

In the case of the DP800 steel, even if the strain paths are comparable, the FLC from the scaled setups are diverse. The difference on the major strain limit is 0.005 in the biaxial condition, 0.004 under near plane strain and only 0.025 under uniaxial tension condition. The low level of stretching and the combination with a sudden crack with a marginal thinning make the bending effect due to different punch diameters visible.

The AA5182 aluminium alloy shows different deviation behaviour for the several strain paths. Under near uniaxial tension condition, the variation of major strain limit is 0.03 and 0.04 for the down-scaled punch and the up-scaled punch respectively. Considering the strain path under plane strain condition the deviation is reduced at 0.01, while is no difference of forming limits by the biaxial condition. It can be explained considering the PLC-effect and its development in different strain conditions. As validated by several researches, the shear bands in aluminium alloys are influenced by the forming history. In fact, as previously mentioned in section 5.1, under positive stretching up to biaxial strain condition, the shear bands are impeded [116].

Considering the experimental outcomes, the scaling of the setups makes possible the achievement of comparable strain distribution, qualifying up-scaled and down-scaled setups for the evaluation of the FLC. However, the bending should be taken into account due to the combination of punch curvature and sheet thickness. Nevertheless, the experimental evaluation of the bending is strongly limited to the inability to investigate the diverse material layers, making a measurement of the bending effect impossible. Moreover, the evaluation of the FLC is also dependent on the evaluation methods or, in other words, to the standard deviation of the experiments and measurement systems. Therefore, the quantitative analysis of the bending can only occur with a numerical simulation.

## 6.3 Numerical analysis of bending

The numerical model of the Nakajima test allows analysing the strain distribution along the thickness. In order to validate the numerical model for the different geometries, setups and materials, the punch force-displacement curves and the strain paths are considered. The punch force-stroke curves comparisons are depicted in Figure 37 for the setup with a punch diameter of 100 mm.

Comparable outcomes are achieved for the other setups. The numerical results show for all setups a good accordance with the loading condition. The root means square error (RMSE) is calculated as follows:

$$\text{RMSE}=\sqrt{\frac{\sum_{j=1}^{p}(F_{simulation}-F_{experiment})^2}{p}} \tag{7}$$

in which $F_{simulation}$ is the value of punch force in the numerical model, $F_{experiment}$ the correspondent experimental value and p the number of

evaluation points. The RMSE is less than 2 kN and proves the good agreement of the numerical models. The most deviations are shown by the AA5182 aluminium alloy due to the inhomogeneity on the experimental punch force-displacement curve caused by the PLC effect.

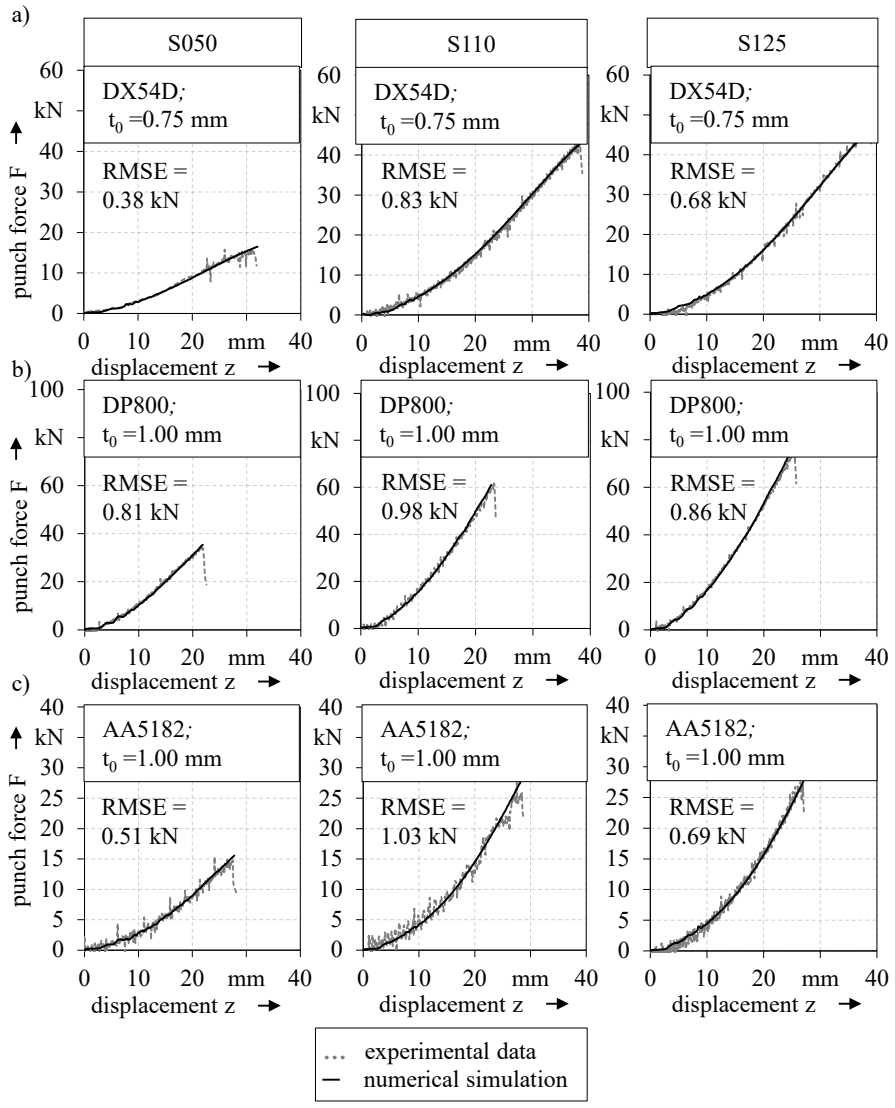


Figure 37: Comparison of the punch force-displacement curve of the Nakajima model for different geometries for the a) DX54D steel b) DP800 steel, c) AA5182 aluminium alloy according to [113].

The numerical approach requires a constitutive model and thus some approximation, such as symmetrical yielding in tension and compression.

The bending contribution has been analysed considering the middle layer bending-free and making the simplification of elastic bending contribution on both layers. The bending contribution is calculated according to the procedure shown in section 6.1. The strains values are evaluated according to the DIN EN ISO 12004-2 with perpendicular sections to the thinning initiation. The results shown in Table 15 are the average of the different strain paths. The bending has been calculated with the equation (6), considering the investigated materials and punch diameters.

Table 15: Numerical results: Bending strain from equation (6), with the middle layer as the neutral axis and evaluating the strain limit for different punch diameters [113].

| | **Bending strain outer surface** | | | | | |
|---|---|---|---|---|---|---|
| | **D = 100 mm** | | **D = 60 mm** | | **D = 360 mm** | |
| | $\varepsilon_{1b}$ | $\varepsilon_{2b}$ | $\varepsilon_{1b}$ | $\varepsilon_{2b}$ | $\varepsilon_{1b}$ | $\varepsilon_{2b}$ |
| DX54D | 0.0023 | 0.0027 | 0.0050 | 0.0051 | 0.0010 | 0.0010 |
| DP800 | 0.0043 | 0.0044 | 0.0070 | 0.0074 | 0.0010 | 0.0017 |
| AA5182 | 0.0050 | 0.0050 | 0.0110 | 0.0122 | 0.0017 | 0.0017 |
| | **Bending strain inner surface** | | | | | |
| | **D = 100 mm** | | **D = 60 mm** | | **D = 360 mm** | |
| | $\varepsilon_{1b}$ | $\varepsilon_{2b}$ | $\varepsilon_{1b}$ | $\varepsilon_{2b}$ | $\varepsilon_{1b}$ | $\varepsilon_{2b}$ |
| DX54D | -0.0015 | -0.0011 | -0.0140 | -0.0056 | -0.0010 | -0.0006 |
| DP800 | -0.0053 | -0.0048 | -0.0080 | -0.0073 | -0.0017 | -0.0013 |
| AA5182 | -0.0053 | -0.0052 | -0.0027 | -0.0049 | -0.0017 | -0.0013 |

The outcomes from the inner and outer surface show discrepancies in general in the order of max. 0.001 and max. 0.01 for the AA5182 aluminium alloy. The results suggest that the consideration of the middle layer as the bending-neutral line is only an approximation. The thinning reduces the distance between the layers. With the limitations given by the element discretisation of the thickness, the bending-free layer is shifting from its middle position. Nevertheless, the bending values are lower by all material and punch diameter combinations compared to the forming limits strains, with the investigated thickness of 1 mm. These outcomes attest what found in [88] that the deviation of the results due bending are lower for sheet under 1.2 mm and increase by higher thickness values.

As expected, by constant punch diameter, the bending contribution increases with the thickness. Exemplarily, Figure 38 depicts the values for the DP800 steel comparing the development of bending by different geometries. It can be noted, that the geometries reach a similar value of bending, proving a poor dependence of the geometry width. Moreover,

the value of reached bending remains under 0.01 up to the thickness 3 mm, comparable with the experimental standard deviation. At 4 mm the bending by the geometry S110 reaches a value of 0.02. However, the discrepancy of this geometry is not directly related to the bending, but rather with the position of the localisation (Figure 38-b). In fact, the high contact force due to the high thickness causes the shifting of the localisation out of the centre of the specimen, even by low friction, reaching the geometrical limit of the setup. Therefore, the cross-section evaluation method does not match properly the strain limit due to the two-peak distribution and thus there are deviations in the bending calculation.

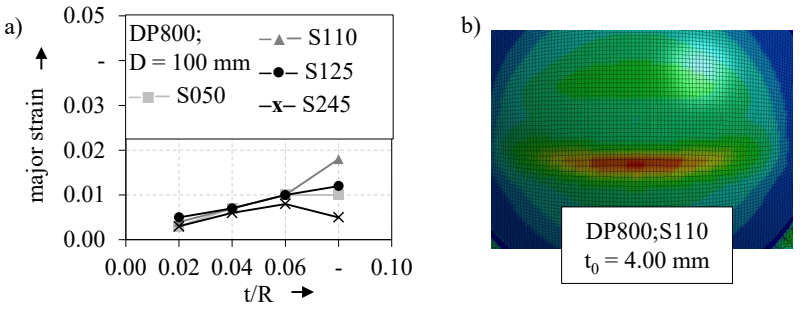


Figure 38: a) Bending contribution for the DP800 steel for different sheet thicknesses. b) Localisation in the numerical simulation of geometry S110 $t_0$ = 4 mm.

Moreover, the full geometry shows lower values than the geometries average. Due to the high thinning under biaxial stretching, the distance between the inner layer, middle layer and outer layer is significantly reduced, causing a reduction of the calculated bending contribution. As exemplarily depicted in Figure 39 for the sheet thickness 4 mm, the thickness distribution reaches a value of 2.4 mm at the centre of the specimen.

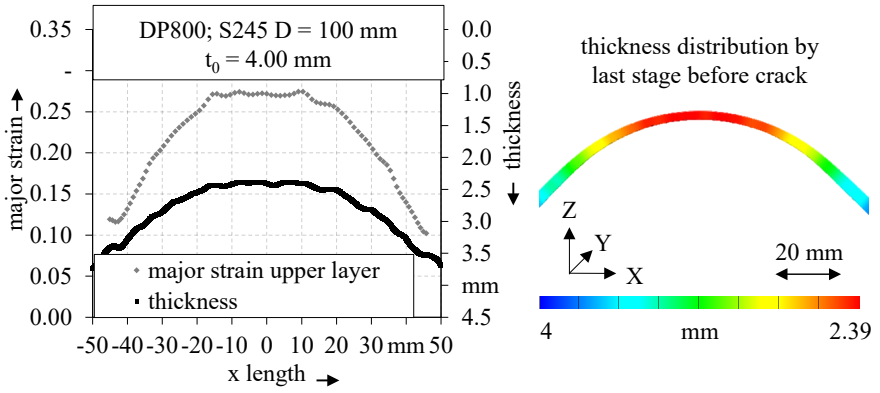


Figure 39: Major and thickness strain distribution at necking for the numerical simulation for the DP800 steel, geometry S245, to = 4 mm.

Considering the bending not relevant for the full geometry, since the values are lower than 0.01, an average value of the rest of the geometry is considered and listed in Table 16. The results are shown exemplarily for the DX54D steel. The increase of the bending with the thickness is visible on the outer as well as on the inner surface. Nevertheless, the two contributions show a light deviation, confirming that the neutral axis may change its position during forming, due to the combination of stretching and bending.

Table 16: Numerical results: Bending strain from equation (6), considering the middle layer as the neutral axis and evaluating the strain limit for different sheet thicknesses.

| **Bending strain outer surface D = 100 mm** | | | | | | | | |
|---|---|---|---|---|---|---|---|---|
| | $t_0$ = 0.75 mm | | $t_0$ = 2 mm | | $t_0$ = 3 mm | | $t_0$ = 4 mm | |
| | $\varepsilon_{1b}$ | $\varepsilon_{2b}$ | $\varepsilon_{1b}$ | $\varepsilon_{1b}$ | $\varepsilon_{2b}$ | $\varepsilon_{2b}$ | $\varepsilon_{1b}$ | $\varepsilon_{1b}$ |
| DX54D | 0.0023 | 0.0027 | 0.006 | 0.004 | 0.008 | 0.006 | 0.014 | 0.011 |
| **Bending strain inner surface D = 100 mm** | | | | | | | | |
| | $t_0$ = 1 mm | | $t_0$ = 2 mm | | $t_0$ = 3 mm | | $t_0$ = 4 mm | |
| | $\varepsilon_{1b}$ | $\varepsilon_{2b}$ | $\varepsilon_{1b}$ | $\varepsilon_{2b}$ | $\varepsilon_{1b}$ | $\varepsilon_{2b}$ | $\varepsilon_{1b}$ | $\varepsilon_{1b}$ |
| DX54D | 0.0015 | 0.0011 | 0.006 | 0.004 | 0.006 | 0.009 | 0.016 | 0.010 |

Another interesting aspect is represented by the comparison of the results by changing the relation $t_o/R$ maintaining the thickness or the diameter constant respectively. Figure 40 shows the average values of bending reached by the different materials considering these two approaches. Despite the outcomes shown by Charpentier in [79], that affirmed that the effect of the thickness appears to be stronger than of curvature, the effects are similar for both. Varying the punch from 60 to 360 mm and the thickness from 1 to 4 mm at punch diameter 100 mm, the reached bending values seems to move linearly by increasing the relation $t_o/R$ independently from what of the two parameters is maintained constant. The discrepancies can be explained considering the differences in the method of investigation.

Firstly, the present outcomes have been obtained by a numerical analysis, avoiding any experimental deviations. Secondly, the scaled setups are qualified to maintain the proportion of inner die diameter and punch diameter, in contrast to the work of Charpentier, in which only the punch form and diameter have been changed. The bending varies also due to the variation of the distance between the inner die corner and punch. Finally, the bending contribution is hereby calculated using the formula

mentioned above, while in the previous paper, the calculated major engineering strain on the surface is considered.

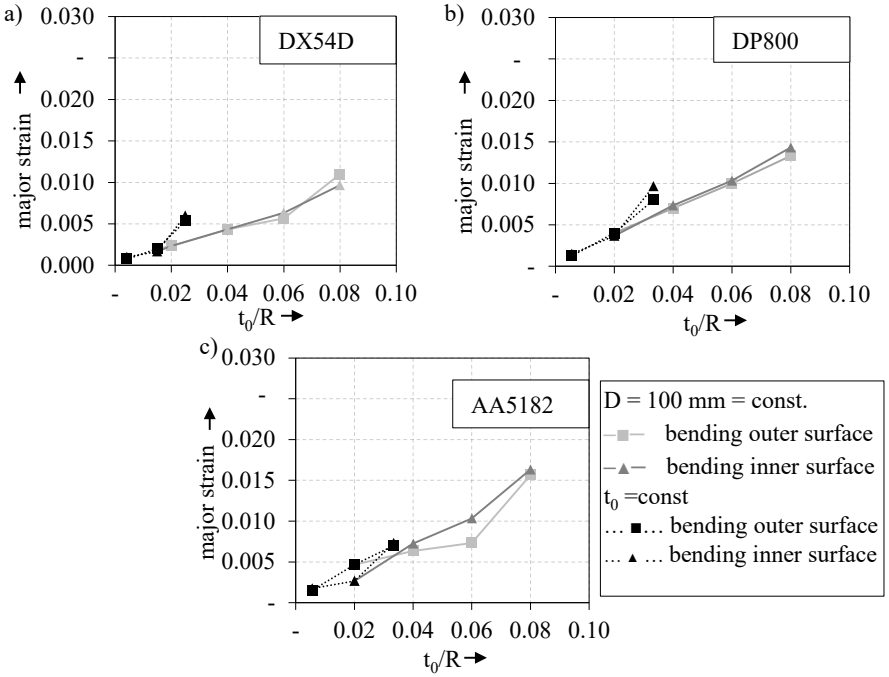


Figure 40: Development of the bending contribution on the outer and inner surface by the a) DX54D steel, b) DP800 steel and c) AA5182 aluminium alloy.

It has also to be noted, that the bending value by changing the punch diameter in the range of the investigated setup, are lower than 0.01. That means, that even by reducing the punch diameter of 60 mm, the maintenance of the size relation with the die and blank holder assures low negligible values of bending. Moreover, the bending by Nakajima tests plays a more important role by low-ductile materials, such as the DP800 steel and the AA5182 aluminium alloy. For those materials, the limits for a minor bending have to been considered at 2 mm of sheet thickness.

## 6.4 Summarizing evaluation and interpretation of the investigation

By evaluating FLC using the Nakajima test, the bending contribution due to the form of the punch and the sheet thickness should be taken into account. It is an undesired effect that may affect the results. Bending does not contribute to the necking initiation but is responsible for an increase

of the strain distribution level on the test surface in comparison to the outer surface. In fact, the outer layer is additionally stretched while the inner layer is compressed. It is expected that the higher is the thickness the higher is the bending contribution. Similarly, lower punch diameters cause a higher level of bending. Nevertheless, the bending is a secondary effect and the forming during Nakajima test occurs basically due stretching. This aspect, together with the difficulties of investigating the strain distribution along the thickness, makes the investigation of the bending difficult. In the presented investigation, the effect of the punch diameters has been experimentally analysed, while the thickness influence has been investigated numerically. The numerical analysis permits the evaluation of the strain distribution on the middle and inner layer. Moreover, it avoids the deviations in the behaviour of sheet metal with different thicknesses.

The investigations using diverse punch diameters have been conducted using scaled setup by maintaining the same relation between inner die diameter and punch diameter. The comparison of the outcomes in term of reached strain in relation to the punch stroke and the strain paths has shown that by maintaining the design relation, the bending contribution for the investigated materials is maintained low. In particular, the ductile DX54D steel show similar FLC values for the up-scaled, the down- scaled as well as the reference setup, while the DP800 steel and the AA5182 aluminium alloy show some discrepancies. Brittle materials are subject to a lower thinning than the ductile material. In fact, the material flow is impeded due to the material structure and the crack initiation is characterised by a minimal or zero localisation. Consequently, the thinning is moderate and the outer and inner layers maintain a distance to the bending free-middle layer.

The numerical analysis conducted varying the material thickness from 1 mm to 4 mm as prescribed by the standard method show level of bending higher of the experimental standard deviation fixed at 0.01. While the geometry width seems to be no effect on the bending, the thickness plays an important role. However, in contrast to the study of Charpentier [79], the influence of the punch diameters is comparable with the influence of the thickness, by maintaining the relation $t_0/R$ constant.

For ductile material the bending is maintained under 0.01 on the investigated range, suggesting that the reduction of the thickness reduce the level of bending. For the DP800 steel and the AA5182 aluminium alloy, the validity of the Nakajima test has to be limited at a thickness of 2 mm.

If the material that has to be tested overcomes this limit in terms of low formability and high thickness, it is suggested to employ an up-scaled setup. The results still are comparable with the standard setup but the influence of the bending can be reduced.

# 7 Investigation of the biaxial pre-straining influence on the determination of the forming limit curve with the Nakajima test

The biaxial pre-stretching by Nakajima tests is an undesired effect caused by the hemispherical geometry of the punch. In the literature, several correction methods for the point the FLC can be found. The methods are based on the definition of the constant equivalent strain [84] other to the calculation of the forming limit stress curve [83]. In particular, the strain-based correction methods on the FLC restrict the investigation in a specific area, not considering the global effect of the biaxial pre-stretching. Moreover, the evaluation of the biaxial contribution is qualitatively calculated considering the strain path deviation of the geometry under plane strain. Finally, it is considered that this effect can be considered constant for all strain paths. In order to achieve a better understanding of the biaxial pre-straining phenomenon during Nakajima tests using the strain measurements, in the present section, a numerical and experimental investigation is conducted. In section 7.1 the phenomenology of the biaxial pre-stretching is described and discussed. The evaluation strategy based on the coefficient of correlation is briefly presented for a better understanding of the next sections. In 7.2 a method based on the coefficient of correlation for the experimental quantification of the pre-stretching is presented. The values for different geometries and materials are compared and analysed. The influence of the setups is investigated thanks to the up-scaled and down-scaled setups. Moreover, strain paths are compared with linear tests such as tensile test and plane strain test. The numerical investigation is presented in section 7.3. Finally, the outcomes are summarised in section 7.4, giving an overview of the biaxial pre-straining during Nakajima tests and its influence on the FLC.

## 7.1 Identification of the biaxial pre-straining in Nakajima tests

The hemispherical form of the Nakajima punch assures lower contact forces in comparison to the Marciniak punch. The contact surface increases with the punch strokes and causes a maximum of the force only at the top of the dome, where the punch displacement direction is perpen-

dicular to the contact surface. Despite this enormous advantage, the hemispherical form is also responsible for a circular symmetry of the material flow. In fact, the progressive increase of the contact surface causes at first a material flow from the top, which is already in contact, to the periphery. As observed in [113], it takes several millimetres of the punch stroke before the maximum contact area is reached. The area interested in forming at the centre of the specimen is also the area with the first contact. In the neighbouring area instead, the contact starts later and at beginning causes a biaxial tension on the top of the specimen. It produces an initial biaxial straining on the top of the specimen. The difference in the punch geometry means, consequently, differences in the strain paths of Nakajima or Marciniak specimens. In Figure 41, the strain path of the DX54D steel for near uniaxial tension and plane strain path from the Nakajima test is compared with the outcome from the Marciniak test. As observed by Hasek in [15], a biaxial pre-stretching followed by a second linear path has the effect to reduce the achieved forming limit due to the fact that a stretching works on the thinning due to the volume constancy and thus reduces the capacity of the material to stand further forming grades. Thus, the FLC points from Nakajima tests present lower major strain values in comparison to the Marciniak results. Moreover, the Nakajima FLC points are globally shifted to higher values of minor strain, as also noted by Leppin et al. in [84].

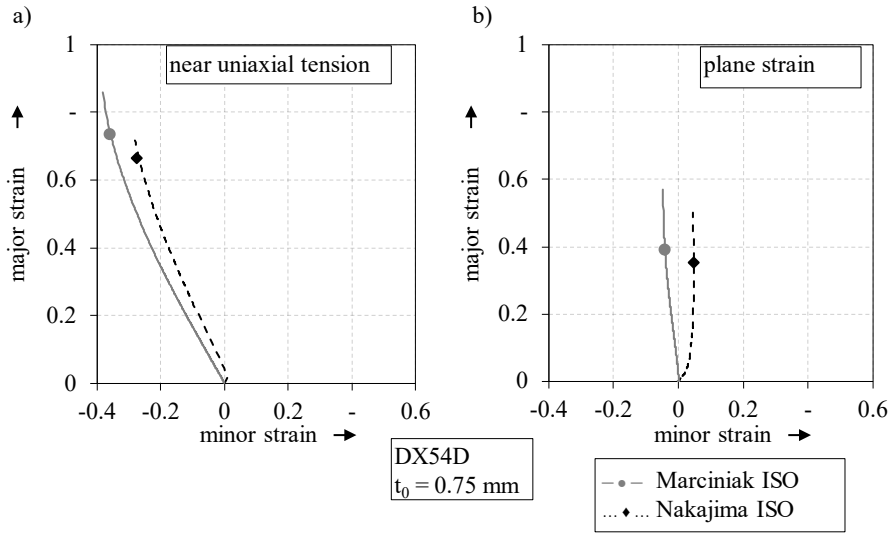


Figure 41: Comparison of forming limit for the DX54D steel between Marciniak and Nakajima tests for the geometry under a) near uniaxial tension and the geometry under b) plane strain [113]

An example of the initial biaxial straining on the strain path at the centre of the specimen is depicted in Figure 42-a.

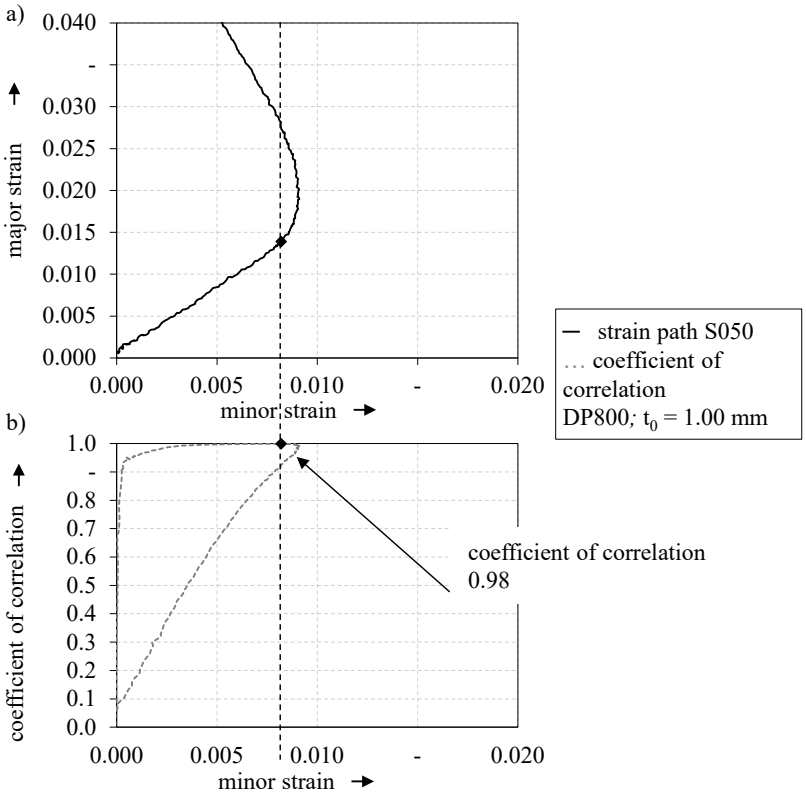


Figure 42: Biaxial pre-straining evaluation with the help of the correlation coefficient method [113].

Due to its complexity in term of space and time development, the evaluation of the biaxial pre-straining can be challenging. The methods presented in section 2 took severe assumptions, like small pre-straining and constant equivalent strain [84], or select a constant value dependent on the material characteristics [102]. In the following, an experimental method based on the coefficient of correlation on the strain path is proposed. The idea is to consider the strain path on the necking zone and its development during the process. Considering an initial linear development by the beginning of the contact, the material flow changes afterwards by reaching the maximum contact areas and develops according to the sample geometry. The transition on the top of the specimen is different depending on the sample. The geometry under uniaxial stain state and in general with a width less than the punch diameter develops to negative strain

values. On the strain paths a sudden change with a sharp angle is recognizable. Geometries with a width comparable with the punch diameter, namely between 100 mm and 110mm, evolve to a constant minor strain going vertically on the strain path. Geometries with a width of 125 mm or full geometry develop maintaining positive minor strain values. Therefore, the detection of the biaxial straining is more difficult by increasing sample width; since the positive contribution on the minor strain is summed to the further positive development of the strain path.

Even there are differences in behaviour by the geometries, the initial biaxial stretching seems to give a linear relationship between major and minor strain. Taking advantage of this aspect and due to the fact that the biaxial pre-stretching should be also linear, the strain path can be divided into a bilinear strain path. The transition between biaxial stretching and the linear strain path occurs gradually causing a non-linearity. However, the change in the path from the two linear developments is not relevant for the calculation of the biaxial pre-straining that precedes it. Thus, for the evaluation of the linear relationship, the Pearson correlation coefficient is used on the strain paths [113]. The Pearson correlation coefficient is the covariance of the two variables divided by the product of the standard deviation [123]:

$$\rho = \mathrm{Cov}(x,y)/(\sigma_x * \sigma_y) \tag{8}$$

The coefficient of correlation decreases by the transition from biaxial to linear strain path and therefore the maximum of its value, in which linearity is near to 1, corresponds to the last strain value under pre-straining. Figure 42-b shows the coefficient of correlation development for the strain path in Figure 42-a.

The hypothesis of strain path linearity is valid only at the top of the specimen. In general, points away from the centre have a non-linear development and their strain paths depend on the geometry and of course on the distance to the centre. For this reason, the DIN EN ISO 12004-2 limits the validity of a Nakajima test to specimens with a crack initiation at the top of the specimen or with a distance less than 15% of the punch diameter. With a punch of 100 mm, the limit is 15 mm distance from the centre. It is expected that the biaxial pre-stretching contribution will differ the more is the distance from the centre. However, as it can be noted in Figure 43, the biaxial contribution calculated with the coefficient of correlation does not take into account the transition part, in which the strain path at the centre and at 15 mm distance strongly differ. It demonstrates that the

method is still valid, even by crack initiation slightly away from the top of the specimen in the range of the test validity.

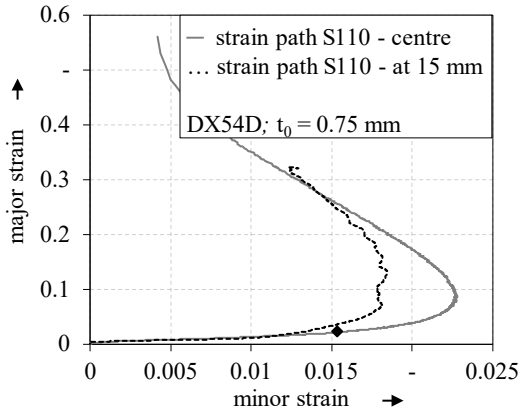


Figure 43: Strain path comparison in the region of validity for the geometry S110: at the centre of the specimen and at 15 mm distance[113].

Moreover, this evaluation method permits to consider the major and minor strain values directly on the strain paths, avoiding the simplification of perfect biaxial relation. In fact, as can be already qualitatively observed in Figure 42-a, the major and minor strain values at pre-straining, in contrast to Leppin et al. [84] that assumed ideally proportional strain paths. The reasons are several and summarised in Figure 44.

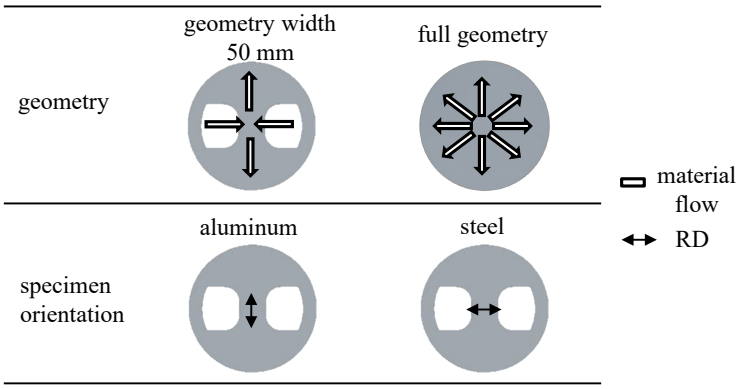


Figure 44: Material flow differences by Nakajima test considering the specimen geometry and orientation.

The specimen width influences the quantity of material that is in contact during the forming along the minor strain direction. Since, the test dimension does not change in the major stain direction, the material flow divergence between those direction increases by decreasing the specimen

width. As schematically depicted in Figure 44, the material flow on the full geometries is equal in all direction, omitting the material anisotropy. On the contrary in the geometry with 50 mm width the material in the forming zone is clamped only in the major strain direction. Thus, the material in the minor strain direction reaches the maximal contact area before than in the perpendicular direction. This circumstance causes that the forming continues in the major strain direction and the not clamped width tends to follow this flow contributing with a material movement from the edge to the centre of the specimen. The other geometries with a width between the extreme 50 mm and the full geometry exhibit a behaviour that looks alike the full geometry or the S050 geometry by increasing or decreasing the width, respectively. The above mentioned considerations do not consider the material anisotropy. However, it is well-know from literature that also the material anisotropy influences the material flow [124], which consequently changes in dependency to the orientation to the rolling direction. According to the standard [13], the specimen orientation is different for aluminium and steel alloy, as depicted in Figure 44. The specimen cut orientation is chosen in order to test the material preferred failure direction. In case of uncertainty the standard suggest defining it by conducting tensile tests. With exception to the full geometry, the principal forming direction is defined from the geometry, as above discussed. Thus, its orientation with respect to the rolling direction can be different for different materials. In conclusion, the combination of the geometry orientation and the material anisotropy, that basically describes the deviation in forming in the different material orientation, affects the material flow during Nakajima-tests. The influence of these two parameters is analysed in the next sections. The above presented method is used hereafter for the calculation of the pre-straining in the experimental as well as in numerical results.

## 7.2 Experimental analysis of biaxial pre-straining

For the evaluation of the linear relationship, the Pearson correlation coefficient is used, as described in the previous section. The outcomes from the experimental evaluation for the DX54D steel are listed in Table 17, together with the deviation between Nakajima and Marciniak FLC. As observed in

Figure 13, the FLC limits of this material are between 0.75 and 0.38 of major strains. The biaxial pre-straining for all geometries is limited between 0.008 and 0.022 that correspond of a 2% of the plane strain FLC point. As

expected, the difference of the FLC Nakajima values in comparison to the Marciniak outcomes show the higher value of minor strains and lower values by the major strain, proving a shifting of the curve in the right-down direction.

Table 17: Biaxial pre-straining in Nakajima tests and the difference of the results in term of major and minor strain between Marciniak and Nakajima result for the DX54D steel [113].

| **DX54D t0=0.75 mm** | | | | |
|---|---|---|---|---|
| **Geometry** | **Biaxial pre-straining** | | **Difference FLC Nakajima/Marciniak** | |
| | $\varepsilon_{1b}$ | $\varepsilon_{2b}$ | $\Delta\varepsilon_1$ | $\Delta\varepsilon_2$ |
| S050 | 0.017 | 0.008 | -0.071 | 0.084 |
| S110 | 0.022 | 0.015 | -0.058 | 0.107 |
| S125 | 0.022 | 0.018 | -0.040 | 0.091 |

The FLC deviation is not proportional and is different for the geometries. Moreover, the biaxial contribution on the major and minor strain direction is not equal. Similar results are achieved with the DP800 steel. The results of biaxial pre-straining and the deviations on major and minor strains of the Nakajima from the Marciniak setup are listed in Table 18. The biaxial pre-straining contribution is limited to a maximum of 0.020. However, the difference of FLC between Marciniak and Nakajima results show some discrepancies in comparison, showing higher major strain values by the Nakajima tests. This outcome can be explained considering the FLC evaluation method and the outcomes from section 5.

The DP800 steel does not show a clear onset of necking and its onset of instability is caused by the development of micro-cracks on the surface. Thus, the standard evaluation method based on the interpolation of the strain development on the section across the crack with a second order function shows for this material weakness. The evaluation of the biaxial pre-strain contribution using the coefficient of correlation is independent on the FLC evaluation and therefore gives the possibility to an objective quantification.

Table 18: Biaxial pre-straining in Nakajima tests and the difference of the results in term of major and minor strain between Marciniak and Nakajima result for the DP800 steel [113].

| **DP800 $t_0$=1.00 mm** | | | | |
|---|---|---|---|---|
| **Geometry** | **Biaxial pre-straining** | | **Difference FLC Nakajima/Marciniak** | |
| | $\varepsilon_{1b}$ | $\varepsilon_{2b}$ | $\Delta\varepsilon_1$ | $\Delta\varepsilon_2$ |
| S050 | 0.014 | 0.008 | -0.041 | 0.048 |
| S110 | 0.015 | 0.013 | 0.011 | 0.055 |
| S125 | 0.020 | 0.018 | 0.063 | 0.040 |

The values for the AA5182 aluminium alloy are listed in Table 19. In the case of the geometry S110, no valid Marciniak tests are achieved. The unstable behaviour of the material together with the high contact forces caused the crack initiation at the punch radius and thus no valid results obtained. That proves the Marciniak setups limitations, in particular for materials with instable peculiarities. The problematic of the PLC effects, however, should not compromise the biaxial pre-straining evaluation, since, as discussed previously, biaxial stresses limit the shear bands development.

Table 19: Biaxial pre-straining in Nakajima tests and the difference of the results in term of major and minor strain between Marciniak and Nakajima result for the AA5182 aluminium alloy [113].

| **AA5182 $t_0$=1.00 mm** | | | | |
|---|---|---|---|---|
| **Geometry** | **Biaxial pre-straining** | | **Difference FLC Nakajima/Marciniak** | |
| | $\varepsilon_{1b}$ | $\varepsilon_{2b}$ | $\Delta\varepsilon_1$ | $\Delta\varepsilon_2$ |
| S050 | 0.019 | 0.006 | -0.003 | 0.044 |
| S110 | 0.026 | 0.020 | - | - |
| S125 | 0.028 | 0.024 | -0.014 | 0.043 |

The biaxial pre-straining by the AA5182 aluminium alloy has a maximum of 0.028 and in general is higher than for the other two materials. Considering the comparison of the different materials according to the geometries depicted in Figure 45, this tendency is attested.

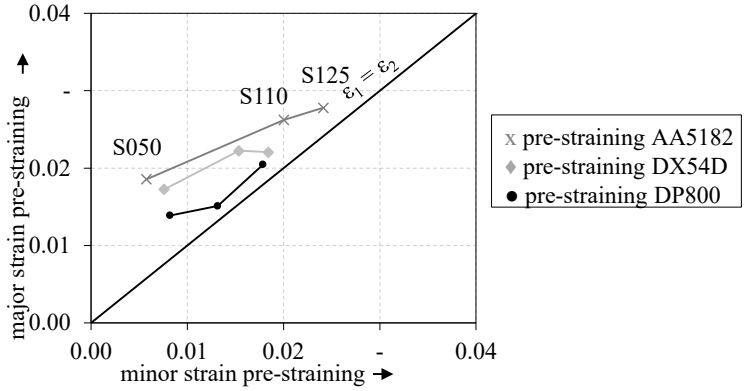


Figure 45: Comparison of the biaxial pre-straining for different materials and Nakajima geometries [113].

It can be attributed, above of other influencing parameters, to the different material hardening behaviours. The hardening plays an important role in the material flow in dependence on the applied forming force. For a

material with a high hardening behaviour, the material flow is impeded from the top to the periphery of the specimen and a higher force is required for further flowing. Therefore, the material is still stretched in both principal directions and the pre-straining increases. Considering the hardening exponent n for the investigated materials, the AA5182 aluminium alloy with n = 0.32 shows the highest pre-straining values.

The DX54D steel with n = 0.23 is followed by the DP800 steel with n = 0.16. The results are in good accordance with the conclusions regarding the general FLC in [85], in which the plane strain point of several materials is compared with the mechanical properties from tensile tests and show an increase of the FLC level by increasing the hardening exponent. The general effect of the hardening exponent is the increase of the FLC value, even by maintaining the other parameters constant, as numerically demonstrated by Hasek in [52].

Regarding the symmetry of the major and minor strain of the pre-straining, it can be observed that the outcomes for the major strains differ from the results for the minor strains. In particular, the assumption that the major strain is equal to the minor strain deviates the more the specimen width decreases. By the specimen S050, the contact area along the minor strain direction is limited and significantly smaller than the area available along the major strain direction. Therefore, the biaxial pre-straining in the minor strain direction is lower than by the major strain. Increasing the geometry width, the contact area is comparable in both directions and the pre-strain contribution tends to be symmetric.

The AA5182 aluminium alloy shows the highest deviation of biaxial symmetry compared with the DP800 steel and the DX54D steel. It may be explained considering the lower value of planar anisotropy of this material. The $\overline{R}$ value for the AA5182 aluminium alloy is lower than 1 and thus the material tends to flow more in the thickness direction than in width direction. Consequently, the strain in minor strain direction evolves slower than in major strain direction due to the compensation along the thickness, causing a lower value of pre-straining in width direction than in the length direction.

For the DX54D steel and the DP800 steel that shows an $\overline{R}$ value near 1 the pre-stretching remains symmetrical. In general, lower values of anisotropy lead with a shifting to the right of the strain path, as observed in [124] and discussed in [1] for the tensile test. This outcome is only apparently in contrast with what is affirmed here. The shifting of the paths to the right in the area of negative minor strain means that the material flows from

the width margin to the centre of the specimen is impeded and thus the strain path evolves faster in the major strain direction and thickness direction than in the width direction. As can be observed in Figure 46-a, the material flow in minor strain direction by the AA5182 aluminium alloy goes slower than by the DX54D steel and thus the minor strain distribution is asymmetric. In the area of positive major strain, in which the biaxial pre-stretching is located, the effect is the same.

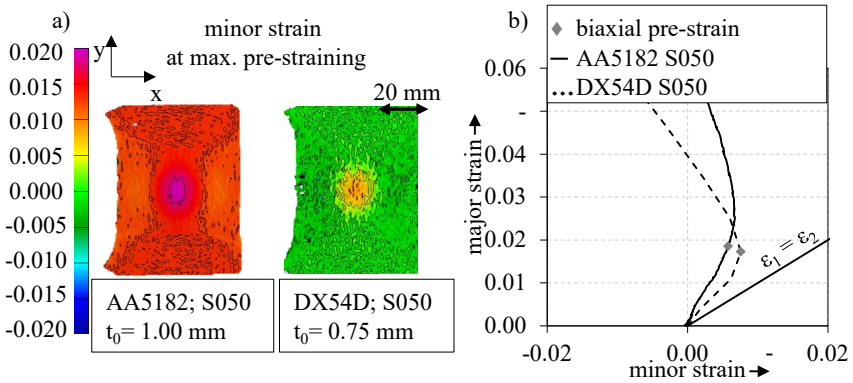


Figure 46: Comparison of the biaxial pre-straining by the geometry S050 for the AA5182 and the DX54D steel: a) minor strain distribution at maximal pre-straining; b) strain paths.

However, the minor strain values are positive and thus the shifting occurs in the other direction. By the comparison of the strain path for the geometry S050 in Figure 46-b, it is visible that the AA5182 aluminium alloy hereby reaches higher values of minor strain: the material flow from the periphery to the centre is hampered by the anisotropy and the compensation of the biaxial pre-straining takes more time. An additional confirmation can be observed by the transition zone between the pre-straining and linear path, which occurs smoothly by the AA5182 aluminium alloy than by the DX54D steel.

## 7.3 Numerical analysis of the biaxial pre-straining

The numerical approach for the investigation of the biaxial pre-stretching during Nakajima tests consents to evaluate the influence of the thickness by maintaining the same material characteristic. As mentioned above, the initial biaxial straining on the top of the specimen is caused by the increase of the contact area between punch and specimen and the consequent material flow from the top to the side.

The increase of the thickness does not change the contact area dimension, since the geometry width is the same. However, due to the increase of the distance between the contact area and specimen surface, the global displacement on the surface increases. Figure 47-a shows the difference on arc length on the surface that occurs by changing the sheet thickness.

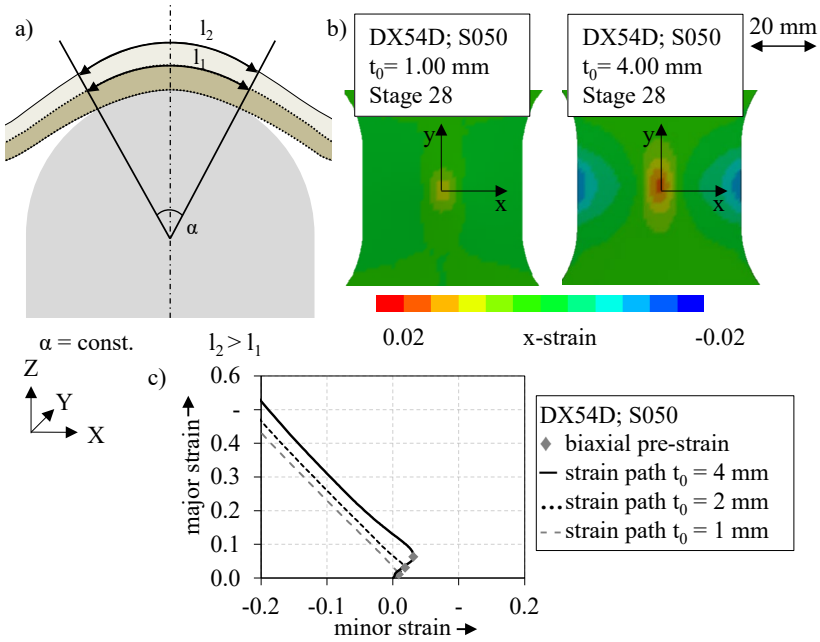


Figure 47: Increase of the biaxial pre straining by increasing the thickness: a) schematic representation; b) numerical comparison of the x-strain for the DX54D steel S050 geometry at the same stage; c) comparison of the strain paths and biaxial pre-straining.

The global development of the strain distribution in the geometry S050 is depicted in Figure 48 for the DX54D steel. Stage 54 represents the condition right after the maximum of the biaxial stretching. A positive stretching is visible on the top of the specimen and the periphery shows slight negative x-strain values. The strain path attests that the strain at the centre evolves to a lower, but positive value of minor strain.

At stage 81 the combination of the stretching and the compression on the periphery causes a zero minor strain at the centre. After this point, the minor strain value at the centre is also negative and the strain distribution shows the typical X pattern. The geometry S050 under near uniaxial tension condition shows a different value of pre-stretching for the major and minor strain.

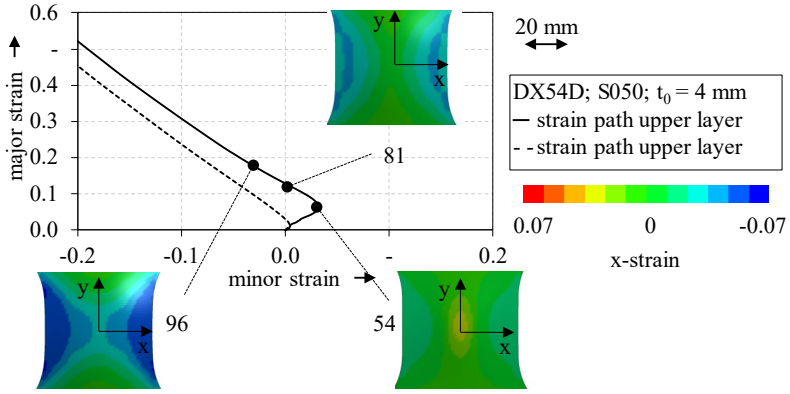


Figure 48: Strain path and x-strain distribution for the DX54D steel, geometry S050 with thickness $t_o$ = 4 mm.

Figure 49 shows the results for the various materials and thicknesses. At thickness 1 mm the values are in accordance with the experimental values depicted in Figure 45.

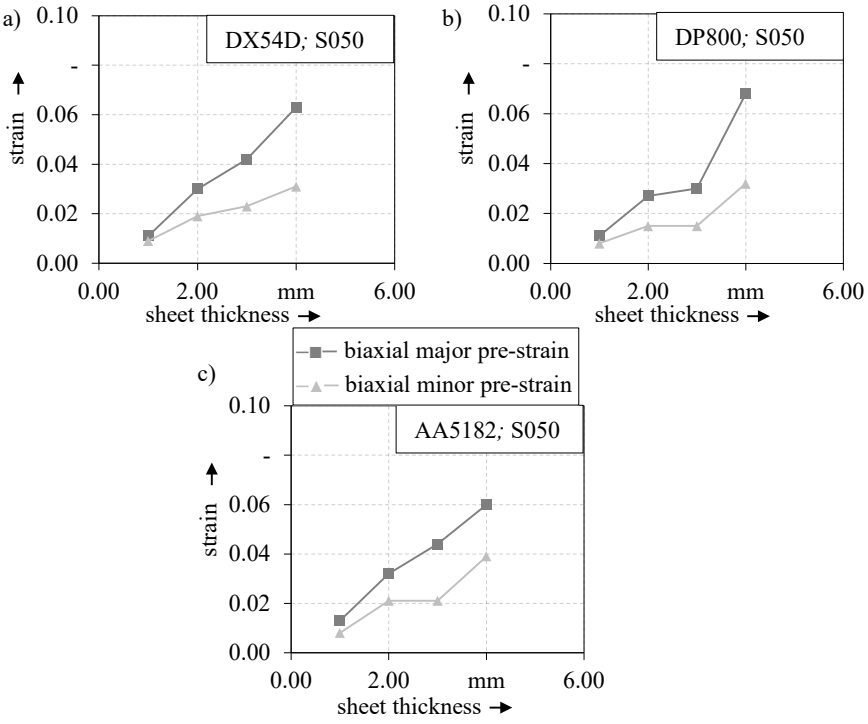


Figure 49: Biaxial pre-strain values for the geometry S050 calculated using the correlation coefficient for a) DX54D steel; b) DP800 steel; c) AA5182 aluminium alloy.

As expected, the pre-straining contribution increases with the thickness for all three materials. Moreover, the discrepancies between major and minor strain contribution increase also with the thickness. It can be explained considering the above-mentioned effect of an increase of the strained area at the surface by increasing the thickness. By higher thickness values the strained area is larger than by lower thickness. That means also that the width of 50 mm is rapidly under stress. Thus, the periphery starts earlier to undergo to negative minor strain and to influence the centre of the specimen, increasing the discrepancy of the strain distribution between major strain and minor strain direction.

The outcomes for the geometry S125 under near plane strain depicted in Figure 50 show that the low value of the planar anisotropy by the AA5182 aluminium alloy causes a discrepancy to the biaxial pre-strain behaviour. As mentioned above, the $\overline{R}$ value for the AA5182 aluminium alloy is lower than 1 and thus the material flow along the thickness is preferred than along the width.

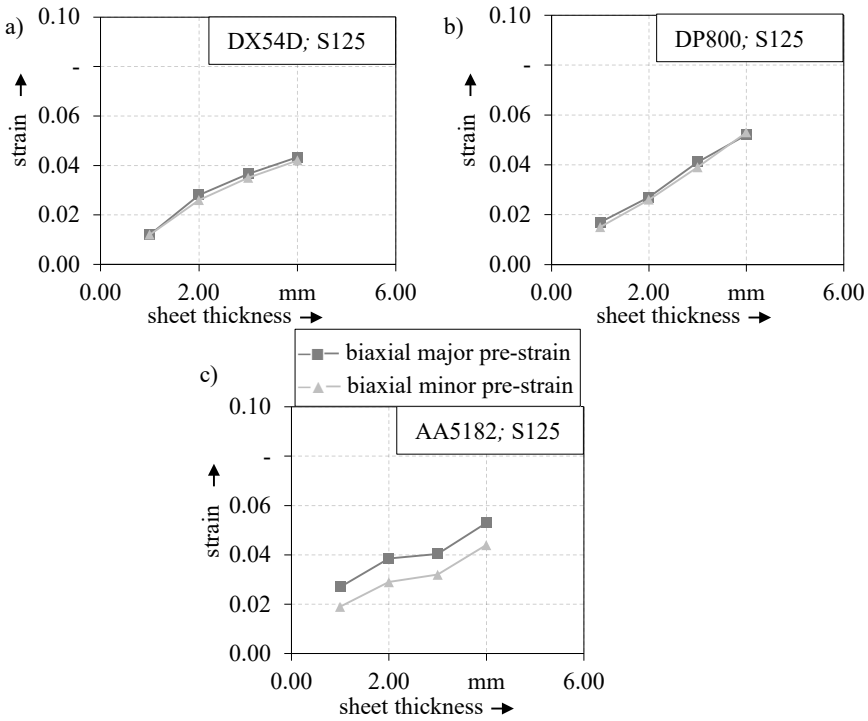


Figure 50: Biaxial pre-strain values for the geometry S125 calculated using the correlation coefficient for a) DX54D steel; b) DP800 steel; c) AA5182 aluminium alloy.

The minor strain direction evolves slower than in major strain direction and therefore discrepancies of the pre-straining values are observed. However, the difference is lower than by the geometry S050. It depends on the fact that the geometry this time has a width higher than the punch diameter. The strained surface area increases with the thickness but this time it does not reach the width margins. Thus, the periphery values in minor strain direction have the same influence of the periphery on the major strain direction thanks to the symmetry in the geometry. Continuing with the forming, the strain distribution on the width tends to a light compression form the margin to the top and thus the minor strain value is kept almost constant on the top of the specimen. The evaluation of the biaxial pre-stretching has been conducted considering the strain development on the surface. It implies that the quantification includes also the bending contribution. An alternative can be the correction of the bending effect and the successive evaluation of the biaxial pre-stretching, as investigated in [43]. The correction on the surface is equivalent to considering the strain distribution on the middle layers. However, since the biaxial pre-straining is observed basically on the surface and occurs simultaneously with the bending, the effect of the thickness in relation to the combination of the two effects should be investigated. In Figure 51 the strain path of the upper and middle layer are compared for the geometry S050 and S125, exemplary for the DX54D steel with a thickness of 2 mm. The stage for the biaxial pre-stretching evaluation is calculated with the coefficient correlation method on the surface. The same stage is considered in the middle layer. The method is still suitable even by considering the middle layer since the selected stage corresponds to the transition on the strain path also for this layer. Both geometries, however, shows higher values of biaxial pre-straining on the surface than on the middle layer.

That is attributable to the bending on the upper surface, that generally increases the strain level and development. Even if a pre-stretching is detectable on the middle layer, caution should be taken by considering a correction of the bending and successive evaluation of the pre-straining. On the one hand, in the hypothesis that the middle layer is bending-free, its position is shifted to an half of the thickness and thus the layer is no more representative. For example, considering the thickness of 2 mm, the middle layer should be positioned at 1 mm. However, the results of straining are not comparable with a material with thickness of 1 mm, since the middle layer would be shifted at 0.5 mm. On the other hand, the biaxial pre-stretching development can be different on the layers. By geometry S050, the middle layer evolves in a near plane strain condition with a biax-

ial pre-stretching of 0.003 minor strain. In Min et al. [83] the authors partially come to the same conclusion, calculating the strain considering the current curvature and thickness. They found that the middle surface goes into a compressive state, however considering it as a small error in the thickness calculation. The geometry S125 shows a positive biaxial pre-straining on both layers, proving that the dependence of the geometry on the effect as well as the no-symmetry of the stretching should not be ignored.

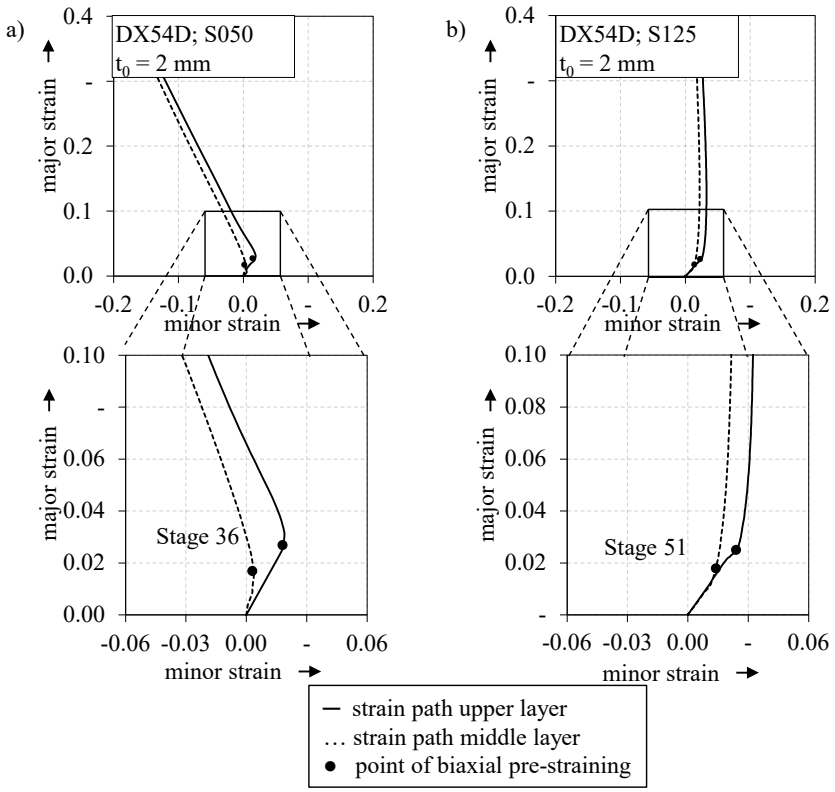


Figure 51: Comparison of pre-stretching on the upper and middle layer for the DX54D steel a) geometry S050 and b) geometry S125 with thickness $t_0$ = 2 mm

## 7.4 Summarizing evaluation and interpretation of the investigation

The biaxial pre-stretching is a process effect caused by the hemispherical punch form. The contact with the specimen evolves gradually from the middle point to higher contact surface with a maximum that depends on the geometry width. The evaluation of the biaxial pre-stretching at the

centre of the specimen by linear strain path is difficult since the transition from the pre-straining to the effective strain development due to the geometry occurs gradually, as observed in Figure 42. Moreover, the general assumption of ideally proportional strain paths by the pre-straining [84] is not always valid, in particular by materials with high hardening exponent (Figure 45).

In this section, an evaluation method based on the correlation coefficient has been proposed. Considering the linearity of the pre-straining, the coefficient of correlation calculated on the global strain path reaches a maximum value by the transition between the two developments. Regarding the influence of the material characteristics, such as the hardening exponent and the anisotropy coefficient, the results are in good accordance with the general effect on the forming limit curve observed in the literature. The increase of the hardening exponent implies an increase of the biaxial pre-straining contribution. Planar anisotropy values lower than 1 have the consequence to reduce the symmetry of the pre-straining in major and minor strain direction.

The material thickness not only influences the bending contribution, as observed in section 6 but also the pre-stretching. The effect is in general higher by higher thickness, due to the increase of the contact arc by constant contact angle. Moreover, the biaxial pre-stretching evaluated on the outer surface is always affected by the bending concurrence. The main investigated influencing parameters and their effects on the biaxial-pre straining by Nakajima tests are summarised in Table 20.

Table 20: Influencing parameters overview and their effects on the pre-straining by Nakajima test.

| influencing parameters | investigated range |
|---|---|
| anisotropy $\bar{R}$ | <1 → 1<br>pre-straining asymmetry decreasing |
| sheet thickness t | 0.75 mm → 4<br>pre-straining increasing |
| hardening exponent n | 0.16 → 0.32<br>pre-straining increasing |

In particular, the effect evaluation conducted in section 7 has pointed out, that the range of thickness in which the FLC is considered valid by the standard should be revised. Sheet metals from up to 4 mm not only may have different material characteristics due to different fabric procedures, but also have divergent forming limits due the thickness itself. In the

range of sheet thickness up to 2 mm the results deviation caused by the undesired effect of biaxial pre-straining is comparable with the standard deviation of the test. By higher value of thickness up to 4 mm the pre-straining as well as the bending seems to be no longer negligible and the effect on the FLC should be taken into account. The suggestion is to limit the validity of the FLC to 2 up to 3 mm, depending on the other two parameters. This statement appears acceptable, since the standard DIN EN ISO 6929 concerning sheet metals and plates set the validity of sheet definition limit to 3 mm [125]. Examples can be find also in the DIN EN 10130 [126]for cold rolled flat products and flat products with high yield strength DIN EN 10268 [127], as well as the standard for the tensile test DIN EN 6892-1 [6]. The validity limit should be defined also considering the hardening exponent as well as the anisotropy, as depicted in Table 20 and reduced to 2 mm for materials with high hardening exponent.

# 8 Scientific assessment of the results

In the present work, the investigation of the failure and necking behaviour during Nakajima tests has been conducted. It was possible to acquire a deeper knowledge of the material mechanism during the forming process, helping by the investigation of the sheet metal forming limit evaluation. The metallographic analysis conducted for different materials and forming levels pointed out that, in general, the material microstructure strongly influences the definition of onset of material instability. In particular, the investigations on the high strength steel and on the aluminium alloy show that the general definition of local necking used for the determination of the forming limit curve does not fit for brittle materials. Other phenomena such as the onset of micro-cracks or shear bands on the surface can be used for evaluating the forming limits. The analysis indicated that these mechanisms are recognizable in form of patterns on the surface as well as on the strain distributions. The classification of the materials patterns for the material investigated in the present work can be used for a new evaluation methodology of the forming limits based on pattern recognition. An automatic evaluation of patterns permits the usage of the whole strain distribution during the forming history, in contrast to the proposed method in the literature discussed in section 2. The main advantage is the direct evaluation of the necking using measured data. Moreover, the computer-aided evaluation contributes to avoiding user-dependence of the results.

In general, pattern recognition is a human capability and deals with the recognition of objects or patterns [128]. Computers can also acquire this ability and employ it in digital data. Even if pattern recognition belongs to engineering, it is often considered a branch of machine learning as computer science [129]. The development of the computational ability and of the computer technology has permitted the increase of the field of applications of pattern recognition. There are successful applications in data mining, biometrics, medical imaging and so on [128]. Even if each application has its peculiarities, the pattern recognition methodology can be summarised in 5 steps: data acquisition, pre-processing, feature extraction, classification and learning. The pipeline is schematically depicted in Figure 52 in the case of image recognition. After the image acquisition, the data are pre-processed with filters or adjustments that help in the recognition, such as the switch in grey levels or the interpolation of data for missing pixels. Afterwards, the data are derived and reduced by evalu-

ating characteristics or features of the labelled data. There are several feature descriptors, such as the histogram of oriented gradient (HoG) or the homogeneity. Further information can be found in the literature, for example in Nixon et al. [130]. Finally, the features are analysed and, based on the information of a learning process, in which similar data have been investigated and evaluated, classified [128]. The classification can occur with supervised or unsupervised techniques. The supervised techniques require a ground truth, namely an external definition of the searched classes. The unsupervised methodology does not require further information and defines the ground truth according to the whole data. Despite a large number of successful applications of pattern recognition, the application on forming processes has been missed. In 2015 Merklein et al. [131] investigated the possibility of using pattern recognition methods in sheet metal forming processes. The investigation started with the classification of crack initiation since its definition is clear and can be easily detected. The analysis covered seven Nakajima geometries for DC04 steel, with three test repetitions, in order to collect a database of images and strain distribution histories. The computer-aided procedure involved machine learning based on the database of the two classes: "failure" and "no failure". The teaching of the classification was made on two of the three repetitions; the third one was used as a control for the quality of the classification, as depicted in Figure 52.

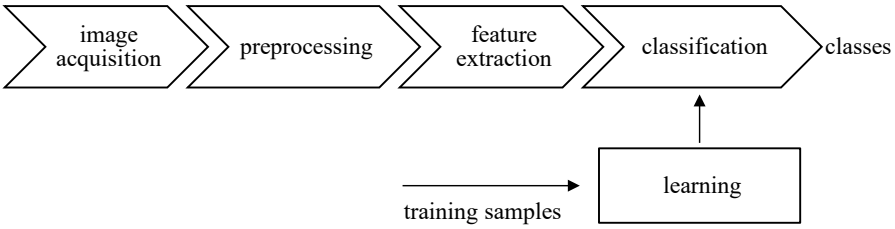


Figure 52: scheme of the pattern recognition procedure [131].

The training approach based on the random forest analysis [132] was conducted combining one sample per width and the available training data across all geometries. The prevision of the classification using only training data from the same sample was correct in 91.26% of the cases in average. The percentage of correct prevision by using all available training data across all sample types improved to 92.04%. It was pointed out, that the accuracy of the pattern recognition reaches good values in case of negative minor strain values, with an average of an absolute error of 2-3 frames instead of 7-8 frames for the geometries on the right side of the

FLC. The strain distribution under positive minor strains develops basically on diffuse necking with a stable and uniform distribution. The localisation and the crack initiation are limited to a few frames collected at the end of the test. There are less training data under unstable behaviour and the classification shows weaknesses. However, this contribution proved the potential of the application of pattern recognition technique for the analysis of the strain distribution during stretching in Nakajima tests.

The investigation continues focusing the classification on the more complex class "onset of necking". A possible way for the definition of the ground truth is the use of the experts' knowledge. Expert annotations are collected and employed to distinguish the different classes. Applications of this methodology can be found in Jaremenko et al. [133] for a medical application. Considering the Nakajima test, the deviation of the homogeneous forming can be interpreted as an anomaly and thus the onset of necking can be recognized. However, as observed during the metallographic analysis, an unequivocal definition of the onset of necking is not possible, since it depends on the material behaviours. Experts in the field of material characterisation are aware of the material behaviour differences and can give an estimation of the onset of necking by visioning the image data during Nakajima tests. They are researchers at the Institute of Manufacturing Technology of the Friedrich-Alexander Universität Erlangen-Nürnberg with at least 5 years experiences in the material characterisation. For the evaluation, they get the strain distribution data of the various materials and geometries and evaluate three classes: homogeneous distribution, the onset of diffuse necking, the onset of necking and crack. The definition of the classes is given by defining the time stage at which each class begins. Moreover, the experts get a guideline of the difference of classes based on the tensile test [134]. Of course, it is expected, that the division of classes according to the uniaxial tension condition fit for the geometries with a small width and the behaviour deviates by increasing the width. Moreover, as discussed in section 5, the definition of the onset of diffuse and local necking deviate for brittle materials. Finally, the strain behaviour is different, considering several strain paths. Also the expert annotations pointed out this heterogeneity. The crack class is well defined and the experts are in accordance. However, while for the uniaxial tension condition the deviation between the classes diffuse and local necking is low, geometries under plane or biaxial strain show discordance between the experts. Moreover, deviations of the interpretation of the classes between ductile and brittle material are observed. The classification is based on the ground truth collected with the majority of the expert annotations

and therefore, the low consistency of the expert decisions affects the evaluation. Considering the class "onset of necking", Figure 53 depicts the results of the expert annotations (experts) as well as the outcomes of the pattern recognition method according to the experts' knowledge and evaluated on other test repetitions using the random forest algorithm (RF experts). While the Experts points are the direct expert decisions for each test, the RF Experts points are obtained dividing the test in training set and test set. The experts' knowledge of the training set is then used for the classification of the test set. The classification is conducted using the random forests [132] algorithm. It is based on the principle of decision trees. Using the learning data set, decisions tree are built. At each node of the tree the data is separated in sub-sequence until no further separation is possible and a decision of class belonging is made. For more information about the random forest refers to [132].

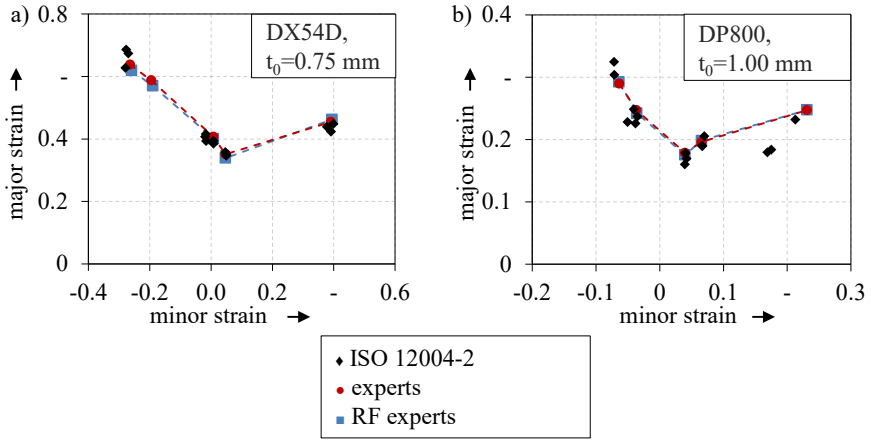


Figure 53: Forming limit evaluation using the pattern recognition method. Comparison of the standard method, experts' annotations and the random forest method based on the experts' interview for the a) DX54D steel and the b) DP800 steel.

It can be observed that despite some differences in expert decisions, the experts' evaluation of the onset of necking for the ductile DX54D steel is in accordance with the experimental results achieved with the standard method. The automatic pattern recognition based on this knowledge shows also comparable conclusions. In the case of the DP800 steel, the experts are in good accordance with the section method as well as with the pattern recognition method with a reduction of the standard deviation. By only using the specialists' knowledge, it is not possible to evaluate the quality of the ground truth, since the experts are affected by their subjectivity and errors can occur. Nevertheless, despite these limitations, the

results demonstrates that they are able to asses material changes during forming and that their annotation can be used for the evaluation of the forming limits using pattern recognition, without the limitation of the evaluation area (ISO method), or limitation on a particular principal strain evaluation (time-dependent methods) [134].

The achieved material mechanisms knowledge during Nakajima tests can be used hereby for the qualification of the pattern recognition methodology. In particular, this comparison is fundamental for the analysis of the results using the unsupervised pattern recognition methodology. The unsupervised pattern recognition does not require experts' annotation. Instead, it permits a probabilistic evaluation of the onset of necking using the achieved forming data. In [135], the One-Class Support Vector Maschine (SVM), based on the objective gradient information, is used [136]. The algorithm is trained on the material homogeneous behaviour (from 4 to 2 mm punch displacement before crack). The deviation from the expected range of gradient in the homogeneous strain distribution is interpreted as anomaly. The SVM values are considered in the time development and thus it is possible to evaluate the different levels of confidence scores assigned to the probability of necking with a GMM (Gaussian mixture model) [137], from <0.01 curve to >0.99. The results, together with the forming stages classified in section 5 are compared with the unsupervised pattern recognition methodology and the standard FLC. The results for the DP800 steel and DX54D steel are depicted in Figure 54.

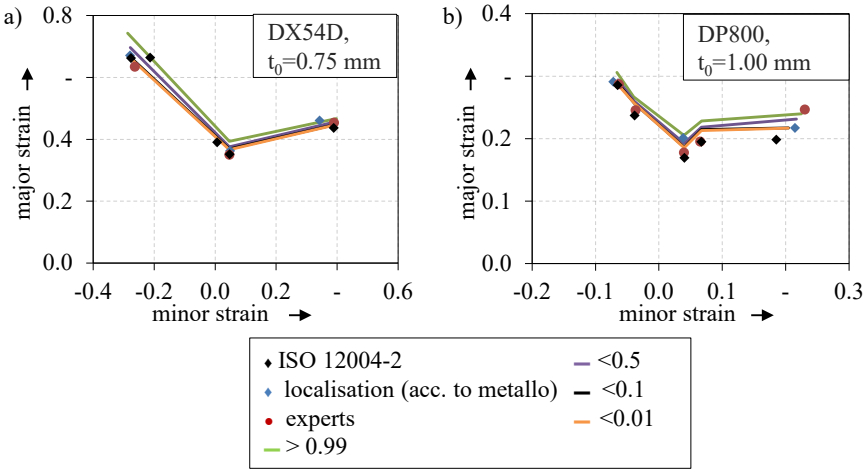


Figure 54: Results of the forming limit evaluation using different learning procedure for the a) DX54D steel and b) DP800 steel. Comparison between the standard method, the metallography knowledge, , the experts' annotations and the unsupervised pattern recognition method at different probability levels, according to [134].

As expected, for the ductile conventional steel, the conventional method predicts the onset of necking accordingly with the metallographic observations of localisation. The estimated probabilistic FLC is in good agreement for all geometries with the experts' annotation as well as with the standard method for the DX54D steel at quantile <0.01, with a slightly underestimation of 0.02 major strain value of the limit from the experts and the standard method compared to the 0.01 probability.

The steel DP800 shows good agreements of the results only for the geometry under uniaxial tension. Hereby, as observed in Section 5, the localisation occurs due to necking and therefore the experts, the standard method and the unsupervised evaluation of the FLC coincide. On the contrary, some divergences are observable for the other geometries. In plan strain condition, the metallographic observation corresponds to the probabilistic <0.5 curve. The experts as well as the ISO standard instead predict a lower limit, suggesting an underestimation of the forming limit. Under biaxial straining, the strain distribution is homogeneous on the surface most of the time and the main straining occurs in the thickness, due to the volume constancy. Therefore, the evaluation of onset of instability for this geometry is still challenging. Nevertheless, the experimental evaluation with metallography agrees with the quantile distribution, confirming that the unsupervised evaluation of the onset of instability is plausible.

The results of the random forest pattern recognition based on the metallographic analysis show that the experts make a conservative decision regarding the onset of instability by the DP800 steel. Moreover, the new method shows a significantly lower deviation in comparison with the standard method. As expected, the geometry under the biaxial condition is challenging, due to the high level of thinning and the consequent sudden crack. Further investigations have been conducted in [135] that tests the consistency of an unsupervised method. The evaluation, compared with the metallographic analysis, prove the qualification of the unsupervised method and give an overview of the level of development of the necking using quantiles.

In section 6 and 7, the undesired secondary effects of bending and biaxial pre-stretching caused by the hemispherical Nakajima punch have been discussed. Regarding the bending, the test setup does not allow a direct measuring of the strain distribution through the thickness. Moreover, the coexistence of stretching and bending makes the investigation of this effect hard. The bending depends on the combination of the punch curvature and the material thickness. The experimental evaluation of the influ-

ence of the punch radius has been conducted using a scaled setup. It has been proven that the scaled setups in the range in which the stretching is predominant are qualified for the evaluation of the forming limits as long as the relation between punch radius and die inner diameter and radius are respected. The effect of the thickness has been numerically investigated, in order to overcome the obstacle by the experimental measurements and also to maintain the material characteristics constant at the different thicknesses. Considering some simplification such as the elastic bending behaviour and the hypothesis that the middle layer is also the bending-free layer, the bending can be calculated as the difference between the outer layer and the middle layer strain. Of course, the bending increases by decreasing the punch diameter. However, the effect is under certain limits negligible. Firstly, the bending contribution is higher than 0.001, namely the experimental standard deviation, only up to a 2 mm thickness. For ductile materials, the thinning is higher and thus the difference between the layers is lower. In this case, a limit of 3 mm thickness can be reached. The validity limit of 4 mm given by the DIN EN ISO 12004-2 seems to be not appropriate. In addition, other standard regarding sheet metals and plate, like the DIN EN ISO 6929 [125] or the tensile test DIN EN 6892-1 [6] set the validity of sheet definition limit to 3 mm. Therefore the recommendation is to reduce the thickness limit by the FLC to 3 mm and give alternative test guidelines for thicknesses up to 4 mm. For example, if a brittle material with a thickness of 4 mm has to been tested, it could be recommended to use an up-scaled setup in order to limit the bending effect. Alternatively, a numerical analysis should be conducted, in order to evaluate the effect and eventually to provide a certain safety factor. In fact, the bending does not contribute to the necking and instead increases the general strain distribution. Thus, if the bending contribution is not negligible, the limits reached are higher than the limits reached by only stretching. The biaxial pre-stretching is caused by the increase of the contact surface between the sheet and the hemispherical punch.

The major effect on the FLC is the general shifting of the points to positive values of minor strain. Even if the effect should be ideally biaxial, namely equal in both principal directions, the investigations show a difference in the values between major and minor strain. For a quantitative evaluation of the phenomenon, a method based on the coefficient of correlation has been proposed. Knowing the strain path on the top of the specimen, the evaluation of the pre-stretching is possible. The pre-stretching causes, in general, a thinning and thus the reached limits val-

ues are lower than by pure linear stretching. Thus, a no consideration of this effect means an underestimation of the material forming potential. The experimental as well as the numerical analysis show that the pre-strain contribution increases with the thickness and the hardening exponent. In the investigated range between 0.16 and 0.32, it was observed, that a high hardening behaviour impedes the material flow from the top to the periphery of the specimen, increasing the required forming force. It causes the increase of the pre-straining force and therefore, for material with a high hardening exponent in the order of 0.3 the pre-straining component should be considered.

The contact area between punch and specimen depends only on the width and thus the thickness increase does not change its dimension. However, the distance between the contact area and specimen surface increases and the global displacement on the surface also rises. The dependency on the width has been also visible by investigating the different pre-stretching levels by the geometries. In general, the behaviour is more symmetrical by increasing the geometry width, namely increasing the geometry symmetry in the principal direction. However, it depends also on the material anisotropy. Lower values of planar anisotropy than 1 cause a material flow more in thickness than in width direction and thus the strain in width direction evolve slower than in the major strain direction due to the thickness compensation. Values of planar anisotropy near to 1 do not cause asymmetry on the strain distribution during pre-stretching.

The pre-stretching reaches, in general, no negligible levels. It should be taken into account, in particular for those applications, in which the full material potential is needed. By material characterisation, it should be given attention to the material hardening and anisotropy as well as the field of strain conditions that are required for the forming process. If the conditions are outside the limits defined in the present investigation, it is suggested to consider the employ of Marciniak tests or alternatively the application of an up-scaled setup. Summarizing the outcomes of the present investigation, a decision chart for the choice of the most appropriate test setup is presented in Figure 55. Regarding the material thickness, for ductile sheet the limit is set to 3 mm, while for brittle material a more conservative thickness of 2 mm should be considered. The second aspect is the hardening evaluation: for low value the standard Nakajima test can be used. For high value of n, like 0.32 for the investigated aluminium alloy AA5182, alternative setup should be considered, in which the pre-straining can be limited (scaled Nakajima test, Marciniak test, etc..).

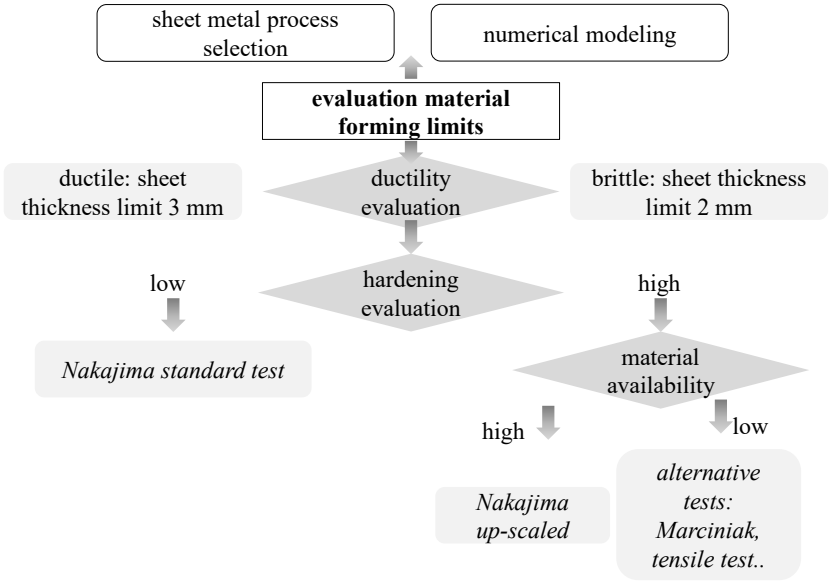


Figure 55: Decision chart for the most appropriate setup for the investigation of the sheet metal forming limits.

Besides the choice of the more appropriate test setups, the definition of the sheet metal forming limits is influenced by the evaluation method [46]. In particular, the conventional method prescribed in the DIN EN ISO 12004-2 seems to be not precise for brittle materials. The metallographic analysis conducted in section 5 indicates that the necking mechanisms are crucial for the correct definition of the forming limits. If the mechanisms are known or it is possible to conduct an investigation for a better understanding, the automatic evaluation of the forming limits using pattern recognition is possible.

The supervised determination can also be conducted if material characterisation experts are available. However, the definition of labels with experts' knowledge requires adequate time making this solution disadvantageous. As proposed in [135], the unsupervised analysis can be easily implemented and the validation can be carried on using metallography outcomes. The possible decision tree for the most appropriate evaluation method is depicted in Figure 56. It has to be noted, that until a new revision of the DIN EN ISO 12004-2, the standard method is still the cross-section method.

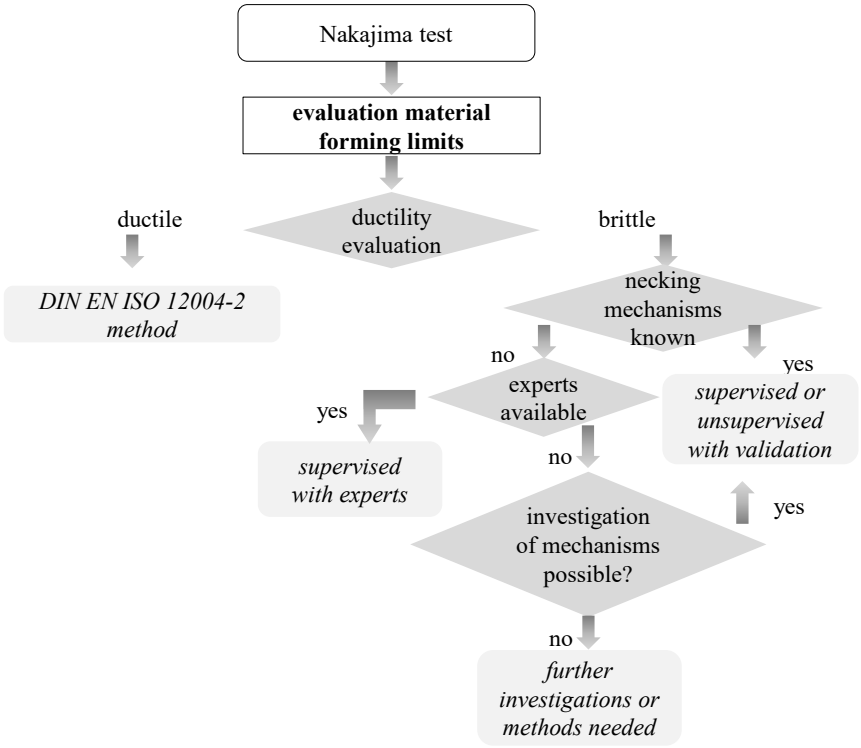


Figure 56: Decision chart for the most appropriate evaluation method for the determination of the forming limits in sheet metals using Nakajima tests.

On the light of the present investigation, a revision of the standard is suggested, in order to consider the pattern recognition as an alternative way to determine the onset of instabilities in sheet metals, in particular for brittle materials. Further investigations should be considered in order to guarantee the universality and the reliability of the method.

The decision charts suggested in Figure 55 and Figure 56 can be applied for the general evaluation of forming limit in the practice. Additionally, the pattern recognition method recommended in Figure 56 can be generally used in order to clearly define the safety margin required in the sheet metal forming production. In production application it is usual to use a safety factor on the FLC conventional estimation, typically 10% on the major stain [138]. Consequently, the production margins are further reduced. The probabilistic FLC mentioned above permits the calculation of the probability of necking instead, allowing more control on the applied safety factor. In Figure 57 the probabilistic FLC and the conventional FLC are compared in an experimental application. The used sample component is modified for academic use, it is not part of a series production and

it is based on a modified exhaust silencer using the deep drawing steel DX54D [43]. By a drawing depth of 73 mm and a blank holder force of 800 kN , the sample is free of failure [43]. Nevertheless, the thickness evaluation conducted with the optical measurement system ATOS (gom GmbH) shows a local thickness reduction.

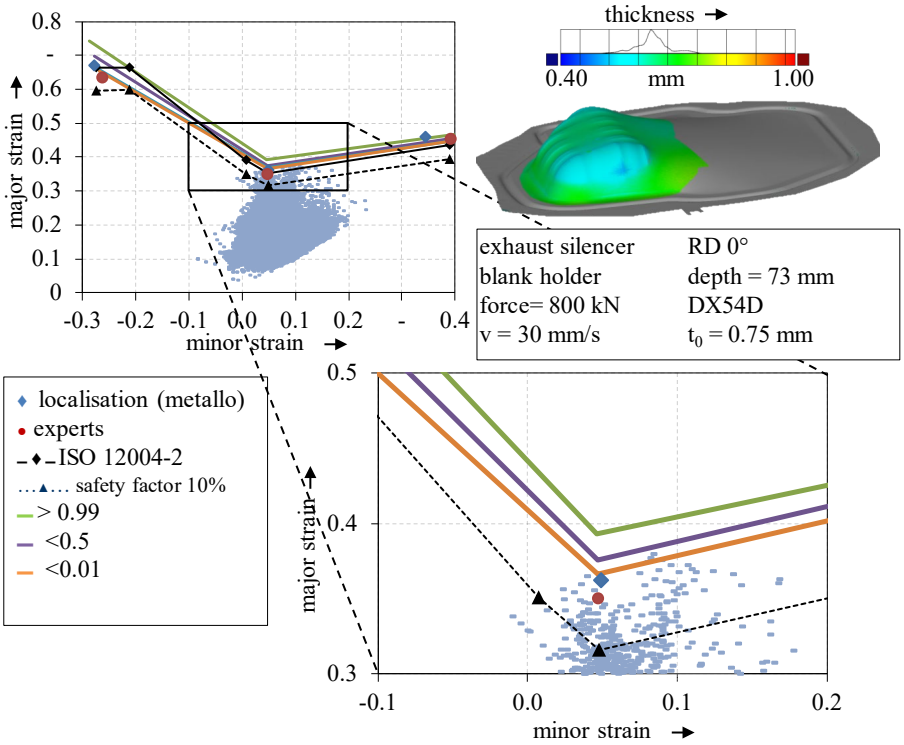


Figure 57: Experimental evaluation of the forming limit of a sample component for academic use according to [43]. The strain distribution is compared to the different FLC evaluation methods.

The experimental strain measurement can be used for the validation of the different FLC evaluations. The comparison confirms the slightly underestimation of the ISO method, since the curve is lower than the probabilistic FLC of 0.001. The limit values gained from the metallography and the experts' evaluation are in accordance with this necking probability. The sample strain value exceeds this curve confirming the onset of necking. That is also observable as a thinning on the sample thickness measurement. The curve with safety factor of 10%, for example, seems to underestimate the limit strains evaluation of 0.05 in comparison to the metallography evaluation and about 0.08 compared to the 0.99 probabil-

ity of necking. As it can be observed, the probabilistic FLC allows defining the safety grades, giving a more precise estimation compared to the normal safety factor of 10% applied in the industry and permits a better understanding of the effective process limit with a controlled estimation of risk.

# 9 Summary and future work

Sheet metal forming belongs to the key processes in the industrial production. The trends go to complex components designs and, in particular in the automotive industries, to lightweight structures. Therefore, the usage of the full formability potential of the employed materials is crucial for the process optimization with numerical analysis. The formability of sheet metals is commonly classified using the forming limit curve (FLC). The FLC collects the major and minor strain pairs at formability limit for different strain path condition. The standard for the testing, measurement and calculation is given by the DIN EN ISO 12004-2. It prescribes the use of a stretching test with a hemispherical Nakajima or a flat Marciniak punch. The forming limit is generally defined as the onset of necking. Thus, the standard evaluation method, based on the interpolation of the strain distribution along sections perpendicular to the crack initialisation, has been basically developed for ductile material, in which the instability corresponds with the localised necking. Thus, for lightweight and in general brittle materials, the method shows weaknesses. Moreover, also by using the standard procedure and setup, FLC results from diverse investigations show discrepancies, suggesting that process- as well as material-dependent parameters, have an influence.

In the present investigation, a detailed analysis of the Nakajima process and the failure mechanisms by different materials classes has been conducted. The objective was to analyse the validity of the FLC definition as the onset of necking also for no ductile material and to use the acquired knowledge for a correct estimation of the forming limits also for materials that do not show localisation. Finally, the investigation should clarify the limit of validity of the standard Nakajima test considering the material thickness and the setup dimension.

Firstly, a characterisation of the material mechanisms at the onset of necking has been conducted using metallography. Several deformation steps have been achieved and analysed in order to evaluate the onset of instability. For ductile materials, such as the DX54D steel, it coincides with the onset of necking, attesting the reliability of the standard method for ductile behaviour. For brittle materials, the onset of instabilities depends on the material structure. For the dual-phase steels, the instability is represented by micro-cracks on the surface that are also recognizable as multiple local maxima in the surface strain distribution. For the aluminium alloy AA5182, the sudden appearance of shear bands makes the evalu-

ation of limit strains hard. However, in the outcomes a trend is recognizable. The bandwidths decrease with the increase of the forming levels and a transition interpretable as the onset of necking is evaluable.

Secondly, an experimental and numerical analysis of the Nakajima test process has been presented. The attention has been focused on the two main effects of bending biaxial pre-stretching. The physical reason for their occurrence has been described and validated. The results indicate a dependence of the material characteristics as well as the strain path on the process effects. In contrast to the literature, it has been shown that some simplifications, such as the symmetrical nature of the pre-straining, as well as the standardisation of the FLC also for material thickness up to 4 mm, cause a deviation of the reached limits that should not be neglected.

Finally, the obtained knowledge has been used to define the validity window of the FLC and to optimize the evaluation of the forming limits, considering the peculiarities of the different material but without losing the universality of the FLC definition. The proposed method is based on the automatic pattern recognition method. Using the information of achieved forming level by the onset of instabilities, the method analyses the strain measurement coming from the optical measurement system and automatically classify the instability. The results are very promising not only using the classification of experts, as normally considered in the classical pattern recognition method but also using the new definition of the necking phases.

The present investigation opens new scenario for future research. Firstly, the transferability of the new evaluation method on other characterisations tests should be investigated. It is expected that for tests with linear strain development, such as tensile test, the classification of necking as well as the related pattern is still valid since the failure mechanisms are the same. More adjustments and adaptation will be required in case of more complex strain development, like out-of-plane condition, for example by bending or hole expansion tests. Secondly, further investigations are required by the validity of the necking phases by other materials with similar materials structures. Here the analysis should be focused on the possibility to group the materials per similar instabilities behaviour, in order to clarify if a generalisation is possible.

# 10 Zusammenfassung und Ausblick

Seit längerem geht der Trend in Richtung komplexer Komponentendesigns und insbesondere in der Autoindustrie hin zu Leichtbaustrukturen. Deshalb ist die Nutzung des vollen Potenzials des Formänderungsvermögens des genutzten Materials entscheidend für die Prozessoptimierung durch numerische Analyse. Das Formänderungsvermögen von Blechen wird dabei üblicherweise durch die Grenzformänderungskurve (GFK) klassifiziert. Die GFK sammelt die Haupt- und Nebenumformgradwerte beim Beginn der Materialinstabilität unter unterschiedliche lineare Dehnungshistorie. Der Standard für die Versuche, Messungen und die Evaluierung ist durch die DIN EN ISO 12004-2 festgelegt. Diese beschreibt den Gebrauch von Spannungstests mit einem hemisphärischen Nakajima- oder flachem Marciniak-Stempel. Die Formänderungsgrenzen sind dabei im Allgemeinen als Einschnürungsbeginn definiert. Somit ist die Standardmethode zur Evaluation, basierend auf der Interpolation der Spannungsverteilung entlang der Bereiche senkrecht zur Bruchinitiierung grundsätzlich für duktile Materialien entwickelt worden, bei denen die Instabilität mit dem lokal begrenzten Einschnürungsbeginn korrespondiert. Dementsprechend zeigt diese Methode für leichte und allgemein für spröde Materialien Schwächen auf. Zusätzlich zeigt die GFK auch beim Gebrauch des Standardverfahrens und -aufbaus bei unterschiedlichen Untersuchungen Diskrepanzen, die einen Einfluss von sowol verfahrens- als auch materialabhängigen Parametern nahelegen.

In der vorliegenden Untersuchung wurde eine detaillierte Analyse des Nakajima-Prozesses und der Versagensmechanismen bei verschiedenen Materialklassen durchgeführt. Ziel war es, die Gültigkeit der Definition der GFK als Einschnürungsbeginn für weniger duktile Materialien zu analysieren und das gewonnene Wissen für eine korrekte Vorhersage der Formänderungsgrenzen zu nutzen, die auch für Materialien gilt, die keine Lokalisierungen zeigen. Zuletzt sollte die Untersuchung die Grenzen der Gültigkeit des üblichen Nakajima-Versuchen unter Beachtung der Materialdicke und der Größe des Aufbaus aufzeigen.

Zuerst wurde eine Charakterisierung der Materialmechanismen beim Einschnürungsbeginn mittels Metallografie durchgeführt. Einige erreichte Deformationsstufen wurden analysiert um den Beginn von Instabilität zu ermitteln. Für duktile Materialien wie den DX54D fällt die Instabilität mit dem Einschnürungsbeginn zusammen, was die Zuverlässigkeit der Standardmethodik für duktiles Verhalten bestätigt. Bei weniger duktilen Ma-

terialien hängt der Beginn der Instabilität von der Materialstruktur ab. Für zweiphasige Stähle repräsentieren Mikrorisse auf der Oberfläche diese Instabilität, die ebenso als mehrere lokale Maxima in der Spannungsverteilung der Oberfläche erkennbar sind. Für die Aluminiumlegierung AA5182 erschwert das plötzliche Auftreten von Scherbändern die Evaluation. Die Bandbreite verringert sich mit steigendem Formänderungslevel und ein Übergang, der sich als Einschnürungsbeginn interpretieren lässt, ist nachweisbar.

Als nächstes wurde eine experimentelle und numerische Analyse des Nakajima-Versuchs präsentiert. Der Fokus lag hierbei auf den beiden Haupteffekten der biaxialen Vordehnung sowie der Biegung. Der physikalische Grund dafür ihres Auftretens konnte beschrieben und ausgewertet werden. Die Ergebnisse weisen auf einen Zusammenhang zwischen Materialcharakterisierungen so wie auch zwischen dem Spannungspfad und den Prozesseffekten auf. Der Literatur widersprechend konnte gezeigt werden, dass einige Vereinfachungen wie die symmetrische Natur der Vordehnung oder auch die Standardisierung der GFK - auch für Materialdicke bis zu 4 mm - eine Abweichung der erreichten Grenzen verursacht, die nicht vernachlässigt werden sollte.

Zuletzt wurden die gewonnenen Erkenntnisse genutzt, um ein Gültigkeitsfenster für die FLC zu definieren und die Evaluation der Formänderungsgrenzen zu optimieren, wobei die Besonderheiten der unterschiedlichen Materialien berücksichtigt wurden, ohne die universelle Gültigkeit der Definition der FLC aus den Augen zu verlieren. Die vorgeschlagene Methode basiert auf der automatischen Mustererkennung. Unter Verwendung der Informationen der erreichten Formänderungsgrenze nutzt die Mustererkennungsmethodik die Dehnungsmessungen, die vom optischen Messsystem geliefert werden und klassifiziert die Instabilität automatisch. Die Resultate sind äußerst vielversprechend, nicht nur bei Gebrauch der Klassifikation von Experten, wie in der klassischen Mustererkennungsmethode veranschlagt, sondern auch unter Gebrauch der neuen Definition der Einschnürungsphasen.

Die vorliegende Untersuchung eröffnet ein neues Szenario für künftige Forschung. Zunächst sollte nun die Übertragbarkeit der neuen Methodik auf anderen Charakterisierungsversuchen festgestellt werden. Es ist zu erwarten, dass bei Tests mit linearer Spannungsentwicklung, wie dem Zugversuch, die Einschnürungsklassifikation wie auch die zugehörigen Muster weiterhin ihre Gültigkeit behalten, da die Versagensmechanismen die gleichen sind. Im Fall komplexerer Spannungszustände würden weite-

re Abstimmungen und Anpassungen erforderlich werden, wie zum Beispiel durch Biegungs- oder Lochaufweitversuch. Daraufhin würden weitere Untersuchungen der Validität der Einschnürungsphasen mit weiteren Materialien mit ähnlichen Materialeigenschaften nötig werden. Dabei sollte die Analyse sich auf die Möglichkeit konzentrieren, die Materialien in Gruppen nach ähnlichem Instabilitätsverhalten aufzuteilen, um eine Generalisierung zu sichern.

# Bibliography


[1] Banabic, D.: Sheet Metal Forming Processes - Constitutive Modelling and numerical simulation. Springer, 2010

[2] Nakajima, K.; Kikuma, T.; Hasuka, K.: Study of formability of steel sheets. Yawata Tech Rep, (1968)264, pp. 8517–8530

[3] Marciniak, Z.: Stability of plastics shells under tension with kinematic boundary condition. Arciwum mechaniki stosowanej, (1965), pp. 577–592

[4] Buchfink, G.: Fascination of sheet metal - A material of limitless possibilities. Vogel Buchverlag, 2006

[5] Merklein, M.: Charakterisierung von Blechwerkstoffen für den LeichtbauMeisenbach, 2006

[6] DIN EN ISO 6892-1: Metallische Werkstoffe – Zugversuch – Teil 1: Prüfverfahren bei Raumtemperatur, 2017

[7] DIN EN ISO 16808: Metallische Werkstoffe – Blech und Band – Bestimmung der biaxialen Spannung/Dehnung-Kurve durch einen hydraulischen Tiefungsversuch mit optischen Messsystemen, 2014

[8] Gensamer, M.: Strength and ductility. Transactions of the A.S.M., (1946)36, pp. 30–60

[9] Col, A.: Forming limit diagrams: a survey. In: Banabic, D. (ed.): The 7th National Conference on Technologies and Machine-Tools for Cold Metal Forming, 2000, pp. 29–53

[10] Keeler, S. P.; Backofen, W. A.: Plastic instability and fracture in sheets stretched over rigid punches. ASM Trans Q., (1963)56, pp. 25–48

[11] Goodwin, G. M.: Application of Strain Analysis to Sheet Metal Forming Problems in the Press Shop. SAE Technical Paper, (1968)680093

[12] Col, A.: FLCs: past, present and future. In: Japanese Deep Drawing Researg Group; Japan Society for Technology of Plasticity; Iron and Steel Institute of Japan (eds.): Proceedings IDDRG 2002 - Information Technology, Global Enviroment and Sheet Metal Forming, 2002, pp. 107–125

[13] DIN EN ISO. 12004-2: Metallische Werkstoffe –Bleche und Bänder - Bestimmung der Grenzformänderungskurve –Teil 2: Bestimmung von Grenzformänderungskurven im Labor, 2008

[14] Hasek, V. V.: Untersuchung und theoretische Beschreibung wichtiger Einflußgrößen auf das Grenzformänderungsschaubild. Teil I. Blech Rohre Profile, (1978)25, pp. 213–220

[15] Hasek, V. V.: Untersuchung und theoretische Beschreibung wichtiger Einflußgrößen auf das Grenzformänderungsschaubild. Teil II. ASM Trans Q., (1978)25, pp. 285–292

[16] Müschenborn, W.; Sonne, H.-M.: Einfluß des Formänderungsweges auf die Grenzformänderungen des Feinblechs. Steel Research International, (1975)46, pp. 597–602

[17] Merklein, M.; Kuppert, A.; Affronti, E.: An Improvement of the Time Dependent Method Based on the Coefficient of Correlation for the Determination of the Forming Limit Curve. AMR 1018(2014), pp. 215–222

[18] Chu, T. C.; Ranson, W. F.; Sutton, M. A.; Peters, W. H.: Applications of digital-image-correlation techniques to experimental mechanics. Exp Mech, (1985)25, pp. 232–244

[19] Bruck, H. A.; McNeill, S. R.; Sutton, M. A.; Peters, W. H.: Digital image correlation using Newton-Raphson method of partial differential correction. Exp Mech 29(1989)3, pp. 261–267

[20] Luo, P. F.; Chao, Y. J.; Sutton, M. A.; Peters, W. H.: Accurate measurement of three-dimensional deformations in deformable and rigid bodies using computer vision. Exp Mech, (1993)33, pp. 123–132

[21] Galanulis, K.; Hofmann, A.: Determination of forming limit diagrams using an optical measurement system. In: Geiger, M.; Kals, H.; Shirvani, B.; Singh, U. P. (eds.): Proceedings of the 7th International Conference on Sheet Metal - SheMet'99. Meisenbach, 1999

[22] Lewison, D. J.; Lee, D.: Assessment of experimental methods for determination of forming limits. NUMISHEET 1999, (1999), pp. 401–406

[23] Vacher, P.; Haddad, A.; Arrieux, R.: Determination of the Forming Limit Diagrams Using Image Analysis by the Corelation Method. CIRP Annals - Manufacturing Technology 48(1999)1, pp. 227–230

[24] Liebertz, H.; Duwel, A.; Hotz, W.; Keeler, S. P.; Köhler, A.; Kroff, A.; Merklein, M.; Rauer, J.; Staubwasser, L.; Steinboch, G.; Vegter, H.: Guideline for the determination of forming limit curves. In: Kergen, R.; Keßler, L.; Langerak, N.; Lenze, F.-J.; Janssen, E.; Steinbeck, G. (eds.): Proceedings IDDRG 2004, 2004, pp. 216–224

[25] Feldmann, P.; Schatz, M.: Effective evaluation of flc-tests with the optical in-process strain analysis system Autogrid. In: Hora, P. (ed.): Numerical and Experimental methods in prediction of forming limits in sheet forming and tube hydroforming processes, 2006, pp. 69–73

[26] Friebe, H.; Galanulis, K.; Erne, O.; Müller, E.: FLC determination and forming analysis by optical measurement systems. In: Hora, P. (ed.): Proceedings of the FLC-Zurich, 2006, pp. 74–81

[27] Bragard, A.; Baret, J.-C.; Bonnarens, H.: Simplified Technique to Determine the FLD on the Onset of Necking. C.R.M., (1972)33, pp. 53–63

[28] Kobayashi, T.; Ishigaki, H.; Abe, T.: Effect of strain ratios on the deforming limit of steel sheet and its application to actual press forming. In: International Deep Drawing Research Group (ed.): Proceedings IDDRG 1972, 1972, pp. 8.1

[29] Marron, G.; Moinier, L.; Patou, P.; Celeski, J. C.: Un nouveau critere de striction pour les courbes limites de formage. Revue de Metallurgie, Cahiers d'Informations Techniques, (1997)6, pp. 837–845

[30] Janssens, K.; Lambert, F.; Vanrostenberghe, S.; Vermeulen, M.: Statistical evaluation of the uncertainty of experimentally characterised forming limits of sheet steel. Journal of Materials Processing Technology 112(2001)2-3, pp. 174–184

[31] Geiger, M.; Merklein, M.: Determination of forming limit diagrams – a new analysis method for characterization of materials' formability. CIRP Annals - Manufacturing Technology 52(2003)1, pp. 213–216

[32] Keeler, S. P.; Brazier, W. G.: Relationship between Laboratory Material Characterization and Press-shop formability. In: International Symposium on High Strength Low Alloy Steel (ed.): Micro Alloyng 75: Proceedings of an international symposium on high-strength, low-alloy steels, 1975, pp. 517–530

[33] The Auto/Steel Partnership Enhanced Forming Limit Diagram Projekt Team(ed.): Keeler, S. P.: Project Team Technology Report: The Enhanced FLC Effect(2003)

[34] Col, A.: FLCs: are we at turn? In: Boudeau, N. (ed.): Proceedings IDDRG 2005, 2005

[35] Hotz, W.: European efforts in standardisation of FLC. In: Hora, P. (ed.): Proceedings of the FLC-Zurich, 2006, pp. 24–25

[36] Hotz, W.; Timm, J.: Experimental determination of forming limit curves (FLC). In: Hora, P. (ed.): NUMISHEET 2008, 2008, pp. 271–278

[37] DIN EN ISO. 12004-1: Metallische Wertkstoffe- Bleche und Bänder-Bestimmung der Grenzformänderungskurve- Teil 1: Messung und Anwendung der Grenzformänderungsdiagrammen in Stanzreien, 2008

[38] Merklein, M.; Kuppert, A.; Mütze, S.; Geffer, A.: New Time dependent method for determination of FLC applied to SZBS800. Proc. 50th of IDDRG 2010, (2010), pp. 489–498

[39] Volk, W.: New experimental and numerical approach in the evaluation of the FLD with the FE-Method. In: Hora, P. (ed.): Proceedings of the FLC-Zurich, 2006, pp. 26–30

[40] Volk, W.; Hora, P.: New Algorithm for a robust user-independent evaluation of beginning instability for the experimental FLC determination. International Journal of Material Forming, (2011)3, pp. 339–346

[41] Volk, W.; Hora, P.: Evaluation of Experimental Forming Limit Curves and Investigation of Strain Rate Sensitivity for the Start of Local Necking. In: Kwansoo Chung; Heung Nam Han; Hoon Huh (Hrsg.). AIP, 2011, pp. 99–106

[42] Eberle, B.; Volk, W.; Hora, P.: Automatic approach in the evaluation of the experimental FLC with a full 2D approach based on a time depending method. In: Hora, P. (ed.): NUMISHEET 2008, 2008, pp. 279–284

[43] Europäische Forschungsgesellschaft für Blechverarbeitung e.V.(ed.): Merklein, M.; Affronti, E.; Volk, W.; Jocham, D.: Verbesserung der zeitlichen Auswertemethoden von Versuchen zur Ermittlung der

Grenzformänderung und Ableitung eines virtuellen Ersatzmodells - Nr.469. (2017)

[44] Sigvant, M.; Mattiasson, K.; Larsson, M.: The definition of incipient necjking and its impact on experimentally or theoretically determined forming limit curves. In: Asnafi, N. (ed.): Proceedings IDDRG 2008, Olofström, Sweden, 2008, pp. 207–218

[45] Merklein, M.; Kuppert, A.; Geiger, M.: Time dependent determination of forming limit diagrams. CIRP Annals - Manufacturing Technology 59(2010)1, pp. 295–298

[46] Hotz, W.; Merklein, M.; Kuppert, A.; Friebe, H.; Möller, T.; Klein, M.: Time dependent FLC Determination- comparison of different algorithms to detect the onset of unstable necking before fracture-necking before fracture. KEM, (2013)549, pp. 397–404

[47] Vysochinskiy, D.; Coudert, T.; Hopperstad, O. S.; Lademo, O.-G.; Reyes, A.: Experimental detection of forming limit strains on samples with multiple local necks. Journal of Materials Processing Technology 227(2016), pp. 216–226

[48] Hill, R.: On discontinuous plastic states, with special reference to localized necking in thin sheets. Journal of the Mechanics and Physics of Solids, (1952)1, pp. 19–30

[49] Marciniak, Z.; Kuczynski, K.: Limit strains in the process of stretch-forming sheet metal. International Journal of Mechanical Science, (1967)9, pp. 609–620

[50] Hutchinson, J. W.; Neale, K. W.: Sheet necking-II. Time-independent behavior. Mechanics of sheet metal forming, (1978), pp. 127–153

[51] Hutchinson, J. W.; Neale, K. W.: Sheet necking-III. Strain-rate effects. Mechanics of sheet metal forming, (1978), pp. 269–285

[52] Hasek, V. V.: Untersuchung und theoretische Beschreibung wichtiger Einflußgrößen auf das Grenzformänderungsschaubild. Teil III. Blech Rohre Profile, (1978)25, pp. 493–499

[53] Chan, K. S.: Effects of plastic anisotropy and yield surface shape on sheet metal stretchability. Metallurgical Transactions A, (1985)16A, pp. 629–639

[54] Butuc, M. C.: A more general model for forming limit diagrams prediction. Journal of Materials Processing Technology, (2002)125, pp. 213–218

[55] Butuc, M. C.; Gracio, J. J.; Barata da Rocha, A.: A theoretical study on forming limit diagrams prediction. Journal of Materials Processing Technology 142(2003)3, pp. 714–724

[56] Aretz, H.: Numerical analysis of diffuse and localized necking in orthotropic sheet metals. International Journal of Plasticity 23(2007)5, pp. 798–840

[57] Banabic, D.; Aretz, H.; Comșa, D. S.; Paraianu, L.: An improved analytical description of orthotropy in metallic sheets. International Journal of Plasticity 21(2005)3, pp. 493–512

[58] Barlat, F.; Brem, J. C.; Yoon, J.-W.; Chung, K.; Dick, R. E.; Lege, D. J.; Pourboghrat, F.; Choi, S.-H.; Chu, E.: Plane stress yield function for aluminum alloy sheets—part 1: theory. International Journal of Plasticity 19(2003)9, pp. 1297–1319

[59] Banabic, D.: A review of recent developments of the MK model. Computer Methods in Materials Science, (2010)10, pp. 225–317

[60] Hora, P.; Tong, L.: Theoretical prediction of the influence of curvature and thickness on the FLC by the enhanced modifies maximum force criterion. In: Hora, P. (ed.): NUMISHEET 2008, 2008, pp. 205–210

[61] El-Magd, E.; Gese, H.; Tham, R.; Hooputra, H.; Werner, H.: Fracture Criteria for Automobile Crashworthiness Simulation of Wrought Aluminium Alloy Components. Mat.-wiss. u. Werkstofftech. 32(2001)9, pp. 712–724

[62] Stören, S.; Rice, J. R.: Localized necking in thin sheets. Journal of the Mechanics and Physics of Solids, (1975)23, pp. 421–441

[63] Ghosh, A. K.: A Criterion for ductile fracture in sheets under biaxial loading. Metallurgical Transactions A, (1976)7, pp. 523–533

[64] Arrieux, R.: Determination and use of the forming limit stress diagrams in sheet metal forming. Journal of Materials Processing Technology 53(1995)1-2, pp. 47–56

[65] Nhat, T. N.; Arrieux, R.: Off-axes forming limit stress diagrams of an anisotropic steel sheet. Materials Processing Technology, (1995)54, pp. 193–198

[66] Arrieux, R.: Determination and use of the forming limit stress surface of orthotropic sheets. Journal of Materials Processing Technology, (1997)64, pp. 25–32

[67] Bleck, W.; Deng, Z.; Papamantellos, K.; Gusek, C. O.: A comparative study of the forming-limit diagram models for sheet steels. Journal of Materials Processing Technology 83(1998)1-3, pp. 223–230

[68] Swift, H. W.: Plastic instability under plane stress. Journal of the Mechanics and Physics of Solids, (1952)1, pp. 1–18

[69] Levy, S. B.: A comparison of empirical forming limit curves for low carbon steel with theoretical forming limit curves of Ramaekers and Bongaerts. In: Tisza, M. (ed.): Proceedings IDDRG 1996, 1996

[70] Cayassials, F.: A new method for predicting FLC. In: CRM; Benelux Deep Drawing Research Group (eds.): Proceedings of IDDRG 1998, 1998, pp. 443–454

[71] Taylor, L.; Cao, J.; Karafillis, A. P.; Boyce, M. C.: Numerical simulations of sheet-metal forming. Journal of Materials Processing Technology 50(1995)1-4, pp. 168–179

[72] Ozturk, F.; Lee, D.: Experimental and numerical analysis of out-of-plane formability test. Journal of Materials Processing Technology 170(2005)1-2, pp. 247–253

[73] Petek A.; Pepelnjak, T.; Kuzman, K.: An improved method for determining a forming limit diagram in digital environment. Journal of Mechanical Engineering, (2005)51, pp. 330–345

[74] Pepelnjak, T.; Kuzman, K.: Determination of forming limit diagrams in cae environment. In: Kuzman, K. (ed.): 5th International Conference on Industrial Tools, 2005, pp. 375–378

[75] Mishra, S. K.; Desai, S. G.; Pant, P.; Narasimhan, K.; Samajdar, I.: Improved predictability of forming limit curves through microstructural inputs. International Journal of Material Forming, (2009)2, pp. 59–67

[76] Hill, R.: A theory of yielding and plastic flow of anisotropic metals. Proc. Roy. Soc. London A, (1948)193, pp. 281–297

[77] Barlat, F.; Lege, D. J.; Brem, J. C.: A six-component yield fucntion for anisotropic materials. International Journal of Plasticity, (1991), pp. 693–712

[78] Mattiasson, K.; Jergeus, J.; Dubois, P.: Models for strain path independent necking prediction in LS-DYNA: 9th European LS-DYNA Conference 2013, 2013

[79] Charpentier, P. L.: Influence of punch curvature on the stretching limits of sheet steel. Metallurgical Transactions A, (1977)6A, pp. 1665–1669

[80] Marciniak, Z.: Sheet metal forming limits. Mechanics of Sheet Metal Forming: Material Behaviour and Deformation Analysis, (1978), pp. 215–236

[81] Merklein, M.: Fundamental investigations concerning forming limit diagrams. In: Kiuchi, M.; Nishimura, H.; Yanagimoto, J. (eds.): Advanced Technology of Plasticity, Proceedings of the 7th ICTP, 2002, pp. 1543–1548

[82] Volk, W.; Gaber, C.: Investigation and Compensation of Biaxial Prestrain During the Standard Nakajima- and Marciniak-test Using Generalized Forming Limit Concept. Procedia Engineering 207(2017), pp. 568–573

[83] Min, J.; Stoughton, T. B.; Carsley, J. E.; Lin, J.: Compensation for process-dependent effects in the determination of localized necking limits. International Journal of Mechanical Science 117(2016), pp. 115–134

[84] Leppin, C.; Li, J.; Daniel, D.: Application of a method to correct the effect of non-proportional strain paths on Nakajima test based forming limit curves. In: Hora, P. (ed.): NUMISHEET 2008, 2008, pp. 217–221

[85] Abspoel, M.; Scholting, M. E.; Droog, J. M.: A new method for predicting Forming Limit Curves from mechanical properties. Journal of Materials Processing Technology 213(2013)5, pp. 759–769

[86] Stoughton, T. B.; Yoon, J. W.: Path independent forming limits in strain and stress spaces. International Journal of Solids and Structures 49(2012)25, pp. 3616–3625

[87] Smith, P. E.; Lee, D.: Determination of forming limits for aluminum alloys. SAE Technical Paper, (1998), pp. 121–127

[88] Dilmec, M.; Halkaci, H. S.; Ozturk, F.; Livatyali, H.; Yigit, O.: Effects of sheet thickness and anisotropy on forming limit curves of AA2024-T4. Int J Adv Manuf Technol 67(2013)9-12, pp. 2689–2700

[89] Merklein, M.; Affronti, E.; Steiner, J.: Numerical Investigation of Dry and Lubricated Sheet Metal Forming Processes. KEM 651-653(2015), pp. 1029–1035

[90] Kuppert, A.: Erweiterung und Verbesserung von Versuchs- und Auswertetechniken für die Bestimmung von Grenzformänderungskurven: Bericht aus dem Lehrstuhl für Fertigungstechnologie Prof. Dr.-Ing. habil. Marion Merklein (Hrsg.): Fertigungstechnik - Erlangen, Meisenbach GmbH Verlag, 2015

[91] Hiroi, T.; Nishimura, H.: The influence of surface defects on the forming-limit diagram of sheet metal. Journal of Materials Processing Technology 72(1997)1, pp. 102–109

[92] Becker, R.: Effects of strain localization on surface roughening during sheet forming. Acta Materialia, (1998)4, pp. 1385–1401

[93] Al-Qureshi, H. A.; Bressan, J. D.: Investigation of the degree of biaxiality on the limit strains in sheet metal stretching. In: Pennsylvania State University (ed.): Proceedings of the Ninth North American Manufacturing Research Conference, 1981, pp. 538–543

[94] Xavier, M. D.; Lima, N. B. de; Plaut, R. L.; Schön, C. G.: Strain path dependence of the FLCo formability parameter in an interstitial free steel. Int J Adv Manuf Technol 80(2015)5-8, pp. 1077–1085

[95] Jocham, D.; Volk, W.: Numerical determination of the onset of local necking using time dependent evaluation method and dynamic material parameters. J. Phys.: Conf. Ser. 734(2016), pp. 32015

[96] Volk, W.; Suh, J.: Reliable and robust evaluation of local necking with a generalized thinning limit diagram. In: Hora, P. (ed.): Proceedings of 5th Forming Technology Forum, 2012, pp. 115–120

[97] Xavier, M. D.; Plaut, R. L.; Schön, C. G.: Uniaxial near plane strain tensile tests applied to the determination of the FLCo formabillity parameter. Mat. Res. 17(2014)4, pp. 982–986

[98] Tasan, C. C.; Hoefnagels, J. P. M.; Horn, C. t. H.; Geers, M. G. D.: Experimental analysis of strain path dependent ductile damage mechanics and forming limits. Mechanics of Materials 41(2009)11, pp. 1264–1276

[99] Tasan, C. C.; Hoefnagels, J. P. M.; Dekkers, E. C. A.; Geers, M. G. D.: Multi-Axial Deformation Setup for Microscopic Testing of Sheet Metal to Fracture. Exp Mech 52(2012)7, pp. 669–678

[100] Tasan, C. C.; Hoefnagels, J. P. M.; Diehl, M.; Yan, D.; Roters, F.; Raabe, D.: Strain localization and damage in dual phase steels investigated by coupled in-situ deformation experiments and crystal plasticity simulations. International Journal of Plasticity 63(2014), pp. 198–210

[101] Jocham, D.; Norz, R.; Volk, W.: Strain rate sensitivity of DC06 for high strains under biaxial stress in hydraulic bulge test and under uniaxial stress in tensile test. Int J Mater Form, (2016)10, pp. 453–461

[102] TATA Steel(ed.): Abspoel, M.; Atzema, E. H.; Droog, J. M.; Khandeparkar, T.; Scholting, M. E.: Inherent influence of strain path in Nakazima FLC - Report. (2011)

[103] Volk, W.; Suh, J.: Prediction of formability for non-linear deformation history using generalized forming limit concept (GFLC). AIP, 2013, pp. 556–561

[104] Stoughton, T. B.; Carsley, J. E.; Min, J.; Lin, J.: Advances in characterization of sheet metal forming limits. J. Phys.: Conf. Ser. 734(2016), pp. 32073

[105] Al-Qureshi, H. A.; Klein, A. N.; Fredel, M. C.: Grain size and surface roughness effect on the instability strains in sheet metal stretching. Journal of Materials Processing Technology 170(2005)1-2, pp. 204–210

[106] Ghadbeigi, H.; Pinna, C.; Celotto, S.; Yates, J. R.: Local plastic strain evolution in a high strength dual-phase steel. Materials Science and Engineering: A 527(2010)18-19, pp. 5026–5032

[107] Merklein, M.; Hofmann, M.: Optimierung und Standardisierung des Zugversuchs mit miniaturisierten Proben zur verbesserten Charakterisierung lokaler Eigenschaften von Bauteilen aus Feinblech - Nr. 467, 2017

[108] DIN EN. 10346: Kontinuierlich schmelztauchveredelte Flacherzeugnisse aus Stahl zum Kaltumformen –Technische Lieferbedingungen, 2015

[109] Picu, R. C.; Vincze, G.; Ozturk, F.; Gracio, J. J.; Barlat, F.; Maniatty, A. M.: Strain rate sensitivity of the commercial aluminum alloy AA5182-O. Materials Science and Engineering: A 390(2005)1-2, pp. 334–343

[110] DIN EN. 573-3: Aluminium und Aluminiumlegierungen- Chemische Zusammensetzung und For von Halbzeug- Teil 3: Chemische Zusammensetzung und Erzeugnisformen, 2009

[111] Hockett, J. E.; Sherby, O. D.: Large strain deformation of polycrystalline metals at low homologous temperatures. Journal of the Mechanics and Physics of Solids, (1975)23, pp. 87–98

[112] Pepelnjak, T.; Petek A.; Kuzman, K.: Analyses of the forming limit diagram in digital environment. Trans Tech Publications, (2005)6, pp. 697–704

[113] Affronti, E.; Merklein, M.: Analysis of the bending effects and the biaxial pre-straining in sheet metal stretch forming processes for the determination of the forming limits. International Journal of Mechanical Sciences 138-139(2018), pp. 295–309

[114] Ahmadi, S.; Eivani, A. R.; Akbarzadeh, A.: Experimental and analytical studies on the prediction of forming limit diagrams. Computational Materials Science, (2009)44, pp. 1252–1257

[115] Tvergaard, V.; Needleman, A.; Lo, K. K.: flow localization in the plane strain tensile test. Journal of the Mechanics and Physics of Solids, (1981)29, pp. 115–142

[116] Romhanji, D.; Glisic, D.; Popovicm M.; Milenkovic, V.: Stress state effect on dynamic strain aging and surface markings during stretching of AlMg7 alloy sheet. Materials Science Forum, (1998)282-283, pp. 309–314

[117] thyssenkrupp Steel Europe AG: Deep-drawing steels DD, DC and DX Product information. URL: https://www.thyssenkrupp-steel.com/media/content_1/publikationen/produktinformationen/dd_dx_dc/thyssenkrupp_dd-dc-dx_product_information_steel_en.pdf

[118] Affronti, E.; Merklein, M.: Metallographic Analysis of Nakajima Tests for the Evaluation of the Failure Developments. Procedia Engineering 183(2017), pp. 83–88

[119] Affronti, E.; Weidinger, M.; Merklein, M.: Metallographic analysis of failure mechanisms during Nakajima tests for the evaluation of forming limits on a dual-phase steel. IOP Conf. Ser.: Mater. Sci. Eng., (2018)418, pp. 12047

[120] Halim, H.; Wilkinson, D. S.; Niewczas, M.: The Portevin–Le Chatelier (PLC) effect and shear band formation in an AA5754 alloy. Acta Materialia 55(2007)12, pp. 4151–4160

[121] Yilmaz, A.: The Portevin-Le Chatelier effect: a review of experimental findings. Science and technology of advanced materials 12(2011)6, pp. 63001

[122] Hezler, C.; Merklein, M.; Hecht, J.; Griesbach, B.: Identification of process-based limit stress states applying a stretch-bending-test: Key Engineering Materials; Material Forming ESAFORM 2012, pp. 47–52

[123] Pearson, K.: Notes on regression and inheritance in the case of two parents. Proceedings of the Royal Society of London, (1895)58, pp. 240–242

[124] Rault, D.: Mise en Forme des Métaux et AlliagesCentre National de la Recherche Scientifique, 1976

[125] ISO 6929:2013: Steel products- Vocabulary,

[126] DIN EN 10130:2006: Kaltgewalzte Flacherzeugnisse aus weichen Stählen zum Kaltumformen – Technische Lieferbedingungen;,

[127] DIN EN 10268:2006+A1:2013: Kaltgewalzte Flacherzeugnisse aus Stählen mit hoher Streckgrenze zum Kaltumformen – Technische Lieferbedingungen;,

[128] Dougherty, G.: Pattern recognition and classification - An introduction. Springer, 2013

[129] Bishop, C. M.: Pattern Recognition and Machine LearningSpringer, 2006

[130] Nixon, M. S.; Aguado, A. A.: Feature extraction and image processing for computer visionAcademic Press, 2012

[131] Merklein, M.; Maier, A.; Kinnstätter, D.; Jaremenko, C.; Affronti, E.: A New Approach to the Evaluation of Forming Limits in Sheet Metal Forming. KEM 639(2015), pp. 333–338

[132] Breiman, L.: Random Forests. Maschine Learning, (2001)45, pp. 5–32

[133] Jaremenko, C.; Maier, A.; Steidl, S.; Hornegger, J.; Oetter, N.; Knipfer, C.; Stelzle, F.; Neumann, H.: Classification of Confocal Laser Endomicroscopic Images of the Oral Cavity to Distinguish Pathological from Healthy Tissue. In: Handels, H.; Deserno, T. M.;

Meinzer, H.-P.; Tolxdorff, T. (Hrsg.). Springer Berlin Heidelberg, 2015, pp. 479–485

[134] Affronti, E.; Jaremenko, C.; Merklein, M.; Maier, A.: Analysis of forming limits in sheet metal forming with pattern recognition methods. Part 1: characterization of onset of necking and expert evaluation. Materials, (2018)11

[135] Jaremenko, C.; Affronti, E.; Maier, A.; Merklein, M.: Analysis of Forming Limits in Sheet Metal Forming with Pattern Recognition Methods. Part 2: Unsupervised Methodology and Application. Materials, (2018)11, pp. 1892

[136] Schölkopf, B.; Platt, J. C.; Shawe-Taylor, J.; Smola, A. J.; Williamson, R. C.: Estimating the support of a high-dimensional distribution. Neural Comput., (2001)13, pp. 1443–1471

[137] Titterington; D.M.; Smith, A.; Makov, U. E.: Statistical analysis of finite mixture distributionsChichester, 1985

[138] Davim, J. P.(ed.): Introduction to mechanical engineeringSpringer, 2018

## Own publications referring to this work

[P1] Affronti, E.; Merklein, M.: Analysis of the bending effects and the biaxial pre-straining in sheet metal stretch forming processes for the determination of the forming limits. International Journal of Mechanical Sciences 138-139(2018), pp. 295–309

[P2] Affronti, E.; Jaremenko, C.; Merklein, M.; Maier, A.: Analysis of forming limits in sheet metal forming with pattern recognition methods. Part 1: characterization of onset of necking and expert evaluation. Materials, (2018)11

[P3] Jaremenko, C.; Affronti, E.; Maier, A.; Merklein, M.: Analysis of Forming Limits in Sheet Metal Forming with Pattern Recognition Methods. Part 2: Unsupervised Methodology and Application. Materials, (2018)11, pp. 1892

[P4] Affronti, E.; Merklein, M.: Metallographic Analysis of Nakajima Tests for the Evaluation of the Failure Developments. Procedia Engineering 183(2017), pp. 83–88

[P5] Jaremenko, C.; Huang, X.; Affronti, E.; Merklein, M.; Maier, A.: Sheet metal forming limits as classification problem. In: Proceedings of the 15th IAPR International Conference on Machine Vision Applications (Machine Vision Applications), Nagoya University, Nagoya, Japan (2017) pp. 100-103

[P6] Merklein, M.; Affronti, E.; Volk, W.; Jocham, D.: Verbesserung der zeitlichen Auswertemethoden von Versuchen zur Ermittlung der Grenzformänderung und Ableitung eines virtuellen Ersatzmodells - Nr.469, 2017

[P7] Lenzen, M.; Affronti, E.; Rosenschon, M.; Merklein, M.: Investigation of the Anisotropic Strain Rate Dependency of AA5182-O and DC04 for Different Stress States. Advanced Materials Research 1140(2016), pp. 35-42

[P8] Merklein, M.; Affronti, E.; Steiner, J.: Numerical Investigation of Dry and Lubricated Sheet Metal Forming Processes. KEM 651-653(2015), pp. 1029–1035

[P9] Merklein, M.; Maier, A.; Kinnstätter, D.; Jaremenko, C.; Affronti, E.: A New Approach to the Evaluation of Forming Limits in Sheet Metal Forming. KEM 639(2015), pp. 333–338

[P10] Merklein, M.; Kuppert, A.; Affronti, E.: An Improvement of the Time Dependent Method Based on the Coefficient of Correlation for the Determination of the Forming Limit Curve. AMR 1018(2014), pp. 215–222

[P11] Merklein, M.; Affronti, E.; Kuppert, A.; Maier, A.; Lechner, M.: The correlation coefficient method: from the beginning to the development. In: Institut für Virtuelle Produktion, ETH Zürich: Workshop Time-dependent Methods for the Evaluation of FLC (2014), pp. 115-122

## Students' theses referring to this work *

[S1] Beneder, M.; Affronti, E.; Merklein, M. Metallographische Analyse des Werkstoffes DC04 für die Bestimmung des Versagensverhaltens im Nakajima-Test. Erlangen, 2015

[S2] Niedenzu, D.; Affronti, E.; Merklein, M. Numerical investigation of time dependent methods for the determination of the forming limit curve. Erlangen, 2015

[S3] Billich, J.; Affronti, E.; Merklein, M. Einflussanalyse eines numerischen Modelles des Nakajima-Versuchs für die Bestimmung der Grenzformänderungskurve. Erlangen, 2016

[S4] Weidinger, M.; Affronti, E.; Merklein, M. Metallographische Analyse des Werkstoffes DP800 für die Bestimmung des Versagensverhalten s im Nakajima-Test, Erlangen, 2017

[S5] Beneder, M.; Affronti, E.; Merklein, M. Experimentelle und numerische Analyse der Effekte der Biegung im Nakajima Versuch, Erlangen, 2017

[S6] Rösch, P.; Affronti, E.; Merklein, M. Experimentelle Untersuchung der Effekte der biaxialen Vordehnung im Nakajima Versuch. Erlangen, 2017

[S7] Scheck, A.; Affronti, E.; Merklein, M. Metallographische Analyse des Werkstoffes HC260LA für die Bestimmung des Versagensverhaltens im Nakajima-Versuch, Erlangen, 2018

[S8] Fan; J.; Affronti, E.; Merklein, M. Numerische Analyse des Marciniak-Versuchs für die Realisierung hochskalierter Versuche; Erlangen, 2018

* The 2nd (3rd) author names the supervisor; the last author is head of the institute

## Reihenübersicht

Koordination der Reihe (Stand 2020):
Geschäftsstelle Maschinenbau, Dr.-Ing. Oliver Kreis, www.mb.fau.de/diss/

Im Rahmen der Reihe sind bisher die nachfolgenden Bände erschienen.

Band 1 – 52
Fertigungstechnik – Erlangen
ISSN 1431-6226
Carl Hanser Verlag, München

Band 53 – 307
Fertigungstechnik – Erlangen
ISSN 1431-6226
Meisenbach Verlag, Bamberg

ab Band 308
FAU Studien aus dem Maschinenbau
ISSN 2625-9974
FAU University Press, Erlangen

Die Zugehörigkeit zu den jeweiligen Lehrstühlen ist wie folgt gekennzeichnet:

Lehrstühle:

| | |
|---|---|
| **FAPS** | Lehrstuhl für Fertigungsautomatisierung und Produktionssystematik |
| **KTmfk** | Lehrstuhl für Konstruktionstechnik |
| **LFT** | Lehrstuhl für Fertigungstechnologie |
| **LPT** | Lehrstuhl für Photonische Technologien |

Band 1: Andreas Hemberger
Innovationspotentiale in der rechnerintegrierten Produktion durch wissensbasierte Systeme
FAPS, 208 Seiten, 107 Bilder. 1988.
ISBN 3-446-15234-2.

Band 2: Detlef Classe
Beitrag zur Steigerung der Flexibilität automatisierter Montagesysteme durch Sensorintegration und erweiterte Steuerungskonzepte
FAPS, 194 Seiten, 70 Bilder. 1988.
ISBN 3-446-15529-5.

Band 3: Friedrich-Wilhelm Nolting
Projektierung von Montagesystemen
FAPS, 201 Seiten, 107 Bilder, 1 Tab. 1989.
ISBN 3-446-15541-4.

Band 4: Karsten Schlüter
Nutzungsgradsteigerung von Montagesystemen durch den Einsatz der Simulationstechnik
FAPS, 177 Seiten, 97 Bilder. 1989.
ISBN 3-446-15542-2.

Band 5: Shir-Kuan Lin
Aufbau von Modellen zur Lageregelung von Industrierobotern
FAPS, 168 Seiten, 46 Bilder. 1989.
ISBN 3-446-15546-5.

Band 6: Rudolf Nuss
Untersuchungen zur Bearbeitungsqualität im Fertigungssystem Laserstrahlschneiden
LFT, 206 Seiten, 115 Bilder, 6 Tab. 1989.
ISBN 3-446-15783-2.

Band 7: Wolfgang Scholz
Modell zur datenbankgestützten Planung automatisierter Montageanlagen
FAPS, 194 Seiten, 89 Bilder. 1989.
ISBN 3-446-15825-1.

Band 8: Hans-Jürgen Wißmeier
Beitrag zur Beurteilung des Bruchverhaltens von Hartmetall-Fließpreßmatrizen
LFT, 179 Seiten, 99 Bilder, 9 Tab. 1989.
ISBN 3-446-15921-5.

Band 9: Rainer Eisele
Konzeption und Wirtschaftlichkeit von Planungssystemen in der Produktion
FAPS, 183 Seiten, 86 Bilder. 1990.
ISBN 3-446-16107-4.

Band 10: Rolf Pfeiffer
Technologisch orientierte Montageplanung am Beispiel der Schraubtechnik
FAPS, 216 Seiten, 102 Bilder, 16 Tab. 1990.
ISBN 3-446-16161-9.

Band 11: Herbert Fischer
Verteilte Planungssysteme zur Flexibilitätssteigerung der rechnerintegrierten Teilefertigung
FAPS, 201 Seiten, 82 Bilder. 1990.
ISBN 3-446-16105-8.

Band 12: Gerhard Kleineidam
CAD/CAP: Rechnergestützte Montagefeinplanung
FAPS, 203 Seiten, 107 Bilder. 1990.
ISBN 3-446-16112-0.

Band 13: Frank Vollertsen
Pulvermetallurgische Verarbeitung eines übereutektoiden verschleißfesten Stahls
LFT, XIII u. 217 Seiten, 67 Bilder, 34 Tab. 1990. ISBN 3-446-16133-3.

Band 14: Stephan Biermann
Untersuchungen zur Anlagen- und Prozeßdiagnostik für das Schneiden mit $CO_2$-Hochleistungslasern
LFT, VIII u. 170 Seiten, 93 Bilder, 4 Tab. 1991. ISBN 3-446-16269-0.

Band 15: Uwe Geißler
Material- und Datenfluß in einer flexiblen Blechbearbeitungszelle
LFT, 124 Seiten, 41 Bilder, 7 Tab. 1991.
ISBN 3-446-16358-1.

Band 16: Frank Oswald Hake
Entwicklung eines rechnergestützten Diagnosesystems für automatisierte Montagezellen
FAPS, XIV u. 166 Seiten, 77 Bilder. 1991.
ISBN 3-446-16428-6.

Band 17: Herbert Reichel
Optimierung der Werkzeugbereitstellung durch rechnergestützte Arbeitsfolgenbestimmung
FAPS, 198 Seiten, 73 Bilder, 2 Tab. 1991.
ISBN 3-446-16453-7.

Band 18: Josef Scheller
Modellierung und Einsatz von Softwaresystemen für rechnergeführte Montagezellen
FAPS, 198 Seiten, 65 Bilder. 1991.
ISBN 3-446-16454-5.

Band 19: Arnold vom Ende
Untersuchungen zum Biegeumforme mit elastischer Matrize
LFT, 166 Seiten, 55 Bilder, 13 Tab. 1991.
ISBN 3-446-16493-6.

Band 20: Joachim Schmid
Beitrag zum automatisierten Bearbeiten von Keramikguß mit Industrierobotern
FAPS, XIV u. 176 Seiten, 111 Bilder, 6 Tab. 1991. ISBN 3-446-16560-6.

Band 21: Egon Sommer
Multiprozessorsteuerung für kooperierende Industrieroboter in Montagezellen
FAPS, 188 Seiten, 102 Bilder. 1991.
ISBN 3-446-17062-6.

Band 22: Georg Geyer
Entwicklung problemspezifischer Verfahrensketten in der Montage
FAPS, 192 Seiten, 112 Bilder. 1991.
ISBN 3-446-16552-5.

Band 23: Rainer Flohr
Beitrag zur optimalen Verbindungstechnik in der Oberflächenmontage (SMT)
FAPS, 186 Seiten, 79 Bilder. 1991.
ISBN 3-446-16568-1.

Band 24: Alfons Rief
Untersuchungen zur Verfahrensfolge Laserstrahlschneiden und -schweißen in der Rohkarosseriefertigung
LFT, VI u. 145 Seiten, 58 Bilder, 5 Tab. 1991. ISBN 3-446-16593-2.

Band 25: Christoph Thim
Rechnerunterstützte Optimierung von Materialflußstrukturen in der Elektronikmontage durch Simulation
FAPS, 188 Seiten, 74 Bilder. 1992.
ISBN 3-446-17118-5.

Band 26: Roland Müller
$CO_2$ -Laserstrahlschneiden von kurzglasverstärkten Verbundwerkstoffen
LFT, 141 Seiten, 107 Bilder, 4 Tab. 1992.
ISBN 3-446-17104-5.

Band 27: Günther Schäfer
Integrierte Informationsverarbeitung bei der Montageplanung
FAPS, 195 Seiten, 76 Bilder. 1992.
ISBN 3-446-17117-7.

Band 28: Martin Hoffmann
Entwicklung einer CAD/CAM-Prozeßkette für die Herstellung von Blechbiegeteilen
LFT, 149 Seiten, 89 Bilder. 1992.
ISBN 3-446-17154-1.

Band 29: Peter Hoffmann
Verfahrensfolge Laserstrahlschneiden und –schweißen: Prozeßführung und Systemtechnik in der 3D-Laserstrahlbearbeitung von Blechformteilen
LFT, 186 Seiten, 92 Bilder, 10 Tab. 1992.
ISBN 3-446-17153-3.

Band 30: Olaf Schrödel
Flexible Werkstattsteuerung mit objektorientierten Softwarestrukturen
FAPS, 180 Seiten, 84 Bilder. 1992.
ISBN 3-446-17242-4.

Band 31: Hubert Reinisch
Planungs- und Steuerungswerkzeuge zur impliziten Geräteprogrammierung in Roboterzellen
FAPS, XI u. 212 Seiten, 112 Bilder. 1992.
ISBN 3-446-17380-3.

Band 32: Brigitte Bärnreuther
Ein Beitrag zur Bewertung des Kommunikationsverhaltens von Automatisierungsgeräten in flexiblen Produktionszellen
FAPS, XI u. 179 Seiten, 71 Bilder. 1992.
ISBN 3-446-17451-6.

Band 33: Joachim Hutfless
Laserstrahlregelung und Optikdiagnostik in der Strahlführung einer $CO_2$-Hochleistungslaseranlage
LFT, 175 Seiten, 70 Bilder, 17 Tab. 1993.
ISBN 3-446-17532-6.

Band 34: Uwe Günzel
Entwicklung und Einsatz eines Simulationsverfahrens für operative und strategische Probleme der Produktionsplanung und –steuerung
FAPS, XIV u. 170 Seiten, 66 Bilder, 5 Tab. 1993.
ISBN 3-446-17604-7.

Band 35: Bertram Ehmann
Operatives Fertigungscontrolling durch Optimierung auftragsbezogener Bearbeitungsabläufe in der Elektronikfertigung
FAPS, XV u. 167 Seiten, 114 Bilder. 1993.
ISBN 3-446-17658-6.

Band 36: Harald Kolléra
Entwicklung eines benutzerorientierten Werkstattprogrammiersystems für das Laserstrahlschneiden
LFT, 129 Seiten, 66 Bilder, 1 Tab. 1993.
ISBN 3-446-17719-1.

Band 37: Stephanie Abels
Modellierung und Optimierung von Montageanlagen in einem integrierten Simulationssystem
FAPS, 188 Seiten, 88 Bilder. 1993.
ISBN 3-446-17731-0.

Band 38: Robert Schmidt-Hebbel
Laserstrahlbohren durchflußbestimmender Durchgangslöcher
LFT, 145 Seiten, 63 Bilder, 11 Tab. 1993.
ISBN 3-446-17778-7.

Band 39: Norbert Lutz
Oberflächenfeinbearbeitung keramischer Werkstoffe mit XeCl-Excimerlaserstrahlung
LFT, 187 Seiten, 98 Bilder, 29 Tab. 1994.
ISBN 3-446-17970-4.

Band 40: Konrad Grampp
Rechnerunterstützung bei Test und Schulung an Steuerungssoftware von SMD-Bestücklinien
FAPS, 178 Seiten, 88 Bilder. 1995.
ISBN 3-446-18173-3.

Band 41: Martin Koch
Wissensbasierte Unterstützung der Angebotsbearbeitung in der Investitionsgüterindustrie
FAPS, 169 Seiten, 68 Bilder. 1995.
ISBN 3-446-18174-1.

Band 42: Armin Gropp
Anlagen- und Prozeßdiagnostik beim Schneiden mit einem gepulsten Nd:YAG-Laser
LFT, 160 Seiten, 88 Bilder, 7 Tab. 1995.
ISBN 3-446-18241-1.

Band 43: Werner Heckel
Optische 3D-Konturerfassung und on-line Biegewinkelmessung mit dem Lichtschnittverfahren
LFT, 149 Seiten, 43 Bilder, 11 Tab. 1995.
ISBN 3-446-18243-8.

Band 44: Armin Rothhaupt
Modulares Planungssystem zur Optimierung der Elektronikfertigung
FAPS, 180 Seiten, 101 Bilder. 1995.
ISBN 3-446-18307-8.

Band 45: Bernd Zöllner
Adaptive Diagnose in der Elektronikproduktion
FAPS, 195 Seiten, 74 Bilder, 3 Tab. 1995.
ISBN 3-446-18308-6.

Band 46: Bodo Vormann
Beitrag zur automatisierten Handhabungsplanung komplexer Blechbiegeteile
LFT, 126 Seiten, 89 Bilder, 3 Tab. 1995.
ISBN 3-446-18345-0.

Band 47: Peter Schnepf
Zielkostenorientierte Montageplanung
FAPS, 144 Seiten, 75 Bilder. 1995.
ISBN 3-446-18397-3.

Band 48: Rainer Klotzbücher
Konzept zur rechnerintegrierten Materialversorgung in flexiblen Fertigungssystemen
FAPS, 156 Seiten, 62 Bilder. 1995.
ISBN 3-446-18412-0.

Band 49: Wolfgang Greska
Wissensbasierte Analyse und Klassifizierung von Blechteilen
LFT, 144 Seiten, 96 Bilder. 1995.
ISBN 3-446-18462-7.

Band 50: Jörg Franke
Integrierte Entwicklung neuer Produkt- und Produktionstechnologien für räumliche spritzgegossene Schaltungsträger (3-D MID)
FAPS, 196 Seiten, 86 Bilder, 4 Tab. 1995.
ISBN 3-446-18448-1.

Band 51: Franz-Josef Zeller
Sensorplanung und schnelle Sensorregelung für Industrieroboter
FAPS, 190 Seiten, 102 Bilder, 9 Tab. 1995.
ISBN 3-446-18601-8.

Band 52: Michael Solvie
Zeitbehandlung und Multimedia-Unterstützung in Feldkommunikationssystemen
FAPS, 200 Seiten, 87 Bilder, 35 Tab. 1996.
ISBN 3-446-18607-7.

Band 53: Robert Hopperdietzel
Reengineering in der Elektro- und Elektronikindustrie
FAPS, 180 Seiten, 109 Bilder, 1 Tab. 1996.
ISBN 3-87525-070-2.

Band 54: Thomas Rebhahn
Beitrag zur Mikromaterialbearbeitung mit Excimerlasern - Systemkomponenten und Verfahrensoptimierungen
LFT, 148 Seiten, 61 Bilder, 10 Tab. 1996.
ISBN 3-87525-075-3.

Band 55: Henning Hanebuth
Laserstrahlhartlöten mit Zweistrahltechnik
LFT, 157 Seiten, 58 Bilder, 11 Tab. 1996.
ISBN 3-87525-074-5.

Band 56: Uwe Schönherr
Steuerung und Sensordatenintegration für flexible Fertigungszellen mit kooperierenden Robotern
FAPS, 188 Seiten, 116 Bilder, 3 Tab. 1996.
ISBN 3-87525-076-1.

Band 57: Stefan Holzer
Berührungslose Formgebung mit Laserstrahlung
LFT, 162 Seiten, 69 Bilder, 11 Tab. 1996.
ISBN 3-87525-079-6.

Band 58: Markus Schultz
Fertigungsqualität beim 3D-Laserstrahlschweißen von Blechformteilen
LFT, 165 Seiten, 88 Bilder, 9 Tab. 1997.
ISBN 3-87525-080-X.

Band 59: Thomas Krebs
Integration elektromechanischer CA-Anwendungen über einem STEP-Produktmodell
FAPS, 198 Seiten, 58 Bilder, 8 Tab. 1997.
ISBN 3-87525-081-8.

Band 60: Jürgen Sturm
Prozeßintegrierte Qualitätssicherung in der Elektronikproduktion
FAPS, 167 Seiten, 112 Bilder, 5 Tab. 1997.
ISBN 3-87525-082-6.

Band 61: Andreas Brand
Prozesse und Systeme zur Bestückung räumlicher elektronischer Baugruppen (3D-MID)
FAPS, 182 Seiten, 100 Bilder. 1997.
ISBN 3-87525-087-7.

Band 62: Michael Kauf
Regelung der Laserstrahlleistung und der Fokusparameter einer $CO_2$-Hochleistungslaseranlage
LFT, 140 Seiten, 70 Bilder, 5 Tab. 1997.
ISBN 3-87525-083-4.

Band 63: Peter Steinwasser
Modulares Informationsmanagement in der integrierten Produkt- und Prozeßplanung
FAPS, 190 Seiten, 87 Bilder. 1997.
ISBN 3-87525-084-2.

Band 64: Georg Liedl
Integriertes Automatisierungskonzept für den flexiblen Materialfluß in der Elektronikproduktion
FAPS, 196 Seiten, 96 Bilder, 3 Tab. 1997.
ISBN 3-87525-086-9.

Band 65: Andreas Otto
Transiente Prozesse beim Laserstrahlschweißen
LFT, 132 Seiten, 62 Bilder, 1 Tab. 1997.
ISBN 3-87525-089-3.

Band 66: Wolfgang Blöchl
Erweiterte Informationsbereitstellung an offenen CNC-Steuerungen zur Prozeß- und Programmoptimierung
FAPS, 168 Seiten, 96 Bilder. 1997.
ISBN 3-87525-091-5.

Band 67: Klaus-Uwe Wolf
Verbesserte Prozeßführung und Prozeßplanung zur Leistungs- und Qualitätssteigerung beim Spulenwickeln
FAPS, 186 Seiten, 125 Bilder. 1997.
ISBN 3-87525-092-3.

Band 68: Frank Backes
Technologieorientierte Bahnplanung für die 3D-Laserstrahlbearbeitung
LFT, 138 Seiten, 71 Bilder, 2 Tab. 1997.
ISBN 3-87525-093-1.

Band 69: Jürgen Kraus
Laserstrahlumformen von Profilen
LFT, 137 Seiten, 72 Bilder, 8 Tab. 1997.
ISBN 3-87525-094-X.

Band 70: Norbert Neubauer
Adaptive Strahlführungen für $CO_2$-Laseranlagen
LFT, 120 Seiten, 50 Bilder, 3 Tab. 1997.
ISBN 3-87525-095-8.

Band 71: Michael Steber
Prozeßoptimierter Betrieb flexibler Schraubstationen in der automatisierten Montage
FAPS, 168 Seiten, 78 Bilder, 3 Tab. 1997.
ISBN 3-87525-096-6.

Band 72: Markus Pfestorf
Funktionale 3D-Oberflächenkenngrößen in der Umformtechnik
LFT, 162 Seiten, 84 Bilder, 15 Tab. 1997.
ISBN 3-87525-097-4.

Band 73: Volker Franke
Integrierte Planung und Konstruktion von Werkzeugen für die Biegebearbeitung
LFT, 143 Seiten, 81 Bilder. 1998.
ISBN 3-87525-098-2.

Band 74: Herbert Scheller
Automatisierte Demontagesysteme und recyclinggerechte Produktgestaltung elektronischer Baugruppen
FAPS, 184 Seiten, 104 Bilder, 17 Tab. 1998.
ISBN 3-87525-099-0.

Band 75: Arthur Meßner
Kaltmassivumformung metallischer Kleinstteile - Werkstoffverhalten, Wirkflächenreibung, Prozeßauslegung
LFT, 164 Seiten, 92 Bilder, 14 Tab. 1998.
ISBN 3-87525-100-8.

Band 76: Mathias Glasmacher
Prozeß- und Systemtechnik zum Laserstrahl-Mikroschweißen
LFT, 184 Seiten, 104 Bilder, 12 Tab. 1998.
ISBN 3-87525-101-6.

Band 77: Michael Schwind
Zerstörungsfreie Ermittlung mechanischer Eigenschaften von Feinblechen mit dem Wirbelstromverfahren
LFT, 124 Seiten, 68 Bilder, 8 Tab. 1998.
ISBN 3-87525-102-4.

Band 78: Manfred Gerhard
Qualitätssteigerung in der Elektronikproduktion durch Optimierung der Prozeßführung beim Löten komplexer Baugruppen
FAPS, 179 Seiten, 113 Bilder, 7 Tab. 1998.
ISBN 3-87525-103-2.

Band 79: Elke Rauh
Methodische Einbindung der Simulation in die betrieblichen Planungs- und Entscheidungsabläufe
FAPS, 192 Seiten, 114 Bilder, 4 Tab. 1998.
ISBN 3-87525-104-0.

Band 80: Sorin Niederkorn
Meßeinrichtung zur Untersuchung der Wirkflächenreibung bei umformtechnischen Prozessen
LFT, 99 Seiten, 46 Bilder, 6 Tab. 1998.
ISBN 3-87525-105-9.

Band 81: Stefan Schuberth
Regelung der Fokuslage beim Schweißen mit CO2-Hochleistungslasern unter Einsatz von adaptiven Optiken
LFT, 140 Seiten, 64 Bilder, 3 Tab. 1998.
ISBN 3-87525-106-7.

Band 82: Armando Walter Colombo
Development and Implementation of Hierarchical Control Structures of Flexible Production Systems Using High Level Petri Nets
FAPS, 216 Seiten, 86 Bilder. 1998.
ISBN 3-87525-109-1.

Band 83: Otto Meedt
Effizienzsteigerung bei Demontage und Recycling durch flexible Demontagetechnologien und optimierte Produktgestaltung
FAPS, 186 Seiten, 103 Bilder. 1998.
ISBN 3-87525-108-3.

Band 84: Knuth Götz
Modelle und effiziente Modellbildung zur Qualitätssicherung in der Elektronikproduktion
FAPS, 212 Seiten, 129 Bilder, 24 Tab. 1998.
ISBN 3-87525-112-1.

Band 85: Ralf Luchs
Einsatzmöglichkeiten leitender Klebstoffe zur zuverlässigen Kontaktierung elektronischer Bauelemente in der SMT
FAPS, 176 Seiten, 126 Bilder, 30 Tab. 1998.
ISBN 3-87525-113-7.

Band 86: Frank Pöhlau
Entscheidungsgrundlagen zur Einführung räumlicher spritzgegossener Schaltungsträger (3-D MID)
FAPS, 144 Seiten, 99 Bilder. 1999.
ISBN 3-87525-114-8.

Band 87: Roland T. A. Kals
Fundamentals on the miniaturization of sheet metal working processes
LFT, 128 Seiten, 58 Bilder, 11 Tab. 1999.
ISBN 3-87525-115-6.

Band 88: Gerhard Luhn
Implizites Wissen und technisches Handeln am Beispiel der Elektronikproduktion
FAPS, 252 Seiten, 61 Bilder, 1 Tab. 1999.
ISBN 3-87525-116-4.

Band 89: Axel Sprenger
Adaptives Streckbiegen von Aluminium-Strangpreßprofilen
LFT, 114 Seiten, 63 Bilder, 4 Tab. 1999.
ISBN 3-87525-117-2.

Band 90: Hans-Jörg Pucher
Untersuchungen zur Prozeßfolge Umformen, Bestücken und Laserstrahllöten von Mikrokontakten
LFT, 158 Seiten, 69 Bilder, 9 Tab. 1999.
ISBN 3-87525-119-9.

Band 91: Horst Arnet
Profilbiegen mit kinematischer Gestalterzeugung
LFT, 128 Seiten, 67 Bilder, 7 Tab. 1999.
ISBN 3-87525-120-2.

Band 92: Doris Schubart
Prozeßmodellierung und Technologieentwicklung beim Abtragen mit $CO_2$-Laserstrahlung
LFT, 133 Seiten, 57 Bilder, 13 Tab. 1999.
ISBN 3-87525-122-9.

Band 93: Adrianus L. P. Coremans
Laserstrahlsintern von Metallpulver - Prozeßmodellierung, Systemtechnik, Eigenschaften laserstrahlgesinterter Metallkörper
LFT, 184 Seiten, 108 Bilder, 12 Tab. 1999.
ISBN 3-87525-124-5.

Band 94: Hans-Martin Biehler
Optimierungskonzepte für Qualitätsdatenverarbeitung und Informationsbereitstellung in der Elektronikfertigung
FAPS, 194 Seiten, 105 Bilder. 1999.
ISBN 3-87525-126-1.

Band 95: Wolfgang Becker
Oberflächenausbildung und tribologische Eigenschaften excimerlaserstrahlbearbeiteter Hochleistungskeramiken
LFT, 175 Seiten, 71 Bilder, 3 Tab. 1999.
ISBN 3-87525-127-X.

Band 96: Philipp Hein
Innenhochdruck-Umformen von Blechpaaren: Modellierung, Prozeßauslegung und Prozeßführung
LFT, 129 Seiten, 57 Bilder, 7 Tab. 1999.
ISBN 3-87525-128-8.

Band 97: Gunter Beitinger
Herstellungs- und Prüfverfahren für thermoplastische Schaltungsträger
FAPS, 169 Seiten, 92 Bilder, 20 Tab. 1999.
ISBN 3-87525-129-6.

Band 98: Jürgen Knoblach
Beitrag zur rechnerunterstützten verursachungsgerechten Angebotskalkulation von Blechteilen mit Hilfe wissensbasierter Methoden
LFT, 155 Seiten, 53 Bilder, 26 Tab. 1999.
ISBN 3-87525-130-X.

Band 99: Frank Breitenbach
Bildverarbeitungssystem zur Erfassung der Anschlußgeometrie elektronischer SMT-Bauelemente
LFT, 147 Seiten, 92 Bilder, 12 Tab. 2000.
ISBN 3-87525-131-8.

Band 100: Bernd Falk
Simulationsbasierte Lebensdauervorhersage für Werkzeuge der Kaltmassivumformung
LFT, 134 Seiten, 44 Bilder, 15 Tab. 2000.
ISBN 3-87525-136-9.

Band 101: Wolfgang Schlögl
Integriertes Simulationsdaten-Management für Maschinenentwicklung und Anlagenplanung
FAPS, 169 Seiten, 101 Bilder, 20 Tab. 2000.
ISBN 3-87525-137-7.

Band 102: Christian Hinsel
Ermüdungsbruchversagen hartstoffbeschichteter Werkzeugstähle in der Kaltmassivumformung
LFT, 130 Seiten, 80 Bilder, 14 Tab. 2000.
ISBN 3-87525-138-5.

Band 103: Stefan Bobbert
Simulationsgestützte Prozessauslegung für das Innenhochdruck-Umformen von Blechpaaren
LFT, 123 Seiten, 77 Bilder. 2000.
ISBN 3-87525-145-8.

Band 104: Harald Rottbauer
Modulares Planungswerkzeug zum Produktionsmanagement in der Elektronikproduktion
FAPS, 166 Seiten, 106 Bilder. 2001.
ISBN 3-87525-139-3.

Band 111: Jürgen Göhringer
Integrierte Telediagnose via Internet zum effizienten Service von Produktionssystemen
FAPS, 178 Seiten, 98 Bilder, 5 Tab. 2001.
ISBN 3-87525-147-4.

Band 105: Thomas Hennige
Flexible Formgebung von Blechen durch Laserstrahlumformen
LFT, 119 Seiten, 50 Bilder. 2001.
ISBN 3-87525-140-7.

Band 106: Thomas Menzel
Wissensbasierte Methoden für die rechnergestützte Charakterisierung und Bewertung innovativer Fertigungsprozesse
LFT, 152 Seiten, 71 Bilder. 2001.
ISBN 3-87525-142-3.

Band 107: Thomas Stöckel
Kommunikationstechnische Integration der Prozeßebene in Produktionssysteme durch Middleware-Frameworks
FAPS, 147 Seiten, 65 Bilder, 5 Tab. 2001.
ISBN 3-87525-143-1.

Band 108: Frank Pitter
Verfügbarkeitssteigerung von Werkzeugmaschinen durch Einsatz mechatronischer Sensorlösungen
FAPS, 158 Seiten, 131 Bilder, 8 Tab. 2001.
ISBN 3-87525-144-X.

Band 109: Markus Korneli
Integration lokaler CAP-Systeme in einen globalen Fertigungsdatenverbund
FAPS, 121 Seiten, 53 Bilder, 11 Tab. 2001.
ISBN 3-87525-146-6.

Band 110: Burkhard Müller
Laserstrahljustieren mit Excimer-Lasern - Prozeßparameter und Modelle zur Aktorkonstruktion
LFT, 128 Seiten, 36 Bilder, 9 Tab. 2001.
ISBN 3-87525-159-8.

Band 111: Jürgen Göhringer
Integrierte Telediagnose via Internet zum effizienten Service von Produktionssystemen
FAPS, 178 Seiten, 98 Bilder, 5 Tab. 2001.
ISBN 3-87525-147-4.

Band 112: Robert Feuerstein
Qualitäts- und kosteneffiziente Integration neuer Bauelementetechnologien in die Flachbaugruppenfertigung
FAPS, 161 Seiten, 99 Bilder, 10 Tab. 2001.
ISBN 3-87525-151-2.

Band 113: Marcus Reichenberger
Eigenschaften und Einsatzmöglichkeiten alternativer Elektroniklote in der Oberflächenmontage (SMT)
FAPS, 165 Seiten, 97 Bilder, 18 Tab. 2001.
ISBN 3-87525-152-0.

Band 114: Alexander Huber
Justieren vormontierter Systeme mit dem Nd:YAG-Laser unter Einsatz von Aktoren
LFT, 122 Seiten, 58 Bilder, 5 Tab. 2001.
ISBN 3-87525-153-9.

Band 115: Sami Krimi
Analyse und Optimierung von Montagesystemen in der Elektronikproduktion
FAPS, 155 Seiten, 88 Bilder, 3 Tab. 2001.
ISBN 3-87525-157-1.

Band 116: Marion Merklein
Laserstrahlumformen von Aluminiumwerkstoffen - Beeinflussung der Mikrostruktur und der mechanischen Eigenschaften
LFT, 122 Seiten, 65 Bilder, 15 Tab. 2001.
ISBN 3-87525-156-3.

Band 117: Thomas Collisi
Ein informationslogistisches Architekturkonzept zur Akquisition simulationsrelevanter Daten
FAPS, 181 Seiten, 105 Bilder, 7 Tab. 2002.
ISBN 3-87525-164-4.

Band 118: Markus Koch
Rationalisierung und ergonomische Optimierung im Innenausbau durch den Einsatz moderner Automatisierungstechnik
FAPS, 176 Seiten, 98 Bilder, 9 Tab. 2002.
ISBN 3-87525-165-2.

Band 119: Michael Schmidt
Prozeßregelung für das Laserstrahl-Punktschweißen in der Elektronikproduktion
LFT, 152 Seiten, 71 Bilder, 3 Tab. 2002.
ISBN 3-87525-166-0.

Band 120: Nicolas Tiesler
Grundlegende Untersuchungen zum Fließpressen metallischer Kleinstteile
LFT, 126 Seiten, 78 Bilder, 12 Tab. 2002.
ISBN 3-87525-175-X.

Band 121: Lars Pursche
Methoden zur technologieorientierten Programmierung für die 3D-Lasermikrobearbeitung
LFT, 111 Seiten, 39 Bilder, 0 Tab. 2002.
ISBN 3-87525-183-0.

Band 122: Jan-Oliver Brassel
Prozeßkontrolle beim Laserstrahl-Mikroschweißen
LFT, 148 Seiten, 72 Bilder, 12 Tab. 2002.
ISBN 3-87525-181-4.

Band 123: Mark Geisel
Prozeßkontrolle und -steuerung beim Laserstrahlschweißen mit den Methoden der nichtlinearen Dynamik
LFT, 135 Seiten, 46 Bilder, 2 Tab. 2002.
ISBN 3-87525-180-6.

Band 124: Gerd Eßer
Laserstrahlunterstützte Erzeugung metallischer Leiterstrukturen auf Thermoplastsubstraten für die MID-Technik
LFT, 148 Seiten, 60 Bilder, 6 Tab. 2002.
ISBN 3-87525-171-7.

Band 125: Marc Fleckenstein
Qualität laserstrahl-gefügter Mikroverbindungen elektronischer Kontakte
LFT, 159 Seiten, 77 Bilder, 7 Tab. 2002.
ISBN 3-87525-170-9.

Band 126: Stefan Kaufmann
Grundlegende Untersuchungen zum Nd:YAG- Laserstrahlfügen von Silizium für Komponenten der Optoelektronik
LFT, 159 Seiten, 100 Bilder, 6 Tab. 2002.
ISBN 3-87525-172-5.

Band 127: Thomas Fröhlich
Simultanes Löten von Anschlußkontakten elektronischer Bauelemente mit Diodenlaserstrahlung
LFT, 143 Seiten, 75 Bilder, 6 Tab. 2002.
ISBN 3-87525-186-5.

Band 128: Achim Hofmann
Erweiterung der Formgebungsgrenzen beim Umformen von Aluminiumwerkstoffen durch den Einsatz prozessangepasster Platinen
LFT, 113 Seiten, 58 Bilder, 4 Tab. 2002.
ISBN 3-87525-182-2.

Band 129: Ingo Kriebitzsch
3 - D MID Technologie in der Automobilelektronik
FAPS, 129 Seiten, 102 Bilder, 10 Tab. 2002.
ISBN 3-87525-169-5.

Band 130: Thomas Pohl
Fertigungsqualität und Umformbarkeit laserstrahlgeschweißter Formplatinen aus Aluminiumlegierungen
LFT, 133 Seiten, 93 Bilder, 12 Tab. 2002.
ISBN 3-87525-173-3.

Band 131: Matthias Wenk
Entwicklung eines konfigurierbaren Steuerungssystems für die flexible Sensorführung von Industrierobotern
FAPS, 167 Seiten, 85 Bilder, 1 Tab. 2002.
ISBN 3-87525-174-1.

Band 132: Matthias Negendanck
Neue Sensorik und Aktorik für Bearbeitungsköpfe zum Laserstrahlschweißen
LFT, 116 Seiten, 60 Bilder, 14 Tab. 2002.
ISBN 3-87525-184-9.

Band 133: Oliver Kreis
Integrierte Fertigung - Verfahrensintegration durch Innenhochdruck-Umformen, Trennen und Laserstrahlschweißen in einem Werkzeug sowie ihre tele- und multimediale Präsentation
LFT, 167 Seiten, 90 Bilder, 43 Tab. 2002.
ISBN 3-87525-176-8.

Band 134: Stefan Trautner
Technische Umsetzung produktbezogener Instrumente der Umweltpolitik bei Elektro- und Elektronikgeräten
FAPS, 179 Seiten, 92 Bilder, 11 Tab. 2002.
ISBN 3-87525-177-6.

Band 135: Roland Meier
Strategien für einen produktorientierten Einsatz räumlicher spritzgegossener Schaltungsträger (3-D MID)
FAPS, 155 Seiten, 88 Bilder, 14 Tab. 2002.
ISBN 3-87525-178-4.

Band 136: Jürgen Wunderlich
Kostensimulation - Simulationsbasierte Wirtschaftlichkeitsregelung komplexer Produktionssysteme
FAPS, 202 Seiten, 119 Bilder, 17 Tab. 2002.
ISBN 3-87525-179-2.

Band 137: Stefan Novotny
Innenhochdruck-Umformen von Blechen aus Aluminium- und Magnesiumlegierungen bei erhöhter Temperatur
LFT, 132 Seiten, 82 Bilder, 6 Tab. 2002.
ISBN 3-87525-185-7.

Band 138: Andreas Licha
Flexible Montageautomatisierung zur Komplettmontage flächenhafter Produktstrukturen durch kooperierende Industrieroboter
FAPS, 158 Seiten, 87 Bilder, 8 Tab. 2003.
ISBN 3-87525-189-X.

Band 139: Michael Eisenbarth
Beitrag zur Optimierung der Aufbau- und Verbindungstechnik für mechatronische Baugruppen
FAPS, 207 Seiten, 141 Bilder, 9 Tab. 2003.
ISBN 3-87525-190-3.

Band 140: Frank Christoph
Durchgängige simulationsgestützte Planung von Fertigungseinrichtungen der Elektronikproduktion
FAPS, 187 Seiten, 107 Bilder, 9 Tab. 2003.
ISBN 3-87525-191-1.

Band 141: Hinnerk Hagenah
Simulationsbasierte Bestimmung der zu erwartenden Maßhaltigkeit für das Blechbiegen
LFT, 131 Seiten, 36 Bilder, 26 Tab. 2003.
ISBN 3-87525-192-X.

Band 142: Ralf Eckstein
Scherschneiden und Biegen metallischer Kleinstteile - Materialeinfluss und Materialverhalten
LFT, 148 Seiten, 71 Bilder, 19 Tab. 2003.
ISBN 3-87525-193-8.

Band 143: Frank H. Meyer-Pittroff
Excimerlaserstrahlbiegen dünner metallischer Folien mit homogener Lichtlinie
LFT, 138 Seiten, 60 Bilder, 16 Tab. 2003.
ISBN 3-87525-196-2.

Band 144: Andreas Kach
Rechnergestützte Anpassung von Laserstrahlschneidbahnen an Bauteilabweichungen
LFT, 139 Seiten, 69 Bilder, 11 Tab. 2004.
ISBN 3-87525-197-0.

Band 145: Stefan Hierl
System- und Prozeßtechnik für das simultane Löten mit Diodenlaserstrahlung von elektronischen Bauelementen
LFT, 124 Seiten, 66 Bilder, 4 Tab. 2004.
ISBN 3-87525-198-9.

Band 146: Thomas Neudecker
Tribologische Eigenschaften keramischer Blechumformwerkzeuge- Einfluss einer Oberflächenendbearbeitung mittels Excimerlaserstrahlung
LFT, 166 Seiten, 75 Bilder, 26 Tab. 2004.
ISBN 3-87525-200-4.

Band 147: Ulrich Wenger
Prozessoptimierung in der Wickeltechnik durch innovative maschinenbauliche und regelungstechnische Ansätze
FAPS, 132 Seiten, 88 Bilder, 0 Tab. 2004.
ISBN 3-87525-203-9.

Band 148: Stefan Slama
Effizienzsteigerung in der Montage durch marktorientierte Montagestrukturen und erweiterte Mitarbeiterkompetenz
FAPS, 188 Seiten, 125 Bilder, 0 Tab. 2004.
ISBN 3-87525-204-7.

Band 149: Thomas Wurm
Laserstrahljustieren mittels Aktoren-Entwicklung von Konzepten und Methoden für die rechnerunterstützte Modellierung und Optimierung von komplexen Aktorsystemen in der Mikrotechnik
LFT, 122 Seiten, 51 Bilder, 9 Tab. 2004.
ISBN 3-87525-206-3.

Band 150: Martino Celeghini
Wirkmedienbasierte Blechumformung: Grundlagenuntersuchungen zum Einfluss von Werkstoff und Bauteilgeometrie
LFT, 146 Seiten, 77 Bilder, 6 Tab. 2004.
ISBN 3-87525-207-1.

Band 151: Ralph Hohenstein
Entwurf hochdynamischer Sensor- und Regelsysteme für die adaptive Laserbearbeitung
LFT, 282 Seiten, 63 Bilder, 16 Tab. 2004.
ISBN 3-87525-210-1.

Band 152: Angelika Hutterer
Entwicklung prozessüberwachender Regelkreise für flexible Formgebungsprozesse
LFT, 149 Seiten, 57 Bilder, 2 Tab. 2005.
ISBN 3-87525-212-8.

Band 153: Emil Egerer
Massivumformen metallischer Kleinstteile bei erhöhter Prozesstemperatur
LFT, 158 Seiten, 87 Bilder, 10 Tab. 2005.
ISBN 3-87525-213-6.

Band 154: Rüdiger Holzmann
Strategien zur nachhaltigen Optimierung von Qualität und Zuverlässigkeit in der Fertigung hochintegrierter Flachbaugruppen
FAPS, 186 Seiten, 99 Bilder, 19 Tab. 2005.
ISBN 3-87525-217-9.

Band 155: Marco Nock
Biegeumformen mit Elastomerwerkzeugen Modellierung, Prozessauslegung und Abgrenzung des Verfahrens am Beispiel des Rohrbiegens
LFT, 164 Seiten, 85 Bilder, 13 Tab. 2005.
ISBN 3-87525-218-7.

Band 156: Frank Niebling
Qualifizierung einer Prozesskette zum Laserstrahlsintern metallischer Bauteile
LFT, 148 Seiten, 89 Bilder, 3 Tab. 2005.
ISBN 3-87525-219-5.

Band 157: Markus Meiler
Großserientauglichkeit trockenschmierstoffbeschichteter Aluminiumbleche im Presswerk Grundlegende Untersuchungen zur Tribologie, zum Umformverhalten und Bauteilversuche
LFT, 104 Seiten, 57 Bilder, 21 Tab. 2005.
ISBN 3-87525-221-7.

Band 158: Agus Sutanto
Solution Approaches for Planning of Assembly Systems in Three-Dimensional Virtual Environments
FAPS, 169 Seiten, 98 Bilder, 3 Tab. 2005.
ISBN 3-87525-220-9.

Band 159: Matthias Boiger
Hochleistungssysteme für die Fertigung elektronischer Baugruppen auf der Basis flexibler Schaltungsträger
FAPS, 175 Seiten, 111 Bilder, 8 Tab. 2005.
ISBN 3-87525-222-5.

Band 160: Matthias Pitz
Laserunterstütztes Biegen höchstfester Mehrphasenstähle
LFT, 120 Seiten, 73 Bilder, 11 Tab. 2005.
ISBN 3-87525-223-3.

Band 161: Meik Vahl
Beitrag zur gezielten Beeinflussung des Werkstoffflusses beim Innenhochdruck-Umformen von Blechen
LFT, 165 Seiten, 94 Bilder, 15 Tab. 2005.
ISBN 3-87525-224-1.

Band 162: Peter K. Kraus
Plattformstrategien - Realisierung einer varianz- und kostenoptimierten Wertschöpfung
FAPS, 181 Seiten, 95 Bilder, 0 Tab. 2005.
ISBN 3-87525-226-8.

Band 163: Adrienn Cser
Laserstrahlschmelzabtrag - Prozessanalyse und -modellierung
LFT, 146 Seiten, 79 Bilder, 3 Tab. 2005.
ISBN 3-87525-227-6.

Band 164: Markus C. Hahn
Grundlegende Untersuchungen zur Herstellung von Leichtbauverbundstrukturen mit Aluminiumschaumkern
LFT, 143 Seiten, 60 Bilder, 16 Tab. 2005.
ISBN 3-87525-228-4.

Band 165: Gordana Michos
Mechatronische Ansätze zur Optimierung von Vorschubachsen
FAPS, 146 Seiten, 87 Bilder, 17 Tab. 2005.
ISBN 3-87525-230-6.

Band 166: Markus Stark
Auslegung und Fertigung hochpräziser Faser-Kollimator-Arrays
LFT, 158 Seiten, 115 Bilder, 11 Tab. 2005.
ISBN 3-87525-231-4.

Band 167: Yurong Zhou
Kollaboratives Engineering Management in der integrierten virtuellen Entwicklung der Anlagen für die Elektronikproduktion
FAPS, 156 Seiten, 84 Bilder, 6 Tab. 2005.
ISBN 3-87525-232-2.

Band 168: Werner Enser
Neue Formen permanenter und lösbarer elektrischer Kontaktierungen für mechatronische Baugruppen
FAPS, 190 Seiten, 112 Bilder, 5 Tab. 2005.
ISBN 3-87525-233-0.

Band 169: Katrin Melzer
Integrierte Produktpolitik bei elektrischen und elektronischen Geräten zur Optimierung des Product-Life-Cycle
FAPS, 155 Seiten, 91 Bilder, 17 Tab. 2005.
ISBN 3-87525-234-9.

Band 170: Alexander Putz
Grundlegende Untersuchungen zur Erfassung der realen Vorspannung von armierten Kaltfließpresswerkzeugen mittels Ultraschall
LFT, 137 Seiten, 71 Bilder, 15 Tab. 2006.
ISBN 3-87525-237-3.

Band 171: Martin Prechtl
Automatisiertes Schichtverfahren für metallische Folien - System- und Prozesstechnik
LFT, 154 Seiten, 45 Bilder, 7 Tab. 2006.
ISBN 3-87525-238-1.

Band 172: Markus Meidert
Beitrag zur deterministischen Lebensdauerabschätzung von Werkzeugen der Kaltmassivumformung
LFT, 131 Seiten, 78 Bilder, 9 Tab. 2006.
ISBN 3-87525-239-X.

Band 173: Bernd Müller
Robuste, automatisierte Montagesysteme durch adaptive Prozessführung und montageübergreifende Fehlerprävention am Beispiel flächiger Leichtbauteile
FAPS, 147 Seiten, 77 Bilder, 0 Tab. 2006.
ISBN 3-87525-240-3.

Band 174: Alexander Hofmann
Hybrides Laserdurchstrahlschweißen von Kunststoffen
LFT, 136 Seiten, 72 Bilder, 4 Tab. 2006.
ISBN 978-3-87525-243-9.

Band 175: Peter Wölflick
Innovative Substrate und Prozesse mit feinsten Strukturen für bleifreie Mechatronik-Anwendungen
FAPS, 177 Seiten, 148 Bilder, 24 Tab. 2006.
ISBN 978-3-87525-246-0.

Band 176: Attila Komlodi
Detection and Prevention of Hot Cracks during Laser Welding of Aluminium Alloys Using Advanced Simulation Methods
LFT, 155 Seiten, 89 Bilder, 14 Tab. 2006.
ISBN 978-3-87525-248-4.

Band 177: Uwe Popp
Grundlegende Untersuchungen zum Laserstrahlstrukturieren von Kaltmassivumformwerkzeugen
LFT, 140 Seiten, 67 Bilder, 16 Tab. 2006.
ISBN 978-3-87525-249-1.

Band 178: Veit Rückel
Rechnergestützte Ablaufplanung und Bahngenerierung Für kooperierende Industrieroboter
FAPS, 148 Seiten, 75 Bilder, 7 Tab. 2006.
ISBN 978-3-87525-250-7.

Band 179: Manfred Dirscherl
Nicht-thermische Mikrojustiertechnik mittels ultrakurzer Laserpulse
LFT, 154 Seiten, 69 Bilder, 10 Tab. 2007.
ISBN 978-3-87525-251-4.

Band 180: Yong Zhuo
Entwurf eines rechnergestützten integrierten Systems für Konstruktion und Fertigungsplanung räumlicher spritzgegossener Schaltungsträger (3D-MID)
FAPS, 181 Seiten, 95 Bilder, 5 Tab. 2007.
ISBN 978-3-87525-253-8.

Band 181: Stefan Lang
Durchgängige Mitarbeiterinformation zur Steigerung von Effizienz und Prozesssicherheit in der Produktion
FAPS, 172 Seiten, 93 Bilder. 2007.
ISBN 978-3-87525-257-6.

Band 182: Hans-Joachim Krauß
Laserstrahlinduzierte Pyrolyse präkeramischer Polymere
LFT, 171 Seiten, 100 Bilder. 2007.
ISBN 978-3-87525-258-3.

Band 183: Stefan Junker
Technologien und Systemlösungen für die flexibel automatisierte Bestückung permanent erregter Läufer mit oberflächenmontierten Dauermagneten
FAPS, 173 Seiten, 75 Bilder. 2007.
ISBN 978-3-87525-259-0.

Band 184: Rainer Kohlbauer
Wissensbasierte Methoden für die simulationsgestützte Auslegung wirkmedienbasierter Blechumformprozesse
LFT, 135 Seiten, 50 Bilder. 2007.
ISBN 978-3-87525-260-6.

Band 185: Klaus Lamprecht
Wirkmedienbasierte Umformung tiefgezogener Vorformen unter besonderer Berücksichtigung maßgeschneiderter Halbzeuge
LFT, 137 Seiten, 81 Bilder. 2007.
ISBN 978-3-87525-265-1.

Band 186: Bernd Zolleiß
Optimierte Prozesse und Systeme für die Bestückung mechatronischer Baugruppen
FAPS, 180 Seiten, 117 Bilder. 2007.
ISBN 978-3-87525-266-8.

Band 187: Michael Kerausch
Simulationsgestützte Prozessauslegung für das Umformen lokal wärmebehandelter Aluminiumplatinen
LFT, 146 Seiten, 76 Bilder, 7 Tab. 2007.
ISBN 978-3-87525-267-5.

Band 188: Matthias Weber
Unterstützung der Wandlungsfähigkeit von Produktionsanlagen durch innovative Softwaresysteme
FAPS, 183 Seiten, 122 Bilder, 3 Tab. 2007.
ISBN 978-3-87525-269-9.

Band 189: Thomas Frick
Untersuchung der prozessbestimmenden Strahl-Stoff-Wechselwirkungen beim Laserstrahlschweißen von Kunststoffen
LFT, 104 Seiten, 62 Bilder, 8 Tab. 2007.
ISBN 978-3-87525-268-2.

Band 190: Joachim Hecht
Werkstoffcharakterisierung und Prozessauslegung für die wirkmedienbasierte Doppelblech-Umformung von Magnesiumlegierungen
LFT, 107 Seiten, 91 Bilder, 2 Tab. 2007.
ISBN 978-3-87525-270-5.

Band 191: Ralf Völkl
Stochastische Simulation zur Werkzeuglebensdaueroptimierung und Präzisionsfertigung in der Kaltmassivumformung
LFT, 178 Seiten, 75 Bilder, 12 Tab. 2008.
ISBN 978-3-87525-272-9.

Band 192: Massimo Tolazzi
Innenhochdruck-Umformen verstärkter Blech-Rahmenstrukturen
LFT, 164 Seiten, 85 Bilder, 7 Tab. 2008.
ISBN 978-3-87525-273-6.

Band 193: Cornelia Hoff
Untersuchung der Prozesseinflussgrößen beim Presshärten des höchstfesten Vergütungsstahls 22MnB5
LFT, 133 Seiten, 92 Bilder, 5 Tab. 2008.
ISBN 978-3-87525-275-0.

Band 194: Christian Alvarez
Simulationsgestützte Methoden zur effizienten Gestaltung von Lötprozessen in der Elektronikproduktion
FAPS, 149 Seiten, 86 Bilder, 8 Tab. 2008.
ISBN 978-3-87525-277-4.

Band 195: Andreas Kunze
Automatisierte Montage von makromechatronischen Modulen zur flexiblen Integration in hybride Pkw-Bordnetzsysteme
FAPS, 160 Seiten, 90 Bilder, 14 Tab. 2008.
ISBN 978-3-87525-278-1.

Band 196: Wolfgang Hußnätter
Grundlegende Untersuchungen zur experimentellen Ermittlung und zur Modellierung von Fließortkurven bei erhöhten Temperaturen
LFT, 152 Seiten, 73 Bilder, 21 Tab. 2008.
ISBN 978-3-87525-279-8.

Band 197: Thomas Bigl
Entwicklung, angepasste Herstellungsverfahren und erweiterte Qualitätssicherung von einsatzgerechten elektronischen Baugruppen
FAPS, 175 Seiten, 107 Bilder, 14 Tab. 2008.
ISBN 978-3-87525-280-4.

Band 198: Stephan Roth
Grundlegende Untersuchungen zum Excimerlaserstrahl-Abtragen unter Flüssigkeitsfilmen
LFT, 113 Seiten, 47 Bilder, 14 Tab. 2008.
ISBN 978-3-87525-281-1.

Band 199: Artur Giera
Prozesstechnische Untersuchungen zum Rührreibschweißen metallischer Werkstoffe
LFT, 179 Seiten, 104 Bilder, 36 Tab. 2008.
ISBN 978-3-87525-282-8.

Band 200: Jürgen Lechler
Beschreibung und Modellierung des Werkstoffverhaltens von presshärtbaren Bor-Manganstählen
LFT, 154 Seiten, 75 Bilder, 12 Tab. 2009.
ISBN 978-3-87525-286-6.

Band 201: Andreas Blankl
Untersuchungen zur Erhöhung der Prozessrobustheit bei der Innenhochdruck-Umformung von flächigen Halbzeugen mit vor- bzw. nachgeschalteten Laserstrahlfügeoperationen
LFT, 120 Seiten, 68 Bilder, 9 Tab. 2009.
ISBN 978-3-87525-287-3.

Band 202: Andreas Schaller
Modellierung eines nachfrageorientierten Produktionskonzeptes für mobile Telekommunikationsgeräte
FAPS, 120 Seiten, 79 Bilder, 0 Tab. 2009.
ISBN 978-3-87525-289-7.

Band 203: Claudius Schimpf
Optimierung von Zuverlässigkeitsuntersuchungen, Prüfabläufen und Nacharbeitsprozessen in der Elektronikproduktion
FAPS, 162 Seiten, 90 Bilder, 14 Tab. 2009.
ISBN 978-3-87525-290-3.

Band 204: Simon Dietrich
Sensoriken zur Schwerpunktslagebestimmung der optischen Prozessemissionen beim Laserstrahltiefschweißen
LFT, 138 Seiten, 70 Bilder, 5 Tab. 2009.
ISBN 978-3-87525-292-7.

Band 205: Wolfgang Wolf
Entwicklung eines agentenbasierten Steuerungssystems zur Materialflussorganisation im wandelbaren Produktionsumfeld
FAPS, 167 Seiten, 98 Bilder. 2009.
ISBN 978-3-87525-293-4.

Band 206: Steffen Polster
Laserdurchstrahlschweißen transparenter Polymerbauteile
LFT, 160 Seiten, 92 Bilder, 13 Tab. 2009.
ISBN 978-3-87525-294-1.

Band 207: Stephan Manuel Dörfler
Rührreibschweißen von walzplattiertem Halbzeug und Aluminiumblech zur Herstellung flächiger Aluminiumschaum-Sandwich-Verbundstrukturen
LFT, 190 Seiten, 98 Bilder, 5 Tab. 2009.
ISBN 978-3-87525-295-8.

Band 208: Uwe Vogt
Seriennahe Auslegung von Aluminium Tailored Heat Treated Blanks
LFT, 151 Seiten, 68 Bilder, 26 Tab. 2009.
ISBN 978-3-87525-296-5.

Band 209: Till Laumann
Qualitative und quantitative Bewertung der Crashtauglichkeit von höchstfesten Stählen
LFT, 117 Seiten, 69 Bilder, 7 Tab. 2009.
ISBN 978-3-87525-299-6.

Band 210: Alexander Diehl
Größeneffekte bei Biegeprozessen- Entwicklung einer Methodik zur Identifikation und Quantifizierung
LFT, 180 Seiten, 92 Bilder, 12 Tab. 2010.
ISBN 978-3-87525-302-3.

Band 211: Detlev Staud
Effiziente Prozesskettenauslegung für das Umformen lokal wärmebehandelter und geschweißter Aluminiumbleche
LFT, 164 Seiten, 72 Bilder, 12 Tab. 2010.
ISBN 978-3-87525-303-0.

Band 212: Jens Ackermann
Prozesssicherung beim Laserdurchstrahlschweißen thermoplastischer Kunststoffe
LPT, 129 Seiten, 74 Bilder, 13 Tab. 2010.
ISBN 978-3-87525-305-4.

Band 213: Stephan Weidel
Grundlegende Untersuchungen zum Kontaktzustand zwischen Werkstück und Werkzeug bei umformtechnischen Prozessen unter tribologischen Gesichtspunkten
LFT, 144 Seiten, 67 Bilder, 11 Tab. 2010.
ISBN 978-3-87525-307-8.

Band 214: Stefan Geißdörfer
Entwicklung eines mesoskopischen Modells zur Abbildung von Größeneffekten in der Kaltmassivumformung mit Methoden der FE-Simulation
LFT, 133 Seiten, 83 Bilder, 11 Tab. 2010.
ISBN 978-3-87525-308-5.

Band 215: Christian Matzner
Konzeption produktspezifischer Lösungen zur Robustheitssteigerung elektronischer Systeme gegen die Einwirkung von Betauung im Automobil
FAPS, 165 Seiten, 93 Bilder, 14 Tab. 2010.
ISBN 978-3-87525-309-2.

Band 216: Florian Schüßler
Verbindungs- und Systemtechnik für thermisch hochbeanspruchte und miniaturisierte elektronische Baugruppen
FAPS, 184 Seiten, 93 Bilder, 18 Tab. 2010.
ISBN 978-3-87525-310-8.

Band 217: Massimo Cojutti
Strategien zur Erweiterung der Prozessgrenzen bei der Innhochdruck-Umformung von Rohren und Blechpaaren
LFT, 125 Seiten, 56 Bilder, 9 Tab. 2010.
ISBN 978-3-87525-312-2.

Band 218: Raoul Plettke
Mehrkriterielle Optimierung komplexer Aktorsysteme für das Laserstrahljustieren
LFT, 152 Seiten, 25 Bilder, 3 Tab. 2010.
ISBN 978-3-87525-315-3.

Band 219: Andreas Dobroschke
Flexible Automatisierungslösungen für die Fertigung wickeltechnischer Produkte
FAPS, 184 Seiten, 109 Bilder, 18 Tab. 2011.
ISBN 978-3-87525-317-7.

Band 220: Azhar Zam
Optical Tissue Differentiation for Sensor-Controlled Tissue-Specific Laser Surgery
LPT, 99 Seiten, 45 Bilder, 8 Tab. 2011.
ISBN 978-3-87525-318-4.

Band 221: Michael Rösch
Potenziale und Strategien zur Optimierung des Schablonendruckprozesses in der Elektronikproduktion
FAPS, 192 Seiten, 127 Bilder, 19 Tab. 2011.
ISBN 978-3-87525-319-1.

Band 222: Thomas Rechtenwald
Quasi-isothermes Laserstrahlsintern von Hochtemperatur-Thermoplasten - Eine Betrachtung werkstoff-prozessspezifischer Aspekte am Beispiel PEEK
LPT, 150 Seiten, 62 Bilder, 8 Tab. 2011.
ISBN 978-3-87525-320-7.

Band 223: Daniel Craiovan
Prozesse und Systemlösungen für die SMT-Montage optischer Bauelemente auf Substrate mit integrierten Lichtwellenleitern
FAPS, 165 Seiten, 85 Bilder, 8 Tab. 2011.
ISBN 978-3-87525-324-5.

Band 224: Kay Wagner
Beanspruchungsangepasste Kaltmassivumformwerkzeuge durch lokal optimierte Werkzeugoberflächen
LFT, 147 Seiten, 103 Bilder, 17 Tab. 2011.
ISBN 978-3-87525-325-2.

Band 225: Martin Brandhuber
Verbesserung der Prognosegüte des Versagens von Punktschweißverbindungen bei höchstfesten Stahlgüten
LFT, 155 Seiten, 91 Bilder, 19 Tab. 2011.
ISBN 978-3-87525-327-6.

Band 226: Peter Sebastian Feuser
Ein Ansatz zur Herstellung von pressgehärteten Karosseriekomponenten mit maßgeschneiderten mechanischen Eigenschaften: Temperierte Umformwerkzeuge. Prozessfenster, Prozesssimulation und funktionale Untersuchung
LFT, 195 Seiten, 97 Bilder, 60 Tab. 2012.
ISBN 978-3-87525-328-3.

Band 227: Murat Arbak
Material Adapted Design of Cold Forging Tools Exemplified by Powder Metallurgical Tool Steels and Ceramics
LFT, 109 Seiten, 56 Bilder, 8 Tab. 2012.
ISBN 978-3-87525-330-6.

Band 228: Indra Pitz
Beschleunigte Simulation des Laserstrahlumformens von Aluminiumblechen
LPT, 137 Seiten, 45 Bilder, 27 Tab. 2012.
ISBN 978-3-87525-333-7.

Band 229: Alexander Grimm
Prozessanalyse und -überwachung des Laserstrahlhartlötens mittels optischer Sensorik
LPT, 125 Seiten, 61 Bilder, 5 Tab. 2012.
ISBN 978-3-87525-334-4.

Band 230: Markus Kaupper
Biegen von höhenfesten Stahlblechwerkstoffen - Umformverhalten und Grenzen der Biegbarkeit
LFT, 160 Seiten, 57 Bilder, 10 Tab. 2012.
ISBN 978-3-87525-339-9.

Band 231: Thomas Kroiß
Modellbasierte Prozessauslegung für die Kaltmassivumformung unter Brücksichtigung der Werkzeug- und Pressenauffederung
LFT, 169 Seiten, 50 Bilder, 19 Tab. 2012.
ISBN 978-3-87525-341-2.

Band 232: Christian Goth
Analyse und Optimierung der Entwicklung und Zuverlässigkeit räumlicher Schaltungsträger (3D-MID)
FAPS, 176 Seiten, 102 Bilder, 22 Tab. 2012.
ISBN 978-3-87525-340-5.

Band 233: Christian Ziegler
Ganzheitliche Automatisierung mechatronischer Systeme in der Medizin am Beispiel Strahlentherapie
FAPS, 170 Seiten, 71 Bilder, 19 Tab. 2012.
ISBN 978-3-87525-342-9.

Band 234: Florian Albert
Automatisiertes Laserstrahllöten und -reparaturlöten elektronischer Baugruppen
LPT, 127 Seiten, 78 Bilder, 11 Tab. 2012.
ISBN 978-3-87525-344-3.

Band 235: Thomas Stöhr
Analyse und Beschreibung des mechanischen Werkstoffverhaltens von presshärtbaren Bor-Manganstählen
LFT, 118 Seiten, 74 Bilder, 18 Tab. 2013.
ISBN 978-3-87525-346-7.

Band 236: Christian Kägeler
Prozessdynamik beim Laserstrahlschweißen verzinkter Stahlbleche im Überlappstoß
LPT, 145 Seiten, 80 Bilder, 3 Tab. 2013.
ISBN 978-3-87525-347-4.

Band 237: Andreas Sulzberger
Seriennahe Auslegung der Prozesskette zur wärmeunterstützten Umformung von Aluminiumblechwerkstoffen
LFT, 153 Seiten, 87 Bilder, 17 Tab. 2013.
ISBN 978-3-87525-349-8.

Band 238: Simon Opel
Herstellung prozessangepasster Halbzeuge mit variabler Blechdicke durch die Anwendung von Verfahren der Blechmassivumformung
LFT, 165 Seiten, 108 Bilder, 27 Tab. 2013.
ISBN 978-3-87525-350-4.

Band 239: Rajesh Kanawade
In-vivo Monitoring of Epithelium Vessel and Capillary Density for the Application of Detection of Clinical Shock and Early Signs of Cancer Development
LPT, 124 Seiten, 58 Bilder, 15 Tab. 2013.
ISBN 978-3-87525-351-1.

Band 240: Stephan Busse
Entwicklung und Qualifizierung eines Schneidclinchverfahrens
LFT, 119 Seiten, 86 Bilder, 20 Tab. 2013.
ISBN 978-3-87525-352-8.

Band 241: Karl-Heinz Leitz
Mikro- und Nanostrukturierung mit kurz und ultrakurz gepulster Laserstrahlung
LPT, 154 Seiten, 71 Bilder, 9 Tab. 2013.
ISBN 978-3-87525-355-9.

Band 242: Markus Michl
Webbasierte Ansätze zur ganzheitlichen technischen Diagnose
FAPS, 182 Seiten, 62 Bilder, 20 Tab. 2013.
ISBN 978-3-87525-356-6.

Band 243: Vera Sturm
Einfluss von Chargenschwankungen auf die Verarbeitungsgrenzen von Stahlwerkstoffen
LFT, 113 Seiten, 58 Bilder, 9 Tab. 2013.
ISBN 978-3-87525-357-3.

Band 244: Christian Neudel
Mikrostrukturelle und mechanisch-technologische Eigenschaften widerstandspunktgeschweißter Aluminium-Stahl-Verbindungen für den Fahrzeugbau
LFT, 178 Seiten, 171 Bilder, 31 Tab. 2014.
ISBN 978-3-87525-358-0.

Band 245: Anja Neumann
Konzept zur Beherrschung der Prozessschwankungen im Presswerk
LFT, 162 Seiten, 68 Bilder, 15 Tab. 2014.
ISBN 978-3-87525-360-3.

Band 246: Ulf-Hermann Quentin
Laserbasierte Nanostrukturierung mit optisch positionierten Mikrolinsen
LPT, 137 Seiten, 89 Bilder, 6 Tab. 2014.
ISBN 978-3-87525-361-0.

Band 247: Erik Lamprecht
Der Einfluss der Fertigungsverfahren auf die Wirbelstromverluste von Stator-Einzelzahnblechpaketen für den Einsatz in Hybrid- und Elektrofahrzeugen
FAPS, 148 Seiten, 138 Bilder, 4 Tab. 2014.
ISBN 978-3-87525-362-7.

Band 248: Sebastian Rösel
Wirkmedienbasierte Umformung von Blechhalbzeugen unter Anwendung magnetorheologischer Flüssigkeiten als kombiniertes Wirk- und Dichtmedium
LFT, 148 Seiten, 61 Bilder, 12 Tab. 2014.
ISBN 978-3-87525-363-4.

Band 249: Paul Hippchen
Simulative Prognose der Geometrie indirekt pressgehärteter Karosseriebauteile für die industrielle Anwendung
LFT, 163 Seiten, 89 Bilder, 12 Tab. 2014.
ISBN 978-3-87525-364-1.

Band 250: Martin Zubeil
Versagensprognose bei der Prozesssimulation von Biegeumform- und Falzverfahren
LFT, 171 Seiten, 90 Bilder, 5 Tab. 2014.
ISBN 978-3-87525-365-8.

Band 251: Alexander Kühl
Flexible Automatisierung der Statorenmontage mit Hilfe einer universellen ambidexteren Kinematik
FAPS, 142 Seiten, 60 Bilder, 26 Tab. 2014.
ISBN 978-3-87525-367-2.

Band 252: Thomas Albrecht
Optimierte Fertigungstechnologien für Rotoren getriebeintegrierter PM-Synchronmotoren von Hybridfahrzeugen
FAPS, 198 Seiten, 130 Bilder, 38 Tab. 2014.
ISBN 978-3-87525-368-9.

Band 253: Florian Risch
Planning and Production Concepts for Contactless Power Transfer Systems for Electric Vehicles
FAPS, 185 Seiten, 125 Bilder, 13 Tab. 2014.
ISBN 978-3-87525-369-6.

Band 254: Markus Weigl
Laserstrahlschweißen von Mischverbindungen aus austenitischen und ferritischen korrosionsbeständigen Stahlwerkstoffen
LPT, 184 Seiten, 110 Bilder, 6 Tab. 2014.
ISBN 978-3-87525-370-2.

Band 255: Johannes Noneder
Beanspruchungserfassung für die Validierung von FE-Modellen zur Auslegung von Massivumformwerkzeugen
LFT, 161 Seiten, 65 Bilder, 14 Tab. 2014.
ISBN 978-3-87525-371-9.

Band 256: Andreas Reinhardt
Ressourceneffiziente Prozess- und Produktionstechnologie für flexible Schaltungsträger
FAPS, 123 Seiten, 69 Bilder, 19 Tab. 2014.
ISBN 978-3-87525-373-3.

Band 257: Tobias Schmuck
Ein Beitrag zur effizienten Gestaltung globaler Produktions- und Logistiknetzwerke mittels Simulation
FAPS, 151 Seiten, 74 Bilder. 2014.
ISBN 978-3-87525-374-0.

Band 258: Bernd Eichenhüller
Untersuchungen der Effekte und Wechselwirkungen charakteristischer Einflussgrößen auf das Umformverhalten bei Mikroumformprozessen
LFT, 127 Seiten, 29 Bilder, 9 Tab. 2014.
ISBN 978-3-87525-375-7.

Band 259: Felix Lütteke
Vielseitiges autonomes Transportsystem basierend auf Weltmodellerstellung mittels Datenfusion von Deckenkameras und Fahrzeugsensoren
FAPS, 152 Seiten, 54 Bilder, 20 Tab. 2014.
ISBN 978-3-87525-376-4.

Band 260: Martin Grüner
Hochdruck-Blechumformung mit formlos festen Stoffen als Wirkmedium
LFT, 144 Seiten, 66 Bilder, 29 Tab. 2014.
ISBN 978-3-87525-379-5.

Band 261: Christian Brock
Analyse und Regelung des Laserstrahltiefschweißprozesses durch Detektion der Metalldampffackelposition
LPT, 126 Seiten, 65 Bilder, 3 Tab. 2015.
ISBN 978-3-87525-380-1.

Band 262: Peter Vatter
Sensitivitätsanalyse des 3-Rollen-Schubbiegens auf Basis der Finite Elemente Methode
LFT, 145 Seiten, 57 Bilder, 26 Tab. 2015.
ISBN 978-3-87525-381-8.

Band 263: Florian Klämpfl
Planung von Laserbestrahlungen durch simulationsbasierte Optimierung
LPT, 169 Seiten, 78 Bilder, 32 Tab. 2015.
ISBN 978-3-87525-384-9.

Band 264: Matthias Domke
Transiente physikalische Mechanismen bei der Laserablation von dünnen Metallschichten
LPT, 133 Seiten, 43 Bilder, 3 Tab. 2015.
ISBN 978-3-87525-385-6.

Band 265: Johannes Götz
Community-basierte Optimierung des Anlagenengineerings
FAPS, 177 Seiten, 80 Bilder, 30 Tab. 2015.
ISBN 978-3-87525-386-3.

Band 266: Hung Nguyen
Qualifizierung des Potentials von Verfestigungseffekten zur Erweiterung des Umformvermögens aushärtbarer Aluminiumlegierungen
LFT, 137 Seiten, 57 Bilder, 16 Tab. 2015.
ISBN 978-3-87525-387-0.

Band 267: Andreas Kuppert
Erweiterung und Verbesserung von Versuchs- und Auswertetechniken für die Bestimmung von Grenzformänderungskurven
LFT, 138 Seiten, 82 Bilder, 2 Tab. 2015.
ISBN 978-3-87525-388-7.

Band 268: Kathleen Klaus
Erstellung eines Werkstofforientierten Fertigungsprozessfensters zur Steigerung des Formgebungsvermögens von Aluminiumlegierungen unter Anwendung einer zwischengeschalteten Wärmebehandlung
LFT, 154 Seiten, 70 Bilder, 8 Tab. 2015.
ISBN 978-3-87525-391-7.

Band 269: Thomas Svec
Untersuchungen zur Herstellung von funktionsoptimierten Bauteilen im partiellen Presshärtprozess mittels lokal unterschiedlich temperierter Werkzeuge
LFT, 166 Seiten, 87 Bilder, 15 Tab. 2015.
ISBN 978-3-87525-392-4.

Band 270: Tobias Schrader
Grundlegende Untersuchungen zur Verschleißcharakterisierung beschichteter Kaltmassivumformwerkzeuge
LFT, 164 Seiten, 55 Bilder, 11 Tab. 2015.
ISBN 978-3-87525-393-1.

Band 271: Matthäus Brela
Untersuchung von Magnetfeld-Messmethoden zur ganzheitlichen Wertschöpfungsoptimierung und Fehlerdetektion an magnetischen Aktoren
FAPS, 170 Seiten, 97 Bilder, 4 Tab. 2015.
ISBN 978-3-87525-394-8.

Band 272: Michael Wieland
Entwicklung einer Methode zur Prognose adhäsiven Verschleißes an Werkzeugen für das direkte Presshärten
LFT, 156 Seiten, 84 Bilder, 9 Tab. 2015.
ISBN 978-3-87525-395-5.

Band 273: René Schramm
Strukturierte additive Metallisierung durch kaltaktives Atmosphärendruckplasma
FAPS, 136 Seiten, 62 Bilder, 15 Tab. 2015.
ISBN 978-3-87525-396-2.

Band 274: Michael Lechner
Herstellung beanspruchungsangepasster Aluminiumblechhalbzeuge durch eine maßgeschneiderte Variation der Abkühlgeschwindigkeit nach Lösungsglühen
LFT, 136 Seiten, 62 Bilder, 15 Tab. 2015.
ISBN 978-3-87525-397-9.

Band 275: Kolja Andreas
Einfluss der Oberflächenbeschaffenheit auf das Werkzeugeinsatzverhalten beim Kaltfließpressen
LFT, 169 Seiten, 76 Bilder, 4 Tab. 2015.
ISBN 978-3-87525-398-6.

Band 276: Marcus Baum
Laser Consolidation of ITO Nanoparticles for the Generation of Thin Conductive Layers on Transparent Substrates
LPT, 158 Seiten, 75 Bilder, 3 Tab. 2015.
ISBN 978-3-87525-399-3.

Band 277: Thomas Schneider
Umformtechnische Herstellung dünnwandiger Funktionsbauteile aus Feinblech durch Verfahren der Blechmassivumformung
LFT, 188 Seiten, 95 Bilder, 7 Tab. 2015.
ISBN 978-3-87525-401-3.

Band 278: Jochen Merhof
Sematische Modellierung automatisierter Produktionssysteme zur Verbesserung der IT-Integration zwischen Anlagen-Engineering und Steuerungsebene
FAPS, 157 Seiten, 88 Bilder, 8 Tab. 2015.
ISBN 978-3-87525-402-0.

Band 279: Fabian Zöller
Erarbeitung von Grundlagen zur Abbildung des tribologischen Systems in der Umformsimulation
LFT, 126 Seiten, 51 Bilder, 3 Tab. 2016.
ISBN 978-3-87525-403-7.

Band 280: Christian Hezler
Einsatz technologischer Versuche zur Erweiterung der Versagensvorhersage bei Karosseriebauteilen aus höchstfesten Stählen
LFT, 147 Seiten, 63 Bilder, 44 Tab. 2016.
ISBN 978-3-87525-404-4.

Band 281: Jochen Bönig
Integration des Systemverhaltens von Automobil-Hochvoltleitungen in die virtuelle Absicherung durch strukturmechanische Simulation
FAPS, 177 Seiten, 107 Bilder, 17 Tab. 2016.
ISBN 978-3-87525-405-1.

Band 282: Johannes Kohl
Automatisierte Datenerfassung für diskret ereignisorientierte Simulationen in der energieflexibelen Fabrik
FAPS, 160 Seiten, 80 Bilder, 27 Tab. 2016.
ISBN 978-3-87525-406-8.

Band 283: Peter Bechtold
Mikroschockwellenumformung mittels ultrakurzer Laserpulse
LPT, 155 Seiten, 59 Bilder, 10 Tab. 2016.
ISBN 978-3-87525-407-5.

Band 284: Stefan Berger
Laserstrahlschweißen thermoplastischer Kohlenstofffaserverbundwerkstoffe mit spezifischem Zusatzdraht
LPT, 118 Seiten, 68 Bilder, 9 Tab. 2016.
ISBN 978-3-87525-408-2.

Band 285: Martin Bornschlegl
Methods-Energy Measurement - Eine Methode zur Energieplanung für Fügeverfahren im Karosseriebau
FAPS, 136 Seiten, 72 Bilder, 46 Tab. 2016.
ISBN 978-3-87525-409-9.

Band 286: Tobias Rackow
Erweiterung des Unternehmenscontrollings um die Dimension Energie
FAPS, 164 Seiten, 82 Bilder, 29 Tab. 2016.
ISBN 978-3-87525-410-5.

Band 287: Johannes Koch
Grundlegende Untersuchungen zur Herstellung zyklisch-symmetrischer Bauteile mit Nebenformelementen durch Blechmassivumformung
LFT, 125 Seiten, 49 Bilder, 17 Tab. 2016.
ISBN 978-3-87525-411-2.

Band 288: Hans Ulrich Vierzigmann
Beitrag zur Untersuchung der tribologischen Bedingungen in der Blechmassivumformung - Bereitstellung von tribologischen Modellversuchen und Realisierung von Tailored Surfaces
LFT, 174 Seiten, 102 Bilder, 34 Tab. 2016.
ISBN 978-3-87525-412-9.

Band 289: Thomas Senner
Methodik zur virtuellen Absicherung der formgebenden Operation des Nasspressprozesses von Gelege-Mehrschichtverbunden
LFT, 156 Seiten, 96 Bilder, 21 Tab. 2016.
ISBN 978-3-87525-414-3.

Band 290: Sven Kreitlein
Der grundoperationsspezifische Mindestenergiebedarf als Referenzwert zur Bewertung der Energieeffizienz in der Produktion
FAPS, 185 Seiten, 64 Bilder, 30 Tab. 2016.
ISBN 978-3-87525-415-0.

Band 291: Christian Roos
Remote-Laserstrahlschweißen verzinkter Stahlbleche in Kehlnahtgeometrie
LPT, 123 Seiten, 52 Bilder, 0 Tab. 2016.
ISBN 978-3-87525-416-7.

Band 292: Alexander Kahrimanidis
Thermisch unterstützte Umformung von Aluminiumblechen
LFT, 165 Seiten, 103 Bilder, 18 Tab. 2016.
ISBN 978-3-87525-417-4.

Band 293: Jan Tremel
Flexible Systems for Permanent Magnet Assembly and Magnetic Rotor Measurement / Flexible Systeme zur Montage von Permanentmagneten und zur Messung magnetischer Rotoren
FAPS, 152 Seiten, 91 Bilder, 12 Tab. 2016.
ISBN 978-3-87525-419-8.

Band 294: Ioannis Tsoupis
Schädigungs- und Versagensverhalten hochfester Leichtbauwerkstoffe unter Biegebeanspruchung
LFT, 176 Seiten, 51 Bilder, 6 Tab. 2017.
ISBN 978-3-87525-420-4.

Band 295: Sven Hildering
Grundlegende Untersuchungen zum Prozessverhalten von Silizium als Werkzeugwerkstoff für das Mikroscherschneiden metallischer Folien
LFT, 177 Seiten, 74 Bilder, 17 Tab. 2017.
ISBN 978-3-87525-422-8.

Band 296: Sasia Mareike Hertweck
Zeitliche Pulsformung in der Lasermikromaterialbearbeitung – Grundlegende Untersuchungen und Anwendungen
LPT, 146 Seiten, 67 Bilder, 5 Tab. 2017.
ISBN 978-3-87525-423-5.

Band 297: Paryanto
Mechatronic Simulation Approach for the Process Planning of Energy-Efficient Handling Systems
FAPS, 162 Seiten, 86 Bilder, 13 Tab. 2017.
ISBN 978-3-87525-424-2.

Band 298: Peer Stenzel
Großserientaugliche Nadelwickeltechnik für verteilte Wicklungen im Anwendungsfall der E-Traktionsantriebe
FAPS, 239 Seiten, 147 Bilder, 20 Tab. 2017.
ISBN 978-3-87525-425-9.

Band 299: Mario Lušić
Ein Vorgehensmodell zur Erstellung montageführender Werkerinformationssysteme simultan zum Produktentstehungsprozess
FAPS, 174 Seiten, 79 Bilder, 22 Tab. 2017.
ISBN 978-3-87525-426-6.

Band 300: Arnd Buschhaus
Hochpräzise adaptive Steuerung und Regelung robotergeführter Prozesse
FAPS, 202 Seiten, 96 Bilder, 4 Tab. 2017.
ISBN 978-3-87525-427-3.

Band 301: Tobias Laumer
Erzeugung von thermoplastischen Werkstoffverbunden mittels simultanem, intensitätsselektivem Laserstrahlschmelzen
LPT, 140 Seiten, 82 Bilder, 0 Tab. 2017.
ISBN 978-3-87525-428-0.

Band 302: Nora Unger
Untersuchung einer thermisch unterstützten Fertigungskette zur Herstellung umgeformter Bauteile aus der höherfesten Aluminiumlegierung EN AW-7020
LFT, 142 Seiten, 53 Bilder, 8 Tab. 2017.
ISBN 978-3-87525-429-7.

Band 303: Tommaso Stellin
Design of Manufacturing Processes for the Cold Bulk Forming of Small Metal Components from Metal Strip
LFT, 146 Seiten, 67 Bilder, 7 Tab. 2017.
ISBN 978-3-87525-430-3.

Band 304: Bassim Bachy
Experimental Investigation, Modeling, Simulation and Optimization of Molded Interconnect Devices (MID) Based on Laser Direct Structuring (LDS) / Experimentelle Untersuchung, Modellierung, Simulation und Optimierung von Molded Interconnect Devices (MID) basierend auf Laser Direktstrukturierung (LDS)
FAPS, 168 Seiten, 120 Bilder, 26 Tab. 2017.
ISBN 978-3-87525-431-0.

Band 305: Michael Spahr
Automatisierte Kontaktierungsverfahren für flachleiterbasierte Pkw-Bordnetzsysteme
FAPS, 197 Seiten, 98 Bilder, 17 Tab. 2017.
ISBN 978-3-87525-432-7.

Band 306: Sebastian Suttner
Charakterisierung und Modellierung des spannungszustandsabhängigen Werkstoffverhaltens der Magnesiumlegierung AZ31B für die numerische Prozessauslegung
LFT, 150 Seiten, 84 Bilder, 19 Tab. 2017.
ISBN 978-3-87525-433-4.

Band 307: Bhargav Potdar
A reliable methodology to deduce thermo-mechanical flow behaviour of hot stamping steels
LFT, 203 Seiten, 98 Bilder, 27 Tab. 2017.
ISBN 978-3-87525-436-5.

Band 308: Maria Löffler
Steuerung von Blechmassivumformprozessen durch maßgeschneiderte tribologische Systeme
LFT, viii u. 166 Seiten, 90 Bilder, 5 Tab. 2018. ISBN 978-3-96147-133-1.

Band 309: Martin Müller
Untersuchung des kombinierten Trenn- und Umformprozesses beim Fügen artungleicher Werkstoffe mittels Schneidclinchverfahren
LFT, xi u. 149 Seiten, 89 Bilder, 6 Tab. 2018. ISBN: 978-3-96147-135-5.

Band 310: Christopher Kästle
Qualifizierung der Kupfer-Drahtbondtechnologie für integrierte Leistungsmodule in harschen Umgebungsbedingungen
FAPS, xii u. 167 Seiten, 70 Bilder, 18 Tab. 2018. ISBN 978-3-96147-145-4.

Band 311: Daniel Vipavc
Eine Simulationsmethode für das 3-Rollen-Schubbiegen
LFT, xiii u. 121 Seiten, 56 Bilder, 17 Tab. 2018. ISBN 978-3-96147-147-8.

Band 312: Christina Ramer
Arbeitsraumüberwachung und autonome Bahnplanung für ein sicheres und flexibles Roboter-Assistenzsystem in der Fertigung
FAPS, xiv u. 188 Seiten, 57 Bilder, 9 Tab. 2018. ISBN 978-3-96147-153-9.

Band 313: Miriam Rauer
Der Einfluss von Poren auf die Zuverlässigkeit der Lötverbindungen von Hochleistungs-Leuchtdioden
FAPS, xii u. 209 Seiten, 108 Bilder, 21 Tab. 2018. ISBN 978-3-96147-157-7.

Band 314: Felix Tenner

Kamerabasierte Untersuchungen der Schmelze und Gasströmungen beim Laserstrahlschweißen verzinkter Stahlbleche

LPT, xxiii u. 184 Seiten, 94 Bilder, 7 Tab.
2018. ISBN 978-3-96147-160-7.

Band 315: Aarief Syed-Khaja

Diffusion Soldering for High-temperature Packaging of Power Electronics

FAPS, x u. 202 Seiten, 144 Bilder, 32 Tab.
2018. ISBN 978-3-87525-162-1.

Band 316: Adam Schaub

Grundlagenwissenschaftliche Untersuchung der kombinierten Prozesskette aus Umformen und Additive Fertigung

LFT, xi u. 192 Seiten, 72 Bilder, 27 Tab.
2019. ISBN 978-3-96147-166-9.

Band 317: Daniel Gröbel

Herstellung von Nebenformelementen unterschiedlicher Geometrie an Blechen mittels Fließpressverfahren der Blechmassivumformung

LFT, x u. 165 Seiten, 96 Bilder, 13 Tab.
2019. ISBN 978-3-96147-168-3.

Band 318: Philipp Hildenbrand

Entwicklung einer Methodik zur Herstellung von Tailored Blanks mit definierten Halbzeugeigenschaften durch einen Taumelprozess

LFT, ix u. 153 Seiten, 77 Bilder, 4 Tab.
2019. ISBN 978-3-96147-174-4.

Band 319: Tobias Konrad

Simulative Auslegung der Spann- und Fixierkonzepte im Karosserierohbau: Bewertung der Baugruppenmaßhaltigkeit unter Berücksichtigung schwankender Einflussgrößen

LFT, x u. 203 Seiten, 134 Bilder, 32 Tab.
2019. ISBN 978-3-96147-176-8.

Band 320: David Meinel

Architektur applikationsspezifischer Multi-Physics-Simulationskonfiguratoren am Beispiel modularer Triebzüge

FAPS, xii u. 166 Seiten, 82 Bilder, 25 Tab.
2019. ISBN 978-3-96147-184-3.

Band 321: Andrea Zimmermann

Grundlegende Untersuchungen zum Einfluss fertigungsbedingter Eigenschaften auf die Ermüdungsfestigkeit kaltmassivumgeformter Bauteile

LFT, ix u. 160 Seiten, 66 Bilder, 5 Tab.
2019. ISBN 978-3-96147-190-4.

Band 322: Christoph Amann

Simulative Prognose der Geometrie nassgepresster Karosseriebauteile aus Gelege-Mehrschichtverbunden

LFT, xvi u. 169 Seiten, 80 Bilder, 13 Tab.
2019. ISBN 978-3-96147-194-2.

Band 323: Jennifer Tenner

Realisierung schmierstofffreier Tiefziehprozesse durch maßgeschneiderte Werkzeugoberflächen

LFT, x u. 187 Seiten, 68 Bilder, 13 Tab.
2019. ISBN 978-3-96147-196-6.

Band 324: Susan Zöller

Mapping Individual Subjective Values to Product Design

KTmfk, xi u. 223 Seiten, 81 Bilder, 25 Tab.
2019. ISBN 978-3-96147-202-4.

Band 325: Stefan Lutz

Erarbeitung einer Methodik zur semiempirischen Ermittlung der Umwandlungskinetik durchhärtender Wälzlagerstähle für die Wärmebehandlungssimulation

LFT, xiv u. 189 Seiten, 75 Bilder, 32 Tab. 2019. ISBN 978-3-96147-209-3.

Band 326: Tobias Gnibl

Modellbasierte Prozesskettenabbildung rührreibgeschweißter Aluminiumhalbzeuge zur umformtechnischen Herstellung höchstfester Leichtbaustrukturteile

LFT, xii u. 167 Seiten, 68 Bilder, 17 Tab. 2019. ISBN 978-3-96147-217-8.

Band 327: Johannes Bürner

Technisch-wirtschaftliche Optionen zur Lastflexibilisierung durch intelligente elektrische Wärmespeicher

FAPS, xiv u. 233 Seiten, 89 Bilder, 27 Tab. 2019. ISBN 978-3-96147-219-2.

Band 328: Wolfgang Böhm

Verbesserung des Umformverhaltens von mehrlagigen Aluminiumblechwerkstoffen mit ultrafeinkörnigem Gefüge

LFT, ix u. 160 Seiten, 88 Bilder, 14 Tab. 2019. ISBN 978-3-96147-227-7.

Band 329: Stefan Landkammer

Grundsatzuntersuchungen, mathematische Modellierung und Ableitung einer Auslegungsmethodik für Gelenkantriebe nach dem Spinnenbeinprinzip

LFT, xii u. 200 Seiten, 83 Bilder, 13 Tab. 2019. ISBN 978-3-96147-229-1.

Band 330: Stephan Rapp

Pump-Probe-Ellipsometrie zur Messung transienter optischer Materialeigenschaften bei der Ultrakurzpuls-Lasermaterialbearbeitung

LPT, xi u. 143 Seiten, 49 Bilder, 2 Tab. 2019. ISBN 978-3-96147-235-2.

Band 331: Michael Scholz

Intralogistics Execution System mit integrierten autonomen, servicebasierten Transportentitäten

FAPS, xi u. 195 Seiten, 55 Bilder, 11 Tab. 2019. ISBN 978-3-96147-237-6.

Band 332: Eva Bogner

Strategien der Produktindividualisierung in der produzierenden Industrie im Kontext der Digitalisierung

FAPS, ix u. 201 Seiten, 55 Bilder, 28 Tab. 2019. ISBN 978-3-96147-246-8.

Band 333: Daniel Benjamin Krüger

Ein Ansatz zur CAD-integrierten muskuloskelettalen Analyse der Mensch-Maschine-Interaktion

KTmfk, x u. 217 Seiten, 102 Bilder, 7 Tab. 2019. ISBN 978-3-96147-250-5.

Band 334: Thomas Kuhn

Qualität und Zuverlässigkeit laserdirektstrukturierter mechatronisch integrierter Baugruppen (LDS-MID)

FAPS, ix u. 152 Seiten, 69 Bilder, 12 Tab. 2019. ISBN: 978-3-96147-252-9.

Band 335: Hans Fleischmann
Modellbasierte Zustands- und Prozessüberwachung auf Basis sozio-cyber-physischer Systeme
FAPS, xi u. 214 Seiten, 111 Bilder, 18 Tab.
2019. ISBN: 978-3-96147-256-7.

Band 336: Markus Michalski
Grundlegende Untersuchungen zum Prozess- und Werkstoffverhalten bei schwingungsüberlagerter Umformung
LFT, xii u. 197 Seiten, 93 Bilder, 11 Tab.
2019. ISBN: 978-3-96147-270-3.

Band 337: Markus Brandmeier
Ganzheitliches ontologiebasiertes Wissensmanagement im Umfeld der industriellen Produktion
FAPS, xi u. 255 Seiten, 77 Bilder, 33 Tab.
2020. ISBN: 978-3-96147-275-8.

Band 338: Stephan Purr
Datenerfassung für die Anwendung lernender Algorithmen bei der Herstellung von Blechformteilen
LFT, ix u. 165 Seiten, 48 Bilder, 4 Tab.
2020. ISBN: 978-3-96147-281-9.

Band 339: Christoph Kiener
Kaltfließpressen von gerad- und schrägverzahnten Zahnrädern
LFT, viii u. 151 Seiten, 81 Bilder, 3 Tab.
2020. ISBN 978-3-96147-287-1.

Band 340: Simon Spreng
Numerische, analytische und empirische Modellierung des Heißcrimpprozesses
FAPS, xix u. 204 Seiten, 91 Bilder, 27 Tab.
2020. ISBN 978-3-96147-293-2.

Band 341: Patrik Schwingenschlögl
Erarbeitung eines Prozessverständnisses zur Verbesserung der tribologischen Bedingungen beim Presshärten
LFT, x u. 177 Seiten, 81 Bilder, 8 Tab.
2020. ISBN 978-3-96147-297-0.

Band 342: Emanuela Affronti
Evaluation of failure behaviour of sheet metals
LFT, ix u. 136 Seiten, 57 Bilder, 20 Tab.
2020. ISBN 978-3-96147-303-8.

# Kurzzusammenfassung

Die volle Ausschöpfung der Umformbarkeit von Blechen ist entscheidend für die Prozessoptimierung. Dies gilt insbesondere für die Automobilindustrie, wo der aktuelle Trend in der Entwicklung von Leichtbaustrukturen liegt. Dennoch zeigt die aktuelle Standardevaluierungsmethodik für leichte und spröde Materialien Schwächen auf. In der vorliegenden Untersuchung wurde zur Verbesserung der Evaluierung der Versagensgrenze eine detaillierte Analyse der Versagensmechanismen bei verschiedenen Materialklassen durchgeführt. Ziel war es, die Gültigkeit der Definition des Einschnürungsbeginn zu analysieren und eine korrekte Vorhersage der Formänderungsgrenzen zu gewährleisten, welche auch für Materialien gilt, die keine Lokalisierungen zeigen. Die erarbeiteten Erkenntnisse wurden genutzt, um ein Gültigkeitsfenster mittels Mustererkennungsmethodik für die Grenzformänderungsvermögen zu definieren sowie die Evaluation der Formänderungsgrenzen zu optimieren, ohne die Besonderheiten der unterschiedlichen Materialien aus den Augen zu verlieren.

The full exploitation of sheet metal formability is crucial for process optimization. This applies in particular to the automotive industry, in which the current trend is in the development of lightweight structures. Nevertheless, the standard evaluation methodology shows weaknesses for brittle materials. In the present study, a detailed analysis of the failure mechanisms for different material classes was carried out to improve the failure limit evaluation. The aim was to analyse the validity of the definition of the onset of necking in order to assure the correct prediction of the deformation limits, including those that do not show any localizations. The knowledge gained was used to define a validity window using pattern recognition methodology and to optimize the forming limit evaluation while taking into consideration the peculiarities of the different materials.

ISBN 978-3-96147-303-8

FAU UNIVERSITY PRESS 2020